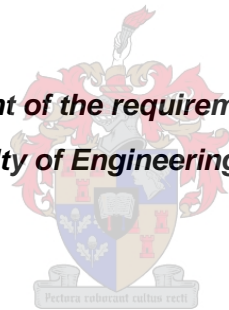


Investigation of Factors Affecting the Load Carrying Capacity of Driven Solar Panel Support Posts

By
Aimable Uwimana

***Thesis presented in fulfilment of the requirements for the degree of Master of
Engineering in the Faculty of Engineering at Stellenbosch University***



Supervisor: DEng PrEng Peter Day

*Technical director at Jones & Wagener
Adjunct Professor: Geotechnical Engineering, Stellenbosch University*

Co-Supervisor: Dr Marius De Wet

Senior Lecturer: Geotechnical Engineering, Stellenbosch University

December 2015

DECLARATION

By submitting this thesis electronically, I declare that the entirety of the work contained therein is my own, original work, that I am the sole author thereof (save to the extent explicitly otherwise stated), that reproduction and publication thereof by Stellenbosch University will not infringe any third party rights and that I have not previously in its entirety or in part submitted it for obtaining any qualification.

August 2015

ABSTRACT

A number of large “solar farms” have already been built in South Africa and more are under construction. Many of these make use of banks of photovoltaic panels mounted on a frame-work supported on columns known as posts. Various methods of founding are used for these posts. One of the founding methods involves driving the post into a predrilled hole filled with granular material. In South Africa, this method is used in semi-arid areas where the sites are frequently underlain by clacretes or by shallow rock. However, there are no clear design guidelines for such foundations. When the installation is not done correctly and the solar panel support structure is subjected to the action of wind and water, the driven posts could settle or be pulled-out of the ground creating failure. Therefore, an investigation of factors affecting the shaft pull-out capacity of driven post is vitally important.

In order to provide a better understanding of load bearing capacity of driven posts in both compression and tension, research has been carried out into the effect of backfill material type, compaction density, compaction moisture content, backfill saturation, post-to-hole area ratio and aging of the backfill. An experimental programme using three types of backfill material, three degrees of compaction, three area ratios and two compaction moisture contents was carried out to assess the influence of these variables on axial and oblique pull-out loading capacity of predrilled driven posts. In addition, the moisture content at the time of loading and the effect of aging of the backfill was considered. Each material was evaluated in terms of particle size distribution, particle shape, and shearing resistance using direct shear tests. The pull-out resistance was evaluated using an Instron load-testing machine on experimental driven posts at half scale.

The results from the direct shear tests revealed an increase in shear strength with an increase in the degree of compaction and normal stress. It also shows that the crusher dust material has higher shear strength than Malmesbury and Philippi sands. However, shear strength reduces with saturation while dilation reduces with an increase of both normal stress and moisture content.

The shaft pull-out capacity results from the experimental model tests confirm the findings of the direct shear tests on material performance. The pull-out resistance increases with both degree of compaction and area ratio. It reduces with saturation. In addition, the pull-out capacity of the post increases significantly with time. Comparing the axial and oblique pull-out capacity, a higher resistance was observed under oblique pull-out loads than for axial pull-out. This helps to explain why posts have been observed to settle under very modest dead loading but are, nevertheless, able to resist significant wind loading on the underside of the panels.

This study contributes to understanding the effect of material type, compaction density, area ratio, water content and aging on the shaft pull-out capacity of driven post foundations for solar panels. Practical specifications and technical guidelines are developed to ensure an improved installation of foundations using this predrilled driven post method.

OPSOMMING

'n Aantal groot sonkrag plase is alreeds in Suid-Afrika gebou en nog meer word tans ontwikkel. Baie van hierdie plase maak gebruik van banke van fotovoltaiëse panele wat op 'n raamwerk gemonteer is. Die raamwerk word ondersteun deur kolomme bekend as pale. Verskeie metodes van fundering word gebruik vir hierdie pale. Een van hierdie metodes behels die indryf van die paal in 'n vooraf-geboorde gat gevul met korrelrige materiaal. In Suid-Afrika word hierdie metode in semi-droë areas gebruik wat dikwels onderlê word deur vlak rots. Daar is egter geen duidelike riglyne vir die ontwerp van sulke fondamente nie. Wanneer die installasie nie reg uitgevoer word nie, en die sonpaneel-struktuur word blootgestel aan die gekombineerde aksie van wind en water, kan die gedrewe pale versak of uit die grond getrek word, wat swigting teweegbring. Om hierdie rede is dit baie belangrik dat die faktore wat die uittrek-kapasiteit van die skag van die gedrewe paal affekteer, ondersoek word.

Om 'n beter begrip van die lasdraende vermoë van gedrewe pale in beide druk en uittrekking te bewerkstellig, is navorsing uitgevoer op die effek van tipe invulmateriaal, kompaksie digtheid, voginhoud by kompaksie, versadiging van invulmateriaal, verhouding van paal-tot gat-deursnitarea en veroudering van terugvulmateriaal. 'n Toetsprogram, waarin drie tipes invulmateriaal, drie grade van kompaksie, drie deursnitarea-verhoudings en twee voginhoud tydens kompaksie gebruik is, is uitgevoer om die invloed van hierdie veranderlikes op aksiale en skuinsuittrekweerstand van vooraf-geboorde gedrewe pale, te bepaal. Daarmee saam is die voginhoud tydens belasting en die effek van veroudering van die invulmateriaal ook beskou. Elke materiaal was geëvalueer in terme van partikelgrootteverspreiding, partikelvorm en skuifweerstand deur direkte skuiftoetse uit te voer. Die uittrekweerstand van eksperimentele gedrewe pale was geëvalueer deur gebruik te maak van 'n Instron toetsapparaat. Die toetsmodel was halfskaalgrootte.

Die resultate van die direkte skuiftoets toon 'n toename in skuifsterkte met 'n toename in die graad van kompaksie en vertikale druk. Dit het ook getoon dat die vergruiser fynstof 'n hoër skuifsterkte as die Malmesbury en Philippi sande het. Die skuifsterkte neem egter af met versadiging terwyl die dilatansie afneem met 'n toename in beide die vertikale spanning en voginhoud.

Die skag uittrekvermoë resultate van die eksperimentele modeltoets bevestig die skuifgedrag van die materiaal. Die uittrekweerstand verhoog met 'n toename in die graad van kompaksie en area verhouding en verlaag met versadiging. Die uittrekvermoë van die pale neem aansienlik toe met tyd. Deur die aksiale en skuinsuittrekvermoë te vergelyk, is 'n hoër weerstand waargeneem met skuinsuittrekbelasting as met aksiale uittrek. Hierdie bevinding verklaar waarom daar al waargeneem is dat pale wat versak onder die invloed van beskeie dooiegegewiglaste, beduidende windbelasting aan die onderkant van panele kan weerstaan.

Hierdie studie dra by tot 'n beter begrip van die effek van materiaal tipe, kompaksiedigtheid, area-verhouding, voginhoud en veroudering op skag-uittrekweerstand van gedrewe paal fondamente vir sonpanele. Praktiese spesifikasies en tegniese riglyne word ontwikkel om

'n verbeterde installasie van fondasies waarin die voorafgeboorde gedrewe paal metode gebruik word, te verseker.

TO MY FAMILY

ACKNOWLEDGMENT

I would like to express my sincere gratitude to the Almighty God for His Grace, strength, protection, and health given. Every good gift and every perfect gift comes from Him.

I am also grateful to the following persons and institutions who have contributed in one way or another to the successful completion of this study:

- My supervisor DEng Peter Day and Co-supervisor Dr. Marius De Wet. I am thankful to DEng Peter Day for his willingness to work with me on this study. Your trust, support, insight guidance, and advices are highly appreciated. My gratitude goes also to Dr. Marius De Wet who not only took part in the guidance of this study but also in academic support and assistance.
- Dr. Gibson Ncube and Ms Rebecca Bisangwa, Mr. Naphtal Ntirenganya, and Torbert Mpano, your assistance in proof reading is appreciated. Special thanks go to Dr. Gibson Ncube and Ms Rebecca Bisangwa for your tireless assistance.
- Mr. Riaan Bride Briedehann (Pavement and geotechnical lab manager) and Mr. Stephan Zeranka (structure lab manager), for your technical assistance in the laboratory.
- Laboratory and workshop personnel, Mr. Gavin Williams and Mr. Colin Isaacs and Mr. Dion Viljion for your assistance in different ways
- The Civil Engineering academic personnel for administrative assistance, special thanks goes to Ms Amanda De Wet and Ms Janine Myburgh.
- Stellenbosch international fellowship (SIF), Bianca Rusu for fellowship and support. Special thanks goes to Rev. Jurie Goosen and his wife Maggie for your love and care.
- Rwandan student association for support.
- The government of Rwanda through Rwanda Education Board for loaning me the money for my studies.
- Friends, who are near or far, who supported me in different ways.
- My entire family especially my late father, Didace Kanyenzi Rusagara for laying the foundation for me. Thanks to my mother, sisters, and brothers for your prayers and support.

TABLE CONTENTS

| | |
|---|------------|
| DECLARATION | I |
| ABSTRACT | II |
| OPSOMMING | III |
| TABLE CONTENTS..... | VII |
| LIST OF TABLES | IX |
| LIST OF FIGURES..... | X |
| LIST OF SYMBOLS AND ABBREVIATIONS | XIV |
| CHAPTER 1 INTRODUCTION | 1 |
| 1.1 BACKGROUND OF THE RESEARCH..... | 1 |
| 1.2 PROBLEM STATEMENT | 3 |
| 1.3 RESEARCH OBJECTIVES..... | 3 |
| 1.4 SCOPE AND LIMITATION..... | 4 |
| 1.5 LAYOUT OF THIS DISSERTATION | 4 |
| CHAPTER 2 LITERATURE STUDY ON SUPPORT STRUCTURES FOR SOLAR PANEL | 6 |
| 2.1 INTRODUCTION | 6 |
| 2.2 DIFFERENT METHODS OF SOLAR PANELS SUPPORTS..... | 7 |
| 2.3 EQUIPMENT AND PROCEDURE INSTALLATION OF DRIVEN POST..... | 10 |
| 2.4 MECHANICAL AND PHYSICAL PROPERTIES AFFECTING THE STRENGTH OF BACKFILL MATERIALS..... | 11 |
| 2.5 COMPARISON OF DIRECT SHEAR BOX AND DRIVEN POST MECHANISM... | 17 |
| 2.6 DIRECT SHEAR TESTING AND THE EFFECT OF SPECIMEN SIZE..... | 22 |
| 2.7 SHAFT CAPACITY OF PILES | 25 |
| 2.8 SOUTH AFRICAN CLIMATIC CONDITIONS | 39 |
| 2.9 SUMMARY OF LITERATURE REVIEW..... | 41 |

| | | |
|------------------------|---|------------|
| CHAPTER 3 | METHODOLOGY AND EXPERIMENT DESIGN | 43 |
| 3.1 | INTRODUCTION | 43 |
| 3.1 | MATERIALS, TEST METHODS AND STANDARDS..... | 43 |
| 3.2 | SHEAR STRENGTH TESTING..... | 47 |
| 3.3 | LOAD EXPERIMENT DESIGN | 53 |
| CHAPTER 4 | LABORATORY TEST RESULTS AND DISCUSSION | 66 |
| 4.1 | CLASSIFICATION TEST RESULTS | 66 |
| 4.2 | DIRECT SHEAR STRENGTH TESTS | 69 |
| 4.3 | DISCUSSION OF RESULTS | 86 |
| CHAPTER 5 | PULL-OUT TEST RESULTS AND DISCUSSION | 87 |
| 5.1 | INTRODUCTION | 87 |
| 5.2 | AXIAL PULL-OUT TEST | 87 |
| 5.3 | OBLIQUE PULL-OUT TEST | 103 |
| 5.4 | DISCUSSION OF RESULTS | 110 |
| CHAPTER 6 | CONCLUSIONS AND RECOMMENDATIONS..... | 112 |
| 6.1 | CONCLUSIONS | 112 |
| 6.2 | RECOMMENDATIONS..... | 113 |
| REFERENCES..... | | 115 |
| APPENDIX..... | | 121 |

LIST OF TABLES

| | |
|--|-----|
| Table 2-1 Summary of standard and modified Proctor compaction test specification ASTM 1557 D-698 and D-1557 and TMH1 (Mod AASHTO) modified from (Das & Sivakugan 2014) | 17 |
| Table 2-2 Shaft resistance per unit area (Byrne & Berry 2008)..... | 26 |
| Table 2-3 Base resistance per unit area (Byrne & Berry 2008) | 27 |
| Table 2-4 Design guideline for non-cohesive soil (API 2000)..... | 28 |
| Table 3-1 Compactor hammer and layer details of CD | 50 |
| Table 4-1 Summary of research materials characteristics | 68 |
| Table 4-2 Summary of Maximum shear stress and horizontal displacement at failure of crusher dust (CD) | 72 |
| Table 4-3 Summary of maximum vertical displacement of crusher dust (CD) | 76 |
| Table 4-4 Summary of maximum vertical displacement and maximum dilation angle of MS | 79 |
| Table 4-5 Summary of shear stress, friction angle, vertical displacement and dilation angle of PS | 81 |
| Table 4-6 A summary of shear maximum shear stress, horizontal displacement, friction angle and cohesion of research materials | 85 |
| Table 4-7 Summary of vertical displacement and dilation angle of the research material | 86 |
| Table 5-1 Area ratio of posts to pipe section | 87 |
| Table 5-2 Summary of maximum of axial pull-out resistance force of the research materials | 102 |
| Table 5-3 Summary of maximum of oblique pull-out resistance and force of the research materials | 109 |

LIST OF FIGURES

| | |
|---|----|
| Figure 1-1 South Africa Photovoltaics growth in Megawatts (Wikipedia 2015)..... | 1 |
| Figure 1-2 Typical support structure including posts for a PV panel array (Day 2014b) | 2 |
| Figure 2-1 Aerial picture of solar panels driven posts (De-Aar Solar Power 2014)..... | 6 |
| Figure 2-2 Types of photovoltaics arrays and panels supports system modified from (Maffei <i>et al.</i> 2013) | 7 |
| Figure 2-3 Ballast footing solar panel support..... | 8 |
| Figure 2-4 Helical pile configuration (Sakr Undated)..... | 9 |
| Figure 2-5 Solar panels embracing the topography | 10 |
| Figure 2-6 GAYK™ Hydraulic ram used in solar panel post installation (Schletter 2010) . | 10 |
| Figure 2-7 Particle distribution curve (Craig 2004)..... | 11 |
| Figure 2-8 Effect of particle distribution on compaction (Whitlow 1995) | 13 |
| Figure 2-9 Particle shape (Das & Sobhan 2013) | 14 |
| Figure 2-10 Sphericity and roundness model determination (Cho <i>et al.</i> 2006)..... | 15 |
| Figure 2-11 Effect of compaction effort (Das 2009) | 16 |
| Figure 2-12 Shear zone representation a) in pile and b) in direct shear box | 18 |
| Figure 2-13 Internal friction sand-sand and interface friction steel-sand in shear box (Lehane <i>et al.</i> 1993) | 19 |
| Figure 2-14 Contribution of shear strength of granular soil (Mitchell & Soga 2005) | 20 |
| Figure 2-15 Soil presentation | 21 |
| Figure 2-16 Effect of decreasing of water in soil modified after (Burland 2012) | 22 |
| Figure 2-17 Effect of specimen size on friction angle (Cerato & Lutenegeger 2006)..... | 23 |
| Figure 2-18 Effect of density and particle size on shear strength and dilation (Simoni & Houlsby 2006) | 24 |
| Figure 2-19 Trend of variation of δ_{cv} with grain size of granular soils shearing against a steel interface (Jardine <i>et al.</i> ,1998, after Jardine <i>et al.</i> ,1992) | 30 |
| Figure 2-20 Interface friction variation with D_{50} after (Lehane <i>et al.</i> 2007) | 32 |

| | |
|---|----|
| Figure 2-21 Definition of the term used in Equation 2-13 and 2-16 (Jardine <i>et al.</i> 1998) .. | 33 |
| Figure 2-22 Behaviour of particles during loading causing dilation (Axelsson 2000) | 34 |
| Figure 2-23 Behaviour of the shear zone during installation and static loading: (a) schematic diagram of the shear zone; (b) variation in the shear zone (Yu & Yang 2012) | 35 |
| Figure 2-24 Effect of dilation and loading type on radial effective stress (Yu & Yang 2012) | 36 |
| Figure 2-25 Reorientation of particles increasing shear zone (Axelsson 2000) | 36 |
| Figure 2-26 Earth pressure distribution (Poulos & Davis 1980) | 38 |
| Figure 2-27 Two tangent methods of load capacity (Bhardwaj & Singh 2013) | 39 |
| Figure 2-28 Solar resource map of South Africa (Solargis 2015) | 40 |
| Figure 2-29 Map of basic wind speeds (SANS10160-3 2011) | 41 |
| Figure 3-1 Research materials a) Crusher dust, b) Malmesbury sand, c) Philippi sand ... | 43 |
| Figure 3-2 Particle size distribution curves of the research materials | 44 |
| Figure 3-3 Particle shape of research materials a) Philippi sand b) Malmesbury sand c) crusher dust | 45 |
| Figure 3-4 Roundness categories, Krumbein images and range of roundness modified from Krumbein (1941) (Edil <i>et al.</i> 2007) | 46 |
| Figure 3-5 Modified AASHTO compactor machine | 47 |
| Figure 3-6 Flowchart of shear test experimental design | 48 |
| Figure 3-7 Shear box compactor | 49 |
| Figure 3-8 Illustration of sample preparation | 50 |
| Figure 3-9 Shear box apparatus set up | 51 |
| Figure 3-10 Shear box apparatus for 60x60 and 100x100 mm | 51 |
| Figure 3-11 Distribution curve of the research material after scalping | 52 |
| Figure 3-12 Summary of experimental program | 54 |
| Figure 3-13 a) Top-hat section of a typical solar project and b) L base section of the research experimental work | 55 |
| Figure 3-14 Experimental pipe and post | 55 |

| | |
|---|----|
| Figure 3-15 Schematic design of oblique pull-out set up | 57 |
| Figure 3-16 Rammer pattern for compaction: a) the one adopted b) TMH1 | 58 |
| Figure 3-17 Laboratory mixer | 59 |
| Figure 3-18 Photograph of Instron 2000 | 60 |
| Figure 3-19 Positioning and push in of the post..... | 61 |
| Figure 3-20 Soil behaviour and condition when a post is been pulled-out..... | 63 |
| Figure 3-21 Axial pull-out test experimental program..... | 64 |
| Figure 3-22 Oblique pull-out test experimental program | 65 |
| Figure 4-1 Compaction curves a) crusher dust b) Malmesbury sand c) Philippi sand | 67 |
| Figure 4-2 Shear stress versus horizontal displacement of crusher dust (CD)..... | 70 |
| Figure 4-3 Relationship of shear stress to normal stress of crusher dust (CD) | 71 |
| Figure 4-4 The effect of normal pressure and compaction effort on maximum shear stress of CD..... | 73 |
| Figure 4-5 The effect of compaction on the friction angle of CD | 74 |
| Figure 4-6 Horizontal versus vertical displacement of crusher dust(CD)..... | 75 |
| Figure 4-7 Shear stress versus horizontal displacement for MS | 77 |
| Figure 4-8 Shear stress versus normal pressure for MS..... | 78 |
| Figure 4-9 Vertical displacement versus horizontal displacement..... | 79 |
| Figure 4-10 Shear stress versus horizontal displacement for PS..... | 80 |
| Figure 4-11 Shear stress versus normal pressure of PS | 82 |
| Figure 4-12 Vertical displacement versus horizontal displacement of PS | 83 |
| Figure 4-13 Maximum shear stress versus normal stress of research materials..... | 84 |
| Figure 5-1 Drive-in force at different Mod AASHTO MDD degrees of CD | 88 |
| Figure 5-2 Drive in force versus displacement at different area ratio of CD | 89 |
| Figure 5-3 Drive-in force compacted at dry and OMC conditions..... | 90 |

| | |
|--|-----|
| Figure 5-4 Pull-out resistance versus displacement of Crusher Dust (CD) at different compaction densities for an area ratio of 3.51% | 91 |
| Figure 5-5 Axial pull-out resistance versus displacement of CD at different area ratio in unsaturated and unsaturated condition..... | 92 |
| Figure 5-6 Axial pull-out resistance tested for dry and unsaturated conditions at 80% and 90% Mod AASHTO compaction density | 93 |
| Figure 5-7 Effect of aging on axial pull-out capacity of CD compacted at 90% Mod ASSHTO | 94 |
| Figure 5-8 Comparison between the effect of compaction density and area on axial pull-out capacity of crusher dust (CD) | 95 |
| Figure 5-9 Drive-in force versus penetration of MS at unsaturated conditions | 96 |
| Figure 5-10 Axial pull-out resistance versus displacement at unsaturated and saturated conditions of MS..... | 97 |
| Figure 5-11 Drive-in force versus penetration of PS tested at 3.51% area ratio at 85% Mod AASHTO | 98 |
| Figure 5-12 Axial pull-out resistance versus displacement of PS..... | 99 |
| Figure 5-13 Driven in force versus displacement of research materials at 85% Mod AASHTO MDD | 100 |
| Figure 5-14 Axial pull-out resistance versus displacement of research materials compacted at 85% Mod AASHTO MDD | 101 |
| Figure 5-15 Oblique pull-out resistance versus displacement of CD at different compaction densities..... | 104 |
| Figure 5-16 Oblique pull-out force versus displacement of CD at different area ratios in unsaturated and unsaturated conditions..... | 105 |
| Figure 5-17 Oblique pull-out force versus displacement of MS at unsaturated and saturated conditions..... | 106 |
| Figure 5-18 Axial pull-out force versus displacement of PS at unsaturated and saturated conditions..... | 107 |
| Figure 5-19 Oblique pull-out force versus displacement of research materials compacted at 85% Mod AASHTO MDD | 108 |

LIST OF SYMBOLS AND ABBREVIATIONS

SYMBOLS

| | |
|----------------|-------------------------------------|
| μ | Coefficient of friction |
| c | Cohesion |
| σ | Stress |
| σ_n | Normal stress |
| σ_{vo} | Vertical effective stress |
| ϕ | Angle of internal friction |
| Ψ | Dilation Angle |
| τ | Shear stress |
| $^{\circ}$ | Degree |
| % | Percentage |
| ϕ_f | Angle of final internal friction |
| ϕ_{crit} | Angle of critique internal friction |
| e_{max} | maximum area ratio |
| e_{min} | Minimum area ratio |
| δ | Interface friction angle |
| d_{50} | Average particle size |
| Δr | Dilation |
| $\Delta\sigma$ | Change in radial stress |
| α | Coefficient of saturation |
| u_w | Water stress |

ABBREVIATIONS

| | |
|--------|--|
| AASHTO | American Association of State Highway and Transportation Officials |
| A_b | Area of base |
| API | American Petroleum Pile |

| | |
|-------|--|
| A_s | Shaft area |
| ASTM | American Society for Testing and Materials |
| CD | Crusher dust |
| CPT | Cone penetration test |
| C_u | Coefficient of uniformity |
| C_z | Coefficient of curvature |
| D | Diameter |
| E | Compaction energy |
| GM | Grading Modulus |
| GW | Gigawatts |
| ICP | imperial College Pile |
| kN | kiloNewtown |
| kPa | kilopascal |
| KWh | kiloWatts hour |
| LL | Liquid Limit |
| MDD | Maximum dry density |
| Mm | millimetre |
| Mod | Modified |
| MS | Malmesbury sand |
| MW | Megawatts |
| N | Normal stress |
| N' | average standard penetration test value |
| OMC | Optimum moisture content |
| PI | Plastic Index |
| PL | Plastic Limit |
| PV | Photovoltaic |
| Q_b | Ultimate base capacity |

Q_s Shaft capacity

SAPEM South African Pavement Engineering Manual

SPT Standard penetration test

TMH Technical Methods for Highways

UWA University of Western Australia

CHAPTER 1 INTRODUCTION

1.1 BACKGROUND OF THE RESEARCH

There is increasing use of renewable energy and the construction of solar Photo Voltaic (PV) farms continues to expand at a rapid rate, with growth in the global capacity averaging almost 55% annually over the past five years. It is reported that one-third of new renewable power capacity installed in 2013 came via solar power (REN21 2014).

Raymond (2010) reported that the combined capacity of solar PV installations around the world was as much as 23 Gigawatts (GW) at the end of 2009, and predicted 186 GW by the end of 2015. Figure 1-1 below shows the manner in which annual global solar PV power output has increased quite rapidly in the past three years in South Africa from around 50 Megawatts (MW) in 2012 to 900 Megawatts cumulative capacity in 2014.

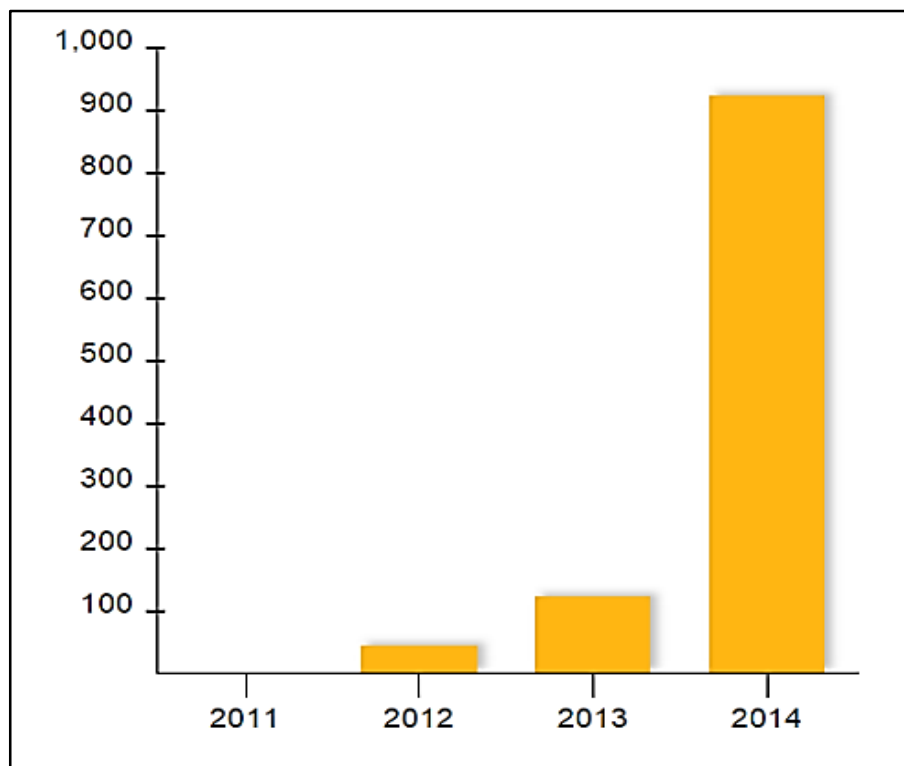


Figure 1-1 South Africa Photovoltaics growth in Megawatts (Wikipedia 2015)

Large scale solar PV farms (>1MW) are gaining market in South Africa and all over the world. One of the factors influencing their growth is the amount of sunshine received annually all over South Africa. The Department of Energy of South Africa (2014) and Mulaudzi *et al.* (2012) have reported that most areas in South Africa average more than 2500 hours of sunshine per year. South Africa is therefore one of the leading countries in the world in terms of best solar resources with an average daily solar radiation that varies between 4.5 and 6.5 KWh/m².

As in the rest of the world, there is a rapid growth in the number of solar power plants. Many of these are located in the more arid areas of the country where the thickness of soil cover to rock or to a pedogenic horizon (typically calcrete) is limited (Day 2014b). Various foundation types are used to support the mounting structures for the solar panels such as driven posts (mini-piles), concrete piers, screw piles, ballasted concrete, etc. Figure 1-2 shows a typical solar panel driven posts in semi-arid area.



Figure 1-2 Typical support structure including posts for a PV panel array (Day 2014b)

Driven posts are installed in various ways. Posts may simply be driven into the ground to the required depth. However, where hard material (typically rock or calcrete) is encountered, one of the methods used is to drill a hole slightly larger than the post using rotary-percussion drilling methods, compact good quality fill material into the hole and then drive the post into the fill. Little research has been conducted on the factors that affect the load bearing capacity of posts installed using this method.

On a recently completed solar project in the Northern Cape, a significant percentage of the posts installed in this manner settled and required remediation. Despite this inability to provide adequate resistance to vertical compressive loading due to dead loads (self weight), the posts appeared to provide adequate resistance to much higher upward-inclined loading due to wind (Day 2014b).

The present research focuses on the factors that affect the capacity of the driven posts installed into pre-drilled holes as described above. It investigates factors that influence the pull-out capacity of the post, some of which include: backfill type, backfill compaction density, compaction moisture content, displacement ratio, effect of time, effect of saturation of the backfill after installation and the direction of loading.

Dilation of material plays an important role in the ability of driven posts to resist the uplift and settlement of the driven posts. The internal angle of friction and shaft capacity are functions of dilation and depend both on the type of soil, relative density and the moisture content. Material type, size distribution and surface roughness are also factors influencing the tension and compression shaft capacity of driven post (Yu & Yang 2012). Therefore, material types, relative density, and moisture content (dry and saturated), as well as the area ratio (section area of post divided by section area of hole) are all factors that affect the pull-out resistance of the posts.

1.2 PROBLEM STATEMENT

This research examines factors affecting load carrying capacity of a solar panel support post, driven into a predrilled hole, which has been backfilled with granular soil. Shear deformation of the fill during loading causes dilation of the fill. This increases the normal effective stress on the soil-pile interface, thereby adding to the load carrying capacity of the post. However, the concern is that if the installation of the posts is not correctly carried out, these posts could be pulled out. If one post in a series pulls, the uplift (wind) forces on the surrounding posts are increased creating the possibility of a chain reaction. If a post settles, the alignment of the panels is affected and the possibility of one panel shading another arises at the ends of each section.

Several empirical studies have been conducted on the effects driven piles of deep foundations in sand, specifically on the dilation and normal stress behaviour generated during the loading. However, dilation does not only occurs around in deep foundation piles, but also around mini piles such as the solar panel posts. This dilation and normal stress govern the shaft capacity of a pile. As such, change in shaft pull-out capacity was investigated by varying factors affecting it such as backfill material, compaction effort and water content and area ratio.

1.3 RESEARCH OBJECTIVES

The main objective of this research was to determine the sensitivity of pull-out resistance, which is mainly governed by the normal stress (σ_n) and friction angle of backfill, to variations in the backfill type, the post section, compaction effort and compaction moisture content. The effect of saturation of the fill after post installation was also investigated.

The specific objectives of in this research were to investigate the effect on pile capacity of:

- Varying the type of the backfill on the axial load capacity (push in and pull-out) of the post
- Varying the displacement ratio (cross-sectional area of the post divided by the cross-sectional area of hole) on the axial load capacity of the post
- Varying the degree of compaction and the moisture content of the backfill on the axial capacity
- Inclination of pull-out load
- Saturation of the backfill prior to loading
- Aging of the fill.

1.4 SCOPE AND LIMITATION

The research was limited on the driven post in predrilled hole that are backfilled with granular soils. Oblique and vertical pull-out tests as well as compressive load tests were conducted in order to analyse the resistance of the post when material type, moisture content, density, and post section have been varied. Static load was used for both push-in and pull-out testing. The tests were conducted on a half-scale model of the post and post hole. These tests simulate the condition of a post hole drilled into rock from the ground surface.

1.5 LAYOUT OF THIS DISSERTATION

Chapter 1: Introduction

This chapter briefly discusses the background of the research project, and then states the problem that has led to the research investigation. Moreover, research objectives are highlighted as well as the scope and limitation of the study.

Chapter 2: Literature review on previous research

The first part focuses on the literature relating to support structures for solar panels. A review of previous studies was done on the types of solar panel foundations, their advantages, and disadvantages. Attention was given to collection of information on the driven post, as well as the procedures and equipment used for the driven post installation.

The second part discusses the shaft capacity of driven piles generally in granular (non-cohesive) materials. Factors affecting the shaft capacity are highlighted.

Chapter 3: Methodology and Experimental design

This chapter begins by explaining the type of materials used in the research, and the standards and procedures followed during the testing of these materials. Thereafter there is an analysis of designing and building of the apparatus used for axial and oblique pull-out tests as well as the test procedures followed.

Chapter 4: Laboratory test results and discussions

Results of classification and shear tests are presented. The effects of compaction effort, material types, and water content on both the angle of friction and dilation are interpreted.

Chapter 5: Axial and oblique pull-out test results and discussions

This section is divided in two parts. The first part is the results and discussion of the axial pull-out tests. Discussion of the effects of compaction effort, displacement ratio as well as water on both push-in and pull-out resistance are discussed.

The second part comprises the interpretation of the oblique pull-out results. Effects of compaction effort, displacement ratio, and water on oblique pull-out are analysed. Moreover, lateral loads effect on pull-out resistance is also interpreted.

Chapter 7: Conclusion and recommendation

This chapter draws general conclusions of the findings presented in the results chapter, provides guidelines for installation of driven posts, and provides recommendations for further study.

CHAPTER 2 LITERATURE STUDY ON SUPPORT STRUCTURES FOR SOLAR PANEL

2.1 INTRODUCTION

Figure 2-1 shows an aerial view of a typical PV solar panel power plant. A 100MW plant may require as many as 50000 individual supports, each carrying loads of around 10kN-12kN. Many of these “solar farms” are often located in semi-arid areas. The sites are frequently underlain by shallow rock or hardpan calcrete.



Figure 2-1 Aerial picture of solar panels driven posts (De-Aar Solar Power 2014)

Solar PV panels have been promoted as a prime source of renewable energy, converting solar energy into electricity. Advanced studies and research have been conducted on the solar module and several different supports structures and founding methods have been used (Maffei *et al.* 2013; Oldcastle Precast Inc. 2009; Sakr Undated). These foundation supports depend on many factors such as topography, scale of the project, environmental factors like wind speed, soil saturation, soil contamination, depth of bedrock, aridity and whether the panels are installed on the roof or not.

Due to the above mentioned factors screw piles, helical piles, precast or cast-in-situ concrete ballast footings, concrete piers and driven piles have been developed for the foundation to suit the ground conditions and minimise the time and cost of construction.

Despite the many solar panel support methods, there are no clear design guidelines for solar panel supports. Installation procedures are normally the proprietary knowledge of the designer or the construction company. Each designer or company may follow its own guidelines.

Brief descriptions of the most common methods are firstly presented in this chapter with emphasis on the driven pile (post) installation and functionality. Secondly, a review of physical and mechanical properties of granular (non-cohesive soil) is carrying out. Finally, evaluation of different shaft capacity methods of pile is discussed as well as the axial and oblique capacities of the pile.

2.2 DIFFERENT METHODS OF SOLAR PANELS SUPPORTS

Different founding methods are used for solar PV panel arrays. Figure 2-2 shows different categories of roof-mounted and ground-mounted systems. The ground-mounted category is the focus of this present research. In the ground-mounted category, two types are used namely pile supported (which includes driven piles and helical piles) and ballasted (which includes precast ballast footings or cast in place ballast). A description of each follows.

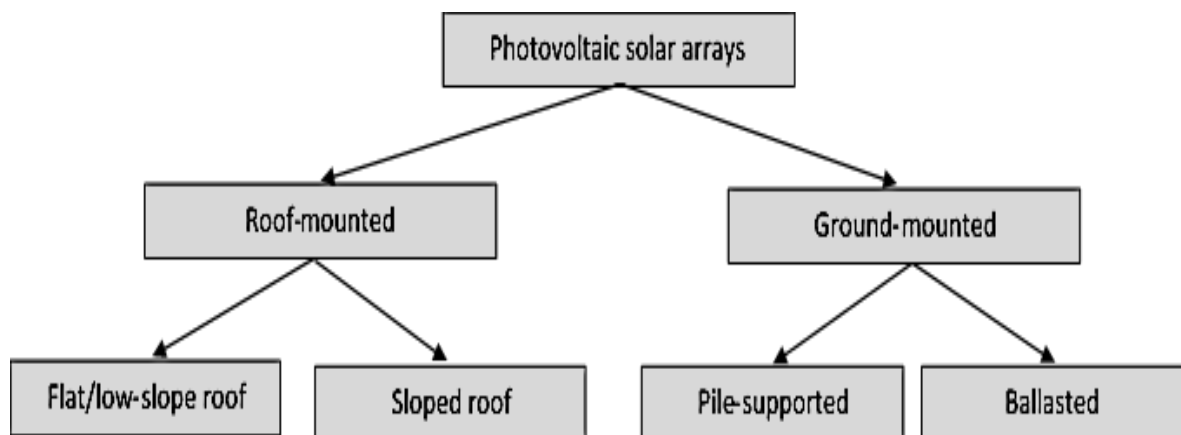


Figure 2-2 Types of photovoltaics arrays and panels supports system modified from (Maffei *et al.* 2013)

2.2.1 PRECAST BALLAST FOOTING

Ballast footing is a heavy concrete element used as foundation to support solar PV panels and to resist uplift forces. This footing can be precast or cast in place concrete (Maffei *et al.* 2013). The precast ballast is preferred to cast in place due to its rapidity in installation. Its installation proceeds faster without issues such as curing time, pouring (Oldcastle Precast Inc. 2009). Figure 2-3 shows a precast ballast footing installed on surface.

Precast ballast footings can be installed, whether on the surface or buried depending on the condition of the ground. The installation ground can be contaminated landfill or bedrock. Precast ballast may be used on a contaminated soils of landfills where driven piles or helical cannot be installed as they will penetrate the contaminated ground. Typically, about a metre thick layer of capping soil is present on landfills before reaching the contaminated soil.

It is for this reason that driven piles and helical piles are excluded, as they cannot efficiently provide support in landfills and may be subject to deterioration in contaminated soil. It is in those situations where precast concrete ballast footings are more advantageous than the rest where penetration is required. In addition, the leading advantage of precast ballast footing, specifically on contaminated and landfill are the needlessness of soil penetration and minimal site excavation (Oldcastle Precast Inc. 2009).

Furthermore, Oldcastle Precast Inc. (2009) stated that precast ballast footings are also gaining popularity in the bedrock where installation of precast ballast foundation does not require any excavation. However, in arid north-western parts of South Africa, predrilled driven posts is a popular method of support even where rock is present due to the speed of installation (Day 2014b).



Figure 2-3 Ballast footing solar panel support

2.2.2 HELICAL PILE

Helical piles are a driven piles with helical bearing plate welded to the steel shaft. Figure 2-4 shows a typical helical solar pile. They are used for their cost effectiveness and their installations are very quick compared to ballast footing. However, they can only be installed on sites where there is sufficient depth of soil cover above the rockhead. In colder climates, helical piles are preferred due to their higher uplift resistance and shorter height length compared to driven piles. However, more torque is required for installation in compact sand (Sakr undated).

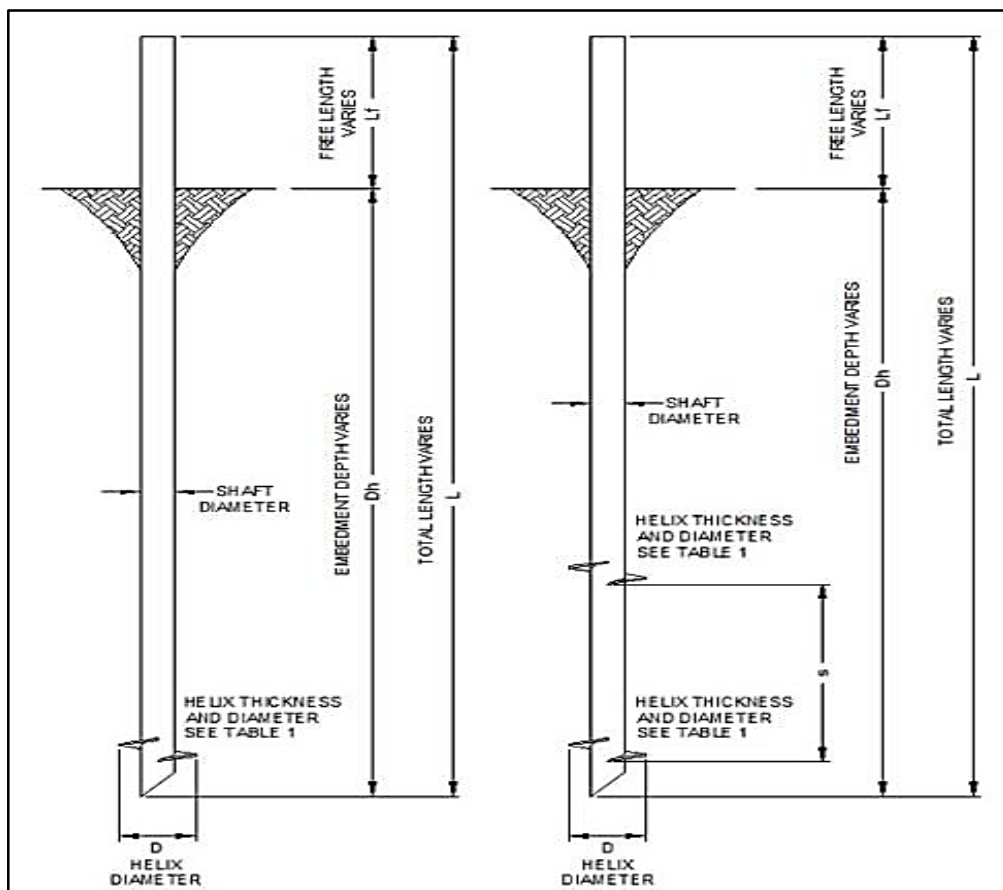


Figure 2-4 Helical pile configuration (Sakr Undated)

2.2.3 DRIVEN PILE

Driven pile or post is a pile driven into soil to offer support or resist forces. It has a function of transmit loads from the structure supporting the PV panels to the underlying soil or rock. This loads are transmitted by means of friction between pile and soil surrounding the post, and by point bearing (Kansas Department of Transportation Undated).

Driven solar panel piles (posts) have many ways of being installed depending on the ground conditions. One method is to drive a post into soil up to a specified depth. The other way of installing the posts is to drill a hole, fill it with compacted material, and then drive the post about 1m-1.5m into the fill (Day 2014b). When the post is loaded in tension or compression, dilation of fill “locks” the post into the hole. The advantage of driven posts is the speed of installation as mentioned before and the ability to follow the topography as it is shown in Figure 2-5.



Figure 2-5 Solar panels embracing the topography

2.3 EQUIPMENT AND PROCEDURE INSTALLATION OF DRIVEN POST

Driven piles are installed using different types of equipment for driving the piles into the ground such as hydraulic jack, percussion hydraulic hammer, driving cylindrical hammer (Prakash 1990; Tomlinson 1994). The key components of driven pile installation equipment are the pile itself, the hammer, and the leader. The leader helps to position the pile at a vertical direction and be aligned axially with the hammer (Figure 2-6). The same mechanism used in heavy piling installation is also applied in solar panel driven pile (mini pile) installation. Schletter (2010) uses GAYK™ Hydraulic rig as shown in Figure 2-6, which has two functions. These functions are to drill a hole and to drive the post using a down-the-hole hammer drilling unit and top-drive hydraulic hammer unit respectively. This allows a quick drilling and installation. The post can be rammed up to 3 - 6 meters (Schletter 2010).

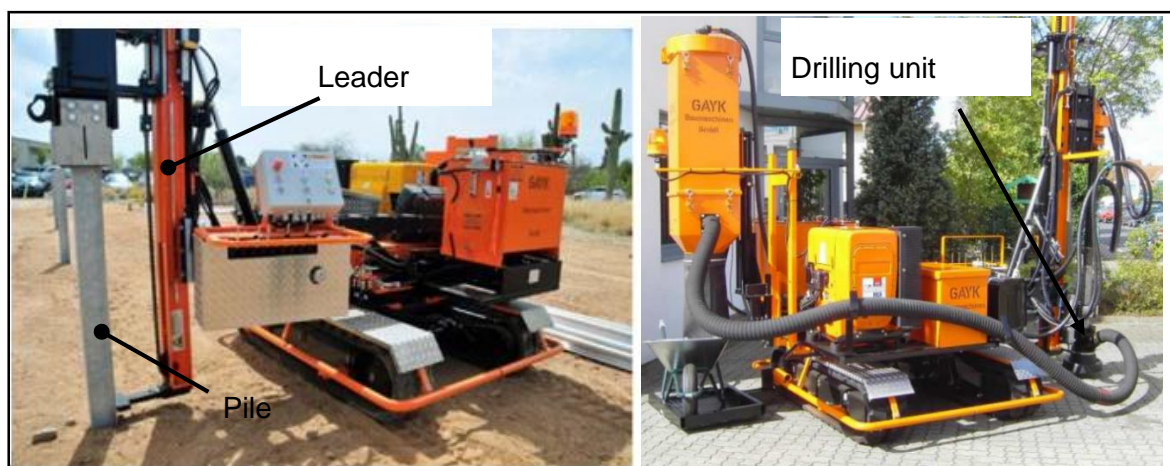


Figure 2-6 GAYK™ Hydraulic ram used in solar panel post installation (Schletter 2010)

2.4 MECHANICAL AND PHYSICAL PROPERTIES AFFECTING THE STRENGTH OF BACKFILL MATERIALS

2.4.1 INTRODUCTION

The ability of driven posts to resist settlement and provide pull-out resistance depends on various factors including the type of backfill material and compaction degree of backfill. This section discusses the most important physical and mechanical properties of the backfill. These properties are particle size distribution, particle shape, degree of compaction, moisture content, and the influence of dilation on the strength of the material.

2.4.2 MATERIAL TYPE AND GRADATION

Particle size distribution of the material plays a significant role in compaction of the backfill. This particle size distribution is determined by sieve analysis; creating distribution curve of cumulative mass passing a sieve. The percentages of particles passing sieves in ordinates and the logarithm of the particles size in abscissa represent the particle distribution. Figure 2-7 illustrates different types of grading of materials. Well graded material has a good representation of particle size over a wide range in other words; each particle size lacks excess in terms of representation. Additionally, it does not have any gaps in particle size distribution. The curve thus is smooth (curve A). However, poor graded material can have a wide range of particle but with gap of particle size (curve C) or have a narrow range of particle size also called uniform material (curve B). Poorly graded material has a steep distribution curve (Craig 2004; Holtz & Kovacs 1981; Terzaghi *et al.* 1996).

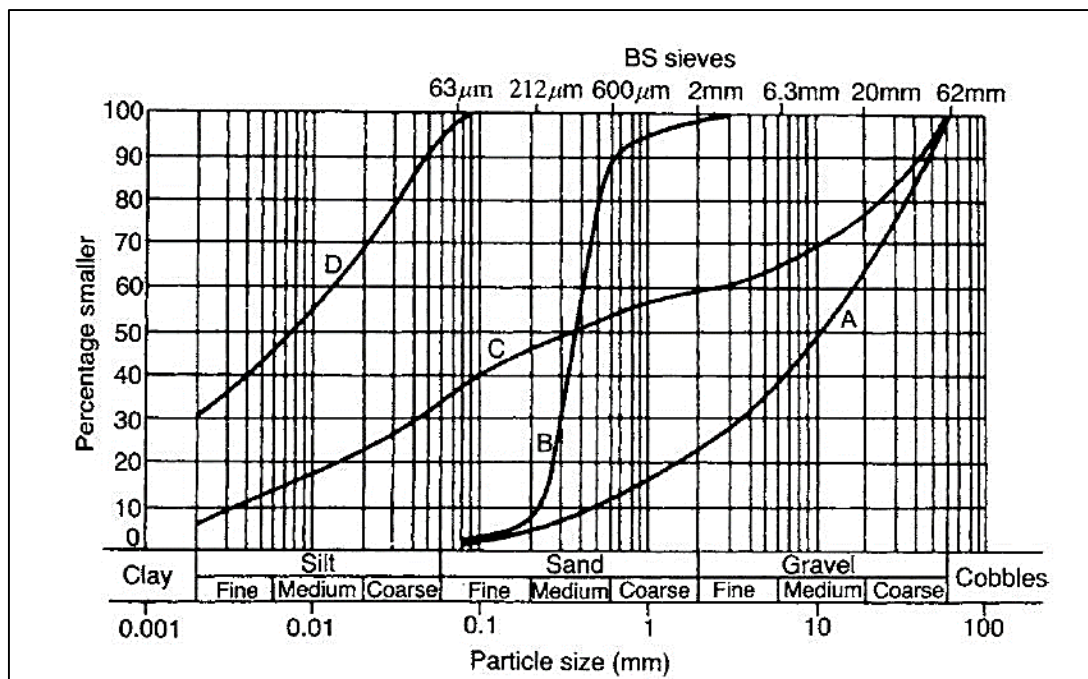


Figure 2-7 Particle distribution curve (Craig 2004)

A grading parameter known as the coefficient of uniformity (C_u) is used to determine whether the material is well graded or not (Smith & Smith 1998). Coefficient of uniformity

and coefficient of curvature (C_z) describe the general shape and slope of distribution curve. C_z for well graded materials is between 1 and 3 (Craig 2004). An equation of each follows.

$$C_u = \frac{D_{60}}{D_{10}} \quad \text{Equation 2-1}$$

$$C_z = \frac{D_{30}^2}{D_{60} \times D_{10}} \quad \text{Equation 2-2}$$

Where D_{60} is a particle diameter at 60% passing, D_{10} the effective size diameter in particle distribution corresponding to 10% passing and D_{30} particle diameter corresponding to 30% passing. D_{10} can be used as an indication of the hydraulic conductivity and drainage through soil. However, Nowak & Gilbert (2015) postulate that the coefficient of uniformity does not identify the gap in a particle distribution. This has a significant effect on the performance of the fill. Consequently, a visual description of the particle distribution curve will be as important as the coefficient of uniformity.

Alternative to coefficient of curvature, the Grading Modulus (GM) is often used to assess the grading of fill materials in South Africa. This following Equation 2-3 measures the GM of the material.

$$GM = \frac{P_{2.00\text{mm}} + P_{0.425\text{mm}} + P_{0.075\text{mm}}}{100} \quad \text{Equation 2-3}$$

Where, P is the cumulative percentage retaining on indicated size.

A material with $GM > 2$ indicates a coarse and good quality material for road construction, whereas $GM < 2$ shows that the material has finer grained of poor quality road construction (SAPEM 2014).

The particle size distribution (well graded, uniform, and poorly graded) contributes significantly to the compaction in terms of maximum dry density and optimum moisture content. A well graded material provides a high maximum dry density at a lower optimum moisture content, however fine uniform material gives lower maximum dry density and higher optimum water content (see Figure 2-8). A high dry density is generally indicative of a good quality backfill material with higher strength.

The reason why the well graded material to have higher maximum dry density (MDD) than poor and uniform materials is that it contains less fine particles than poorly and uniform graded. Moreover, materials with larger particles have higher maximum dry density than materials with smaller particles (Germaine & Germaine 2009).

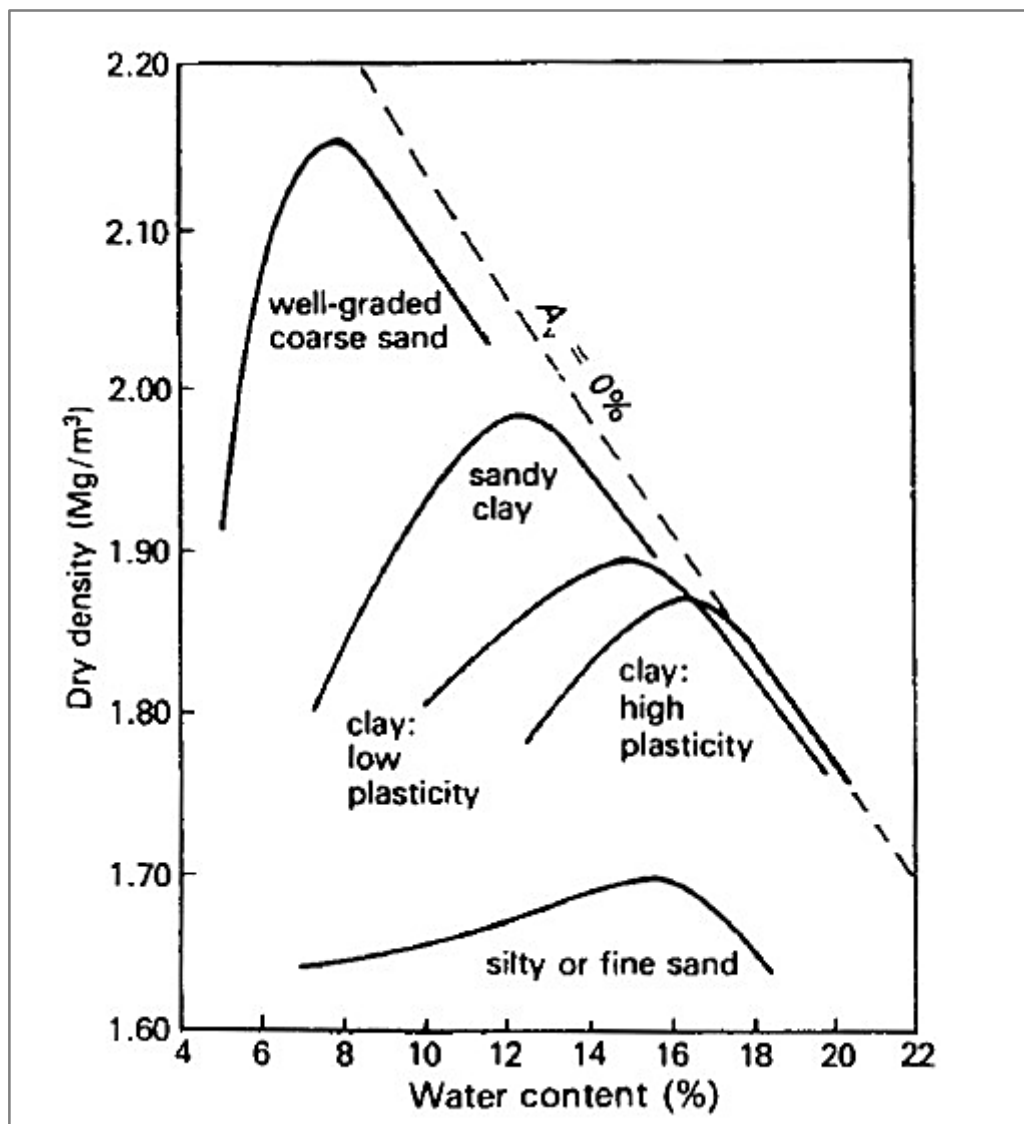


Figure 2-8 Effect of particle distribution on compaction (Whitlow 1995)

2.4.3 PARTICLE SHAPE AND SURFACE TEXTURE

Although, less emphasis is placed on particle shape, Das & Sobhan (2013) assert that particle shape is equally important as the particle size distribution on physical properties of the soil. They identify three major categories depend on the particle size (from boulders to silt size particles). These categories are bulky, flaky and needle particles. The bulky particles (see Figure 2-9) are described in terms of angular, subangular, subrounded and rounded formed by means of mechanical weathering of rock or mineral. Texture of the surface particles is described in term of rough, smooth and polish (Burland 2012).

High angularity of particles results in better interlocking during the densification process. The angularity of the particle increases the strength of materials and the roughness increases the shear resistance of materials. In order for the shear to occur, there has to be an increase in volume or breakage of the interlocking particles. Additionally, higher compaction effort is required for angular and rough particles than for rounded and smooth

because of the resistance generated to compaction. For the same relative compaction, the angular materials produce higher strength than rounded materials. Particles interlock at the point of interparticle contact is higher for rough surface texture than for the smooth one. Particle shape controls primary the dilatancy and the particle texture controls the shear strength (Semmelink, C. J. and Visser 1994).

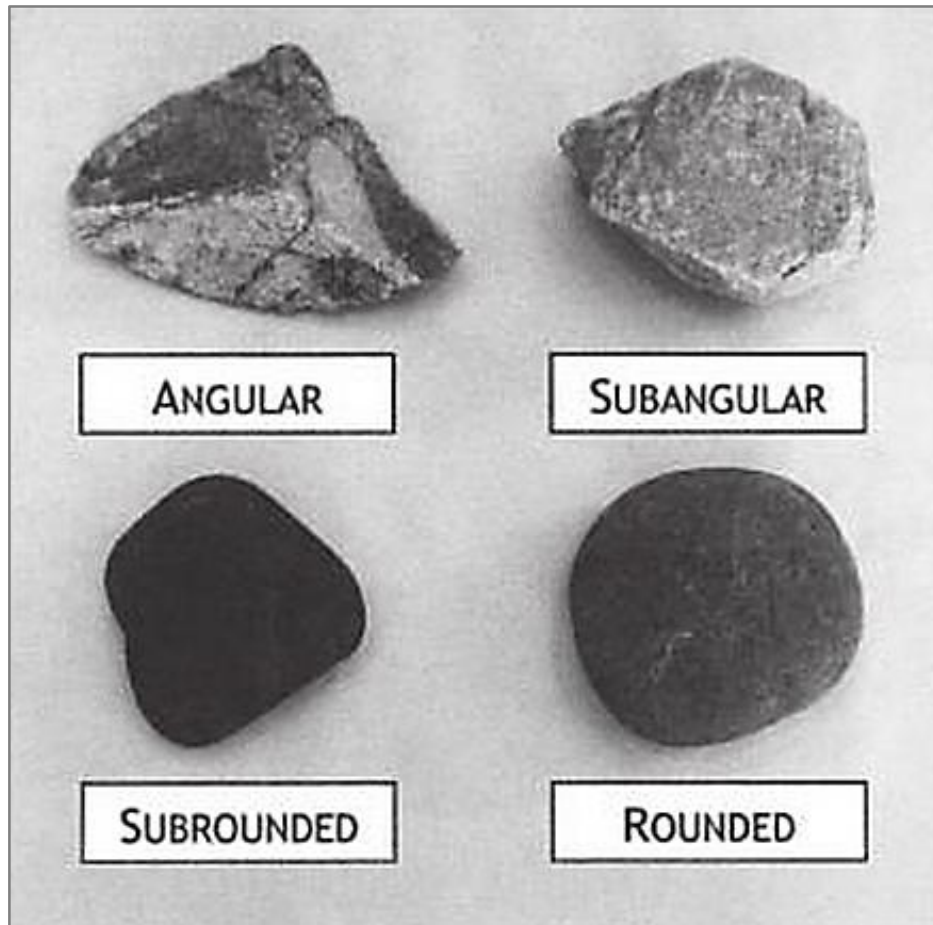


Figure 2-9 Particle shape (Das & Sobhan 2013)

Cho *et al.* (2006) studied the particle shape effects on packing, density and strength using sphericity and roundness as scales. They described sphericity as “the diameter of the largest inscribed sphere relative to the diameter of the smallest circumscribed sphere” and roundness as “the average radius of curvature of surface features relative to the radius of the maximum sphere that can be in the particle” (Figure 2-6). They found that a decrease in sphericity and roundness increased the maximum void ratio (e_{\max}) and minimum void ratio (e_{\min}). Thus the void ratio (i_e) interval increases. Additionally, an increase in the constant volume critical state friction angle was observed when the roundness decreases. In other words, angular materials give high strength performance.

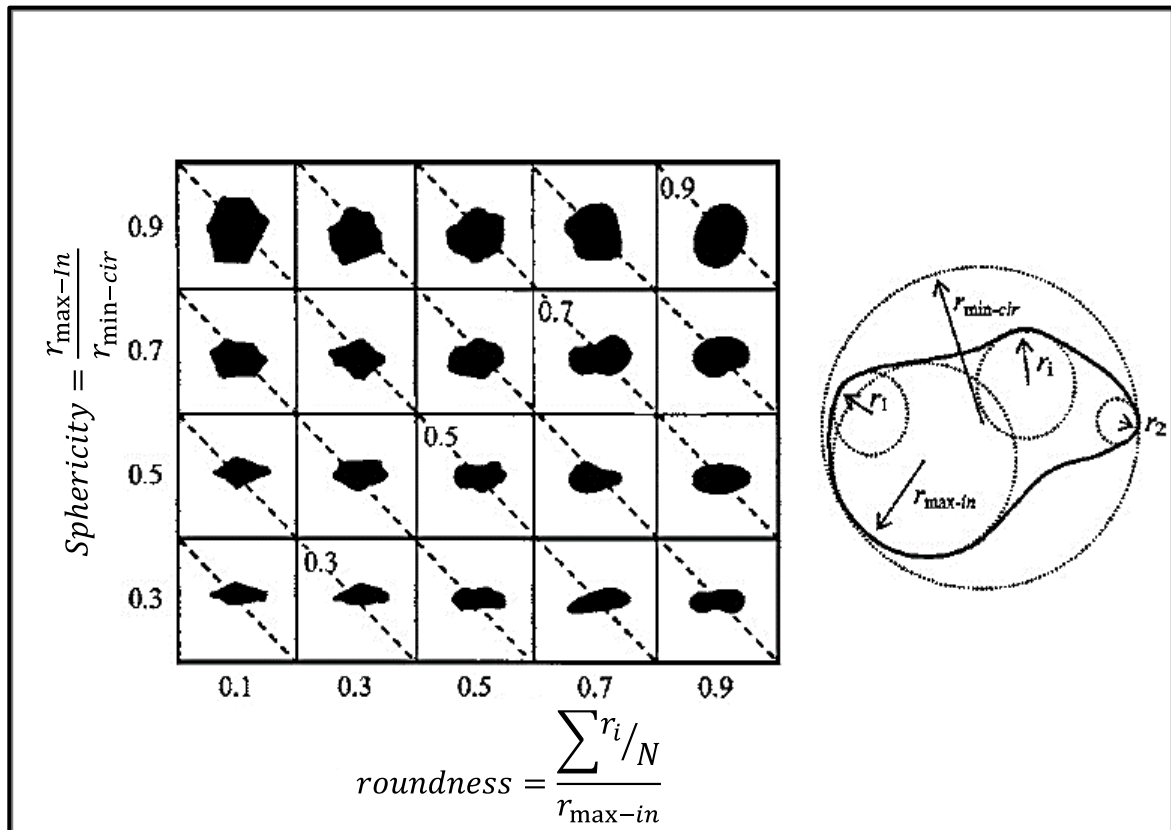


Figure 2-10 Sphericity and roundness model determination (Cho *et al.* 2006)

Particle shape is often overlooked in determining soil parameters. More attention is placed on the particle size distribution in the classification system. Particle shape should be recommended as part of the material classification because it affects not only the compaction but also the shear strength and dilatancy of the sand and gravel materials.

2.4.4 MOISTURE CONTENT AND COMPACTION EFFORT

Compaction effort profoundly influences the Maximum Dry Density (MDD) and the Optimum Moisture Content (OMC). With the increment of compaction effort, the MDD increases and the OMC decreases. Figure 2-11 illustrates the effect of compaction effort on maximum dry density and optimum moisture content.

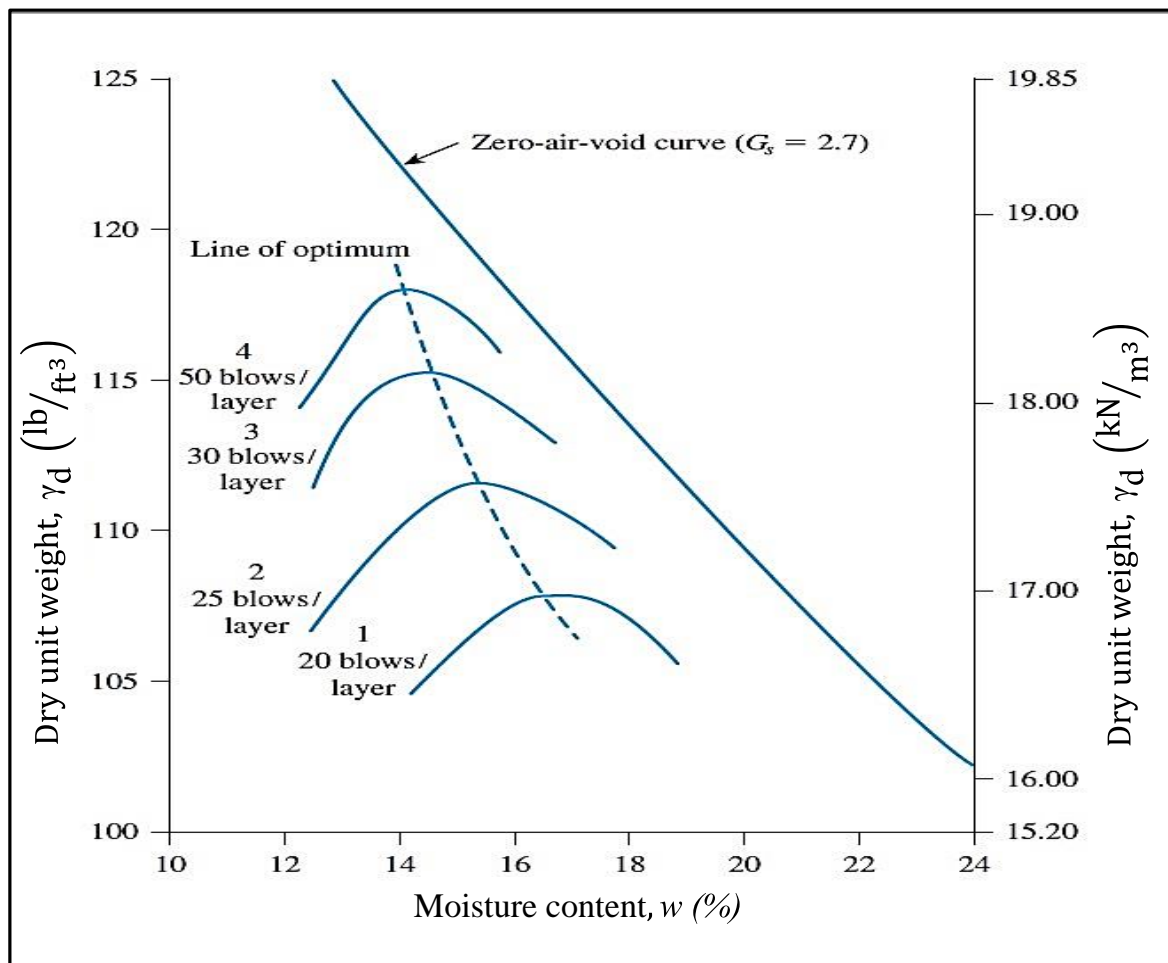


Figure 2-11 Effect of compaction effort (Das 2009)

Different test methods of compaction are used in backfill materials. These methods are standard Proctor, Modified Proctor, vibrator hammer, and other standards developed by countries depending on their type of soil and the availability of compaction plant. Usually, standard Proctor is for fine materials, modified Proctor for coarse materials and vibrator hammer is preferred in road building materials due to its compaction quality for well graded materials. Standard Proctor and modified Proctor use a rammer of 2.5kg and 4.5kg respectively. For instance, in Spain, a modified Proctor rammer compaction (4.5 kg) is preferred due to the arid climate of the country (Nowak & Gilbert 2015).

Moreover, the compaction methods are characterised by number of layers, height drop of the hammer, weight of hammer, number of blows per layer and the size of mould. These variables vary depend on the test methods. The purpose of these variables is to achieve the Maximum Dry Density (MDD) and Optimum Moisture Content (OMC) of a specified material. These MDD and OMC will help to know the energy required to attain a specified degree of compaction. Table 2-1 shows details of standard Proctor and Modified methods and their specifications.

Das & Sobhan (2013) give the compaction energy per unit volume E in Equation 2-4. In addition, details of values of each variables of Equation 2-4 are described in Table 2-1 for both standard proctor and modified methods.

$$E = \frac{\left(\text{Number of blows per layer} \right) \times \left(\text{Number of layers} \right) \times \left(\text{Weight of hammer} \right) \times \left(\text{Height of drop of hammer} \right)}{\text{Volume of mold}} \quad \text{Equation 2-4}$$

Table 2-1 Summary of standard and modified Proctor compaction test specification ASTM 1557 D-698 and D-1557 and TMH1(Mod AASHTO) modified from (Das & Sivakugan 2014)

| | Description | Method A | Method B | Method C | TMH1 |
|-----------------------------|-----------------------|---|---|--|---|
| Physical data for the tests | Material | Passing No. 4 Sieve | Passing $\frac{3}{8}$ in.(9.5 mm) sieve | Passing $\frac{3}{4}$ in.(19.1 mm) sieve | Passing $\frac{3}{4}$ in.(19 mm) sieve |
| Use | use | Used if 20% or less by weight of material is retained on No. 4 (4.75 mm) sieve. | Used if more than 20 % by weight of Material is retained on No. 4 (4.75 mm) sieve and 20 % or less by weight of material is retained on $\frac{3}{8}$ in.(9.5 mm) | used if more than 20% by weight of material is retained on $\frac{3}{8}$ in.(9.5 mm) sieve and less than 30% by weight of material is retained on $\frac{3}{4}$ in.(19.1 mm) sieve | Material passing 19mm sieve. The aggregate retaining through a 19 mm is crushed lightly by means of steel tamper (or laboratory crusher) to pass 19.0 mm and adding to the portion passing the sieve. |
| Mould | Mould volume | $\frac{1}{30}$ ft ³ (0.000094 m ³) | $\frac{1}{30}$ ft ³ (0.000094 m ³) | $\frac{1}{30}$ ft ³ (0.000094 m ³) | 0.002780 m ³ |
| | Mould diameter | 4 in. (101.6 mm) | 4 in. (101.6 mm) | 4 in. (101.6 mm) | 152.4 mm |
| | Mould height | 4.584 in.(116.4 mm) | 4.584 in.(116.4 mm) | 4.584 in.(116.4 mm) | 152.4 mm |
| Standard | Weight of hammer | 5.5 lb (2.5 kg mass) | 5.5 lb (2.5 kg mass) | 5.5 lb (2.5 kg mass) | |
| | Height of drop | 12 in. (304.8 mm) | 12 in. (304.8 mm) | 12 in. (304.8 mm) | |
| | Number of soil layers | 3 | 3 | 3 | |
| | Number of blows/layer | 25 | 25 | 56 | |
| Modified | Weight of hammer | 10 lb (4.54 kg mass) | 10 lb (4.54 kg mass) | 10 lb (4.54 kg mass) | 10 lb (4.54 kg mass) |
| | Height of drop | 18 in. (457.2 mm) | 18 in. (457.2 mm) | 18 in. (457.2 mm) | 18 in. (457.2 mm) |
| | Number of soil layers | 5 | 5 | 5 | 5 |
| | Number of blows/layer | 25 | 25 | 56 | 55 |

2.5 COMPARISON OF DIRECT SHEAR BOX AND DRIVEN POST MECHANISM

The direct shear test is credited as the oldest and simplest method to measure the shear strength of soil (Germaine & Germaine 2009; Lambe & Whitman 1969). The test consists of applying a constant normal force on the specimen placed into a box split into two halves. Then shear force is applied by moving the top half box horizontally forcing the specimen to shear.

Driving the post into the soils displaces material thereby increasing the density of the surrounding soil (Rajapakse 2007). Figure 2-12 a) illustrates a simplified behaviour of the surrounding materials when pile driving is in progress. Houlsby (1991) has likened the thin

band of soil next to the pile as a direct shear test turned through an angle of ninety degrees (Figure 2-12). It has been assumed that the mechanism of failure around the pile is similar to that which occurs on a horizontal plane in the direct shear (Houlsby 1991). This thin band zone is where a large amount of shear displacements are localised (Boulon & Foray 1986; Houlsby 1991).

The process of driving a pile into soil generates shaft friction around the pile. The shaft friction induced during the installation or the pull-out is based on the Coulomb failure criteria as illustrated in Equation 2-5. This shaft friction or shear stress (τ) equals to the radial effective stress acting on the pile (σ_n) (or normal stress in the shear box (N/A)) multiplied by the interface friction at failure $\tan \delta$ (Terzaghi *et al.* 1996).

$$\tau = \sigma_n \tan \delta = \frac{N}{A} \tan \delta$$

Equation 2-5

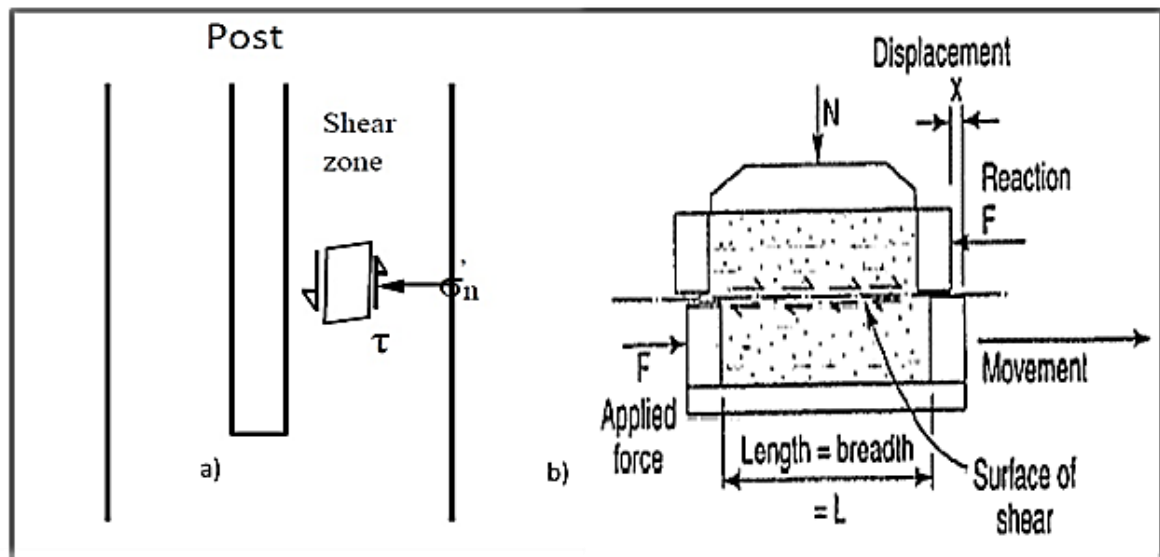


Figure 2-12 Shear zone representation a) in pile and b) in direct shear box

Lehane *et al.* (1993) conducted an investigation on the angle of friction of sand on sand and the interface friction of sand on steel and found that the interface shear results have the same trends in the soil-soil results from the ring shear test at loose and dense conditions. However, the peak values and the constant volume angles of interface friction (δ'_p and δ'_{cv}) were lower and the dilation was constant (Figure 2-13).

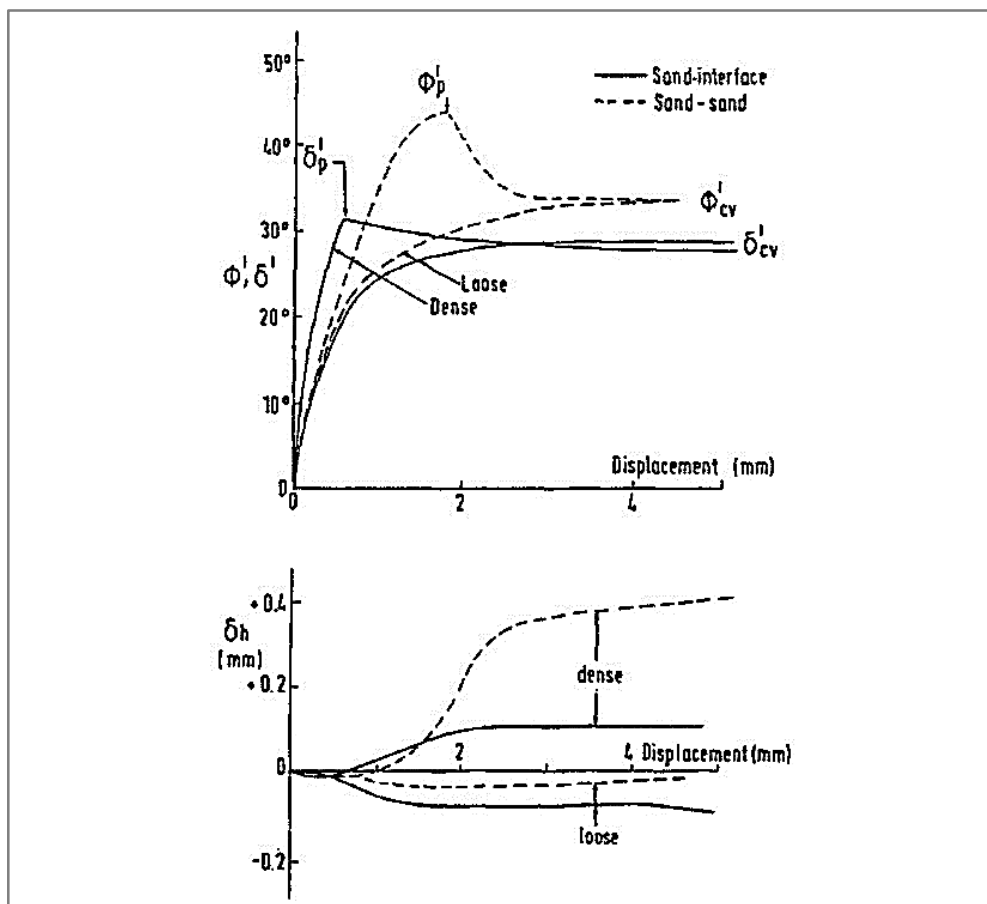


Figure 2-13 Internal friction sand-sand and interface friction steel-sand in shear box (Lehane *et al.* 1993)

2.5.1 EFFECT OF DILATION ON ANGLE OF INTERNAL FRICTION AND SHEAR STRESS

Dilation is the increase of volume of a dense coarse material during the shearing (Craig 2004).

The strength of coarse-grained materials when sheared is not entirely from mineral to mineral friction. Inter-particles friction caused by mineral to mineral contacts are not the only factors affecting the strength but also particles rearrangement, material crushing and dilation contribute to the peak friction angle. Rowe (1962) acknowledged the importance of all these factors, which contribute to the mobilised friction angle during the shearing. Mitchell & Soga (2005) presented in Figure 2-14 an illustration of how the increase of void ratio mobilised the angle of internal friction by taking into account the mentioned factors.

Many authors such as Taylor (1948), Rowe (1962), and Bolton (1986) investigated the relationship of friction angle and dilation and all came up with similar results. Bolton (1986) presented a comprehensive and simple equation based on empirical data. By using 17 types of sand in investigating the strength and dilatancy, he came up with Equation 2-6 where he established a relationship between the angle of friction (ϕ'_{crit}) and angle of dilation (ψ). ϕ'_{crit} describes as friction angle where the granular is at loose condition whereas ψ increases from zero (at loose condition) to a dense condition where the shear stress

reaches its peak value. In other words, the friction angle attains its peak at dense condition where the contribution of the angle of dilation is the highest. The advantage of this relationship is, when any angle of shearing obtained is higher than the friction angle at loose condition, it is definitely due to the geometric expansion (Bolton 1986).

$$\phi' = \phi'_{\text{crit}} + 0.8\psi$$

Equation 2-6

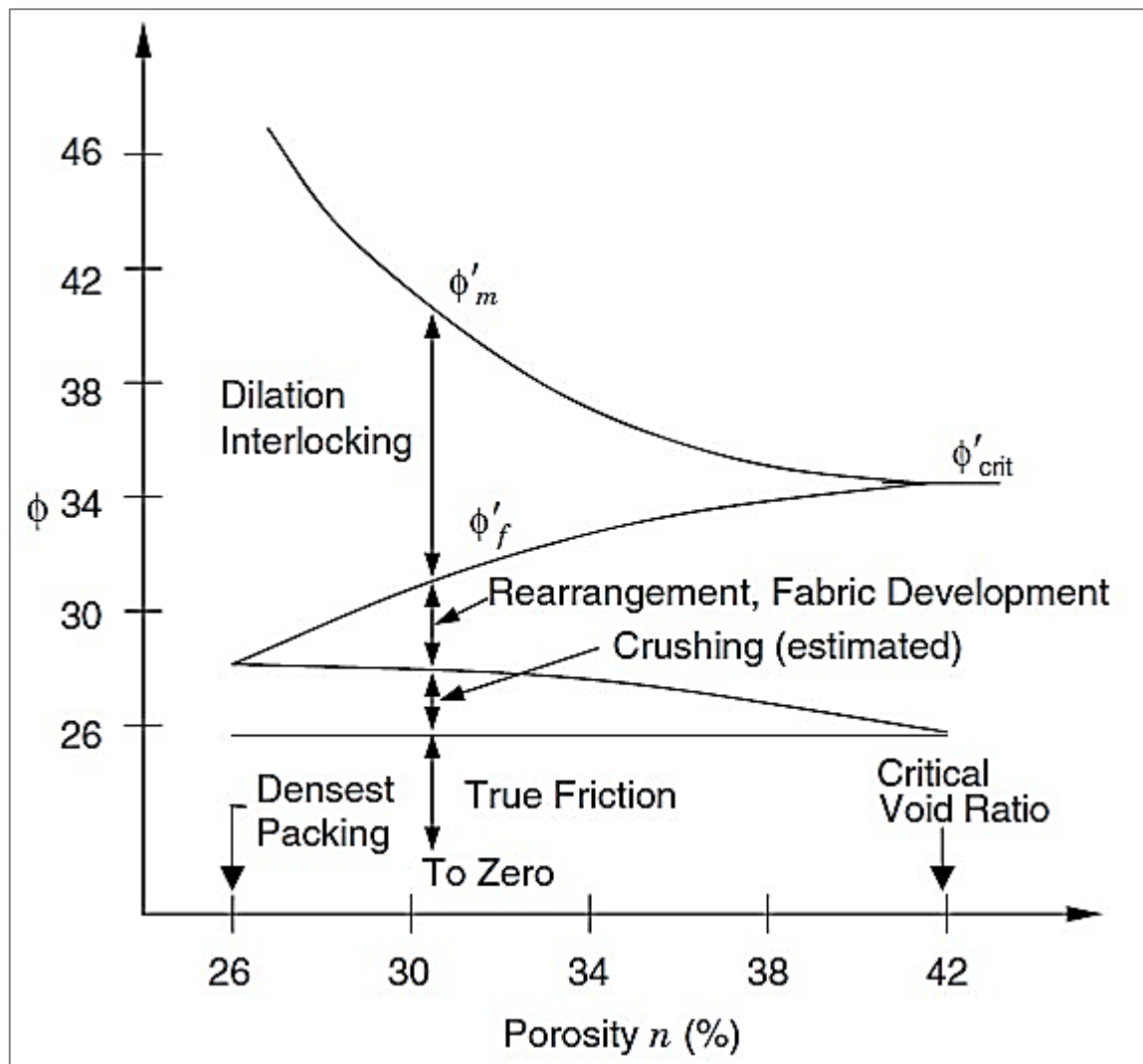


Figure 2-14 Contribution of shear strength of granular soil (Mitchell & Soga 2005)

2.5.2 EFFECT OF SATURATION ON BACKFILL MATERIAL BEHAVIOUR

Particles, air, and water constitute the soil (Figure 2-15). When a soil is unsaturated, the voids contain water and air. However, when soil is saturated, the voids between the particles are full of water alone. Particles of the soil in loose conditions (low dry density) and at low moisture content are bonded whether by lenses water (Figure 2-15) or by bridging colloidal material called clay “bridges” adding strength. In case of lenses water bridging the particles at their contacts, the compression forces generated by lenses water stabilise the grains and increase both the stiffness and the strength of the soil (Burland 2012). The clay “bridges”

also formed at the particle contact add to the strength of the soil at partial saturation and the softening of these clay “bridges” also decreases the strength of soil as it wets up (Schwartz 1985).

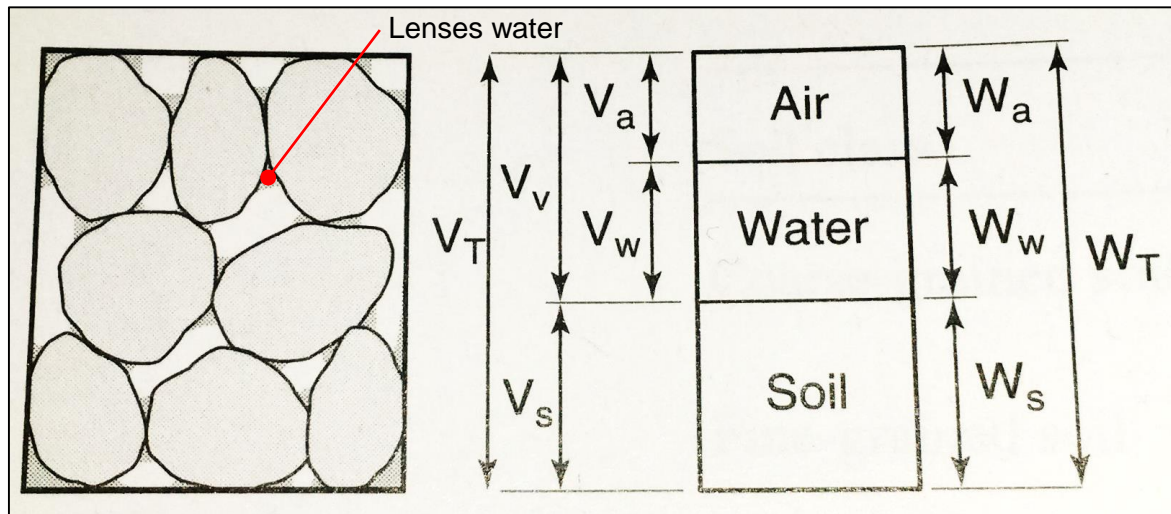


Figure 2-15 Soil presentation

The process of wetting reduces the strength of the loose soil. When soil is moistened, the stabilised force at contact point of particles is removed causing the soil to lose its strength. When this happens to a loose soil, which is under load, reduction of volume occurs. This process of volume reduction is called “collapse of grain structure” and occurs particularly in dry loose sand and also in a backfill material poorly compacted (Burland 2012). Poorly compacted backfill material subjected to water loses its strength and results in volume reduction, which is an unwanted behaviour.

Briaud (2013), in Equation 2-7 gives the effective stress (σ') depending of the total stress σ , α coefficient of saturation ranging between 0 for unsaturated to 1 for saturated soil and u_w water stress.

$$\sigma' = \sigma - \alpha u_w$$

Equation 2-7

It can be observed in Equation 2-7 that as the soil is saturated, the effective stress will be less than the total stress, and when the soil is dry, the negative term will equal to zero, therefore, the effective stress will be equal to the total stress. The product of the coefficient of saturation and water pressure is pore pressure. Figure 2-16 shows how pore water pressure (u) changes with water content. Figure 2-16 a) illustrates an assemblage of particles that is fully saturated, pore water pressure is positive. Then in Figure 2-16 b), water starts reducing due to evaporation or drying, and “surface tension within the curve surface called meniscus” (Burland 2012) forms a compression force P between particles causing sliding resulting in decrease of volume. The assemblage is still fully saturated, but pore pressure is less than the atmospheric. Figure 2-16 c) shows the soils are contained air and water. The lenses generate contact forces P , which are normal to the plane through the particles contact.

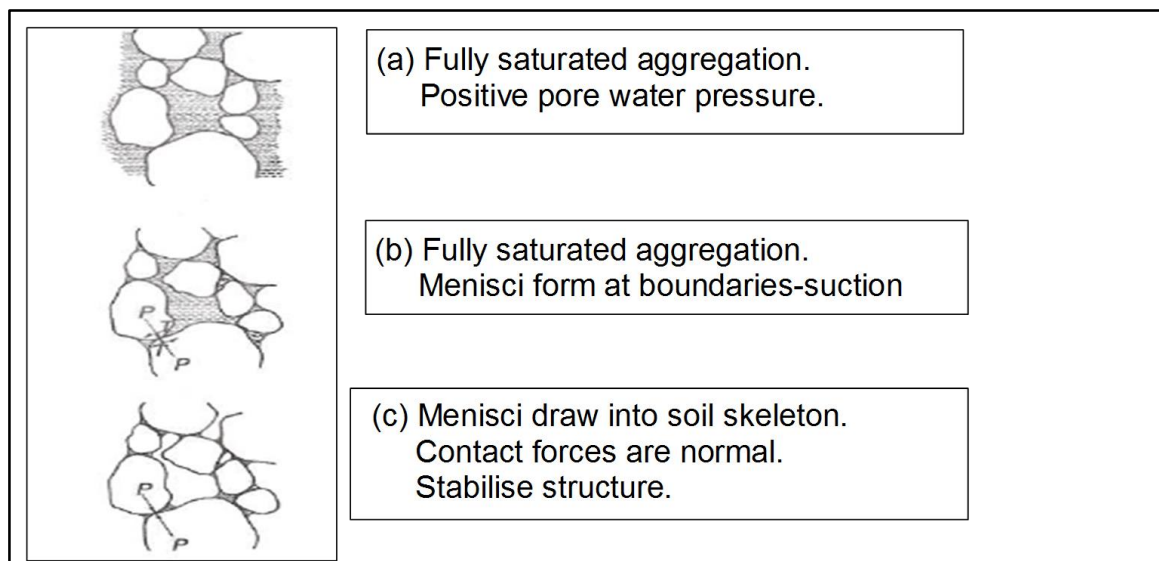


Figure 2-16 Effect of decreasing of water in soil modified after (Burland 2012)

The stress in a soil skeleton has been conceptualised in terms of effective stress. Depending on amount of water in soil, the stress acting on the soil skeleton does not remain the same despite the unchanged external forces acting on it.

Sobolewsky (1995) cited in Axelsson (2000) revealed that dilatant component of shear strength decreases in direct shear by increasing water content. This means that the water content of the soil will affect the dilation of the soil around a driven pile.

2.6 DIRECT SHEAR TESTING AND THE EFFECT OF SPECIMEN SIZE

Direct shear testing is preferred specifically for drained test due to its simplicity. Different sizes of shear apparatus (ASTM 2003; Bareither C.A *et al.* 2008; BSI 1990; Head 2011; Ntirenganya 2015) have been used (60x60mm, 100x100mm, 150x150mm and 300x300mm) with the larger size shear box capable of accommodating the coarse material used in backfill or road building. It has been shown that the particle size of a specimen has a significant influence on friction angle results (Bareither C.A. *et al.* 2008; Cerato & Lutenegegger 2006).

Depending on the size of apparatus, the maximum particle size in the test sample must be limited. ASTM (2003), BSI (1990) and Head (2011) recommend different limit particle size to be used in direct shear. ASTM (2003) suggests that the specimen height in shear box must be at least six times the maximum particle size of the material whereas BSI (1990) recommends that the specimen to be at least ten times the size of maximum particle. Head (2011) supports the specification of BSI (1990). In addition, Jewell & Wroth (1987) recommended that the ratio between shear box length and the average particle size (D_{50}) to be in the range of fifty to three hundred in order to reduce the influence of boundary conditions.

Cerato & Lutenegegger (2006) investigated on five sands the effect of specimen size and scale of shear box on the friction angle using different size of shear box (60x60mm, 100x120 and 120x200mm). Dense, medium, and loose samples were used also to see whether the

density affects also the friction angle. Two of the sands (Winter and GP3) did not meet the criteria of ASTM (2003) and four of the five sands did not meet recommendations of Jewell & Wroth (1987) in 60 mm box. It can be seen in Figure 2-17 that the Winter and GP3 friction angles were more affected by the size of the box specifically in the 60x60 mm box where they did not meet the criteria. On the other hand, the shear box size did not affect Ottawa sand except a slight difference at loose condition.

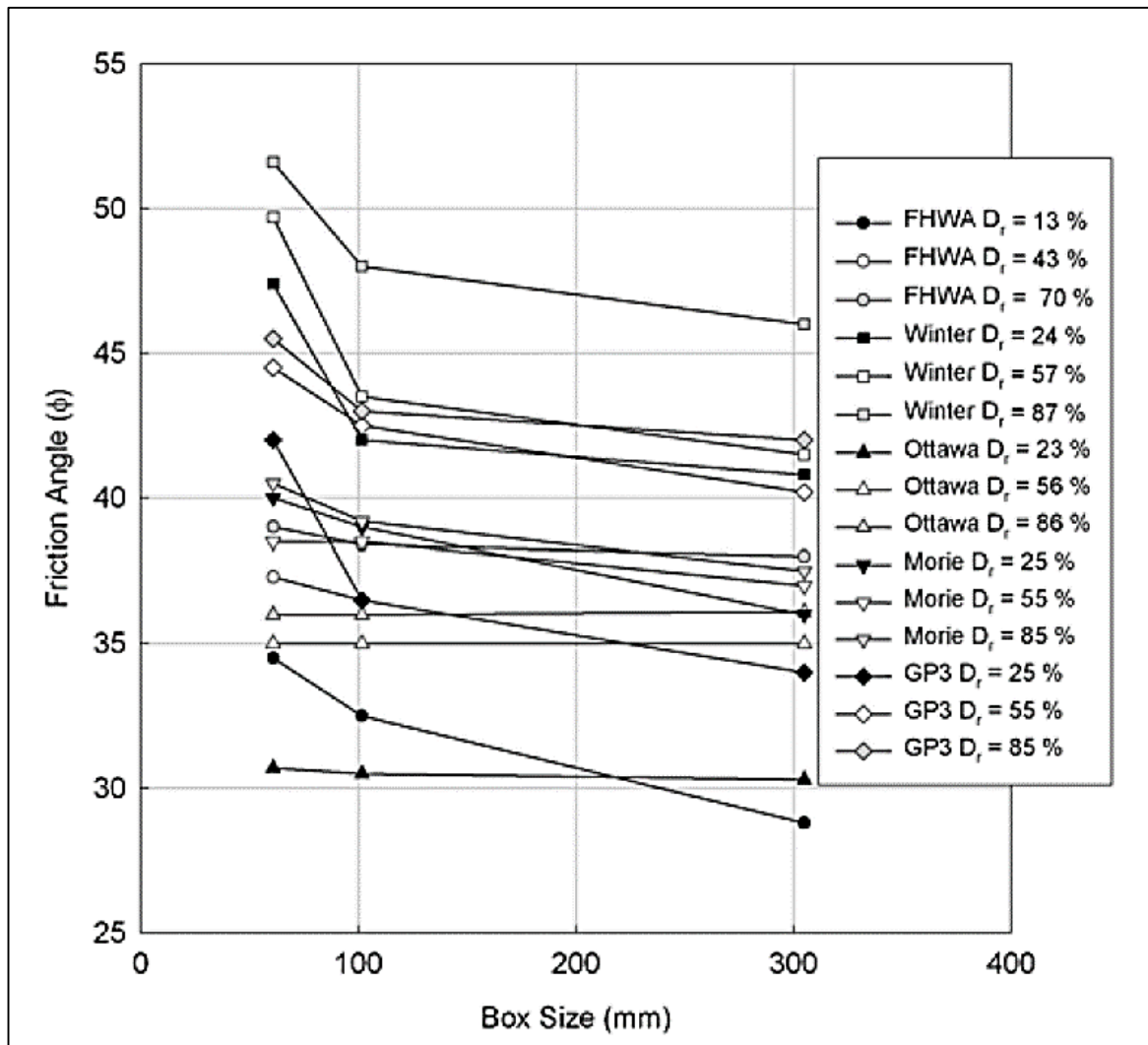


Figure 2-17 Effect of specimen size on friction angle (Cerato & Lutenecker 2006)

Bareither *et al.* (2008) also conducted experiments on the effect of shear strength using small scale and large scale direct shear box (64 mm and 305 mm square). The investigation was on thirty different types of sand. The main objective was to investigate whether the maximum particle size and the shear box size influence the shear strength. By making the initial height of the specimen to be six times the maximum particle size, the friction angles measured were the same in the two shear boxes. Big particle size was removed (scalped) for small-scale apparatus. For small size scale (64mm), 4.75 mm was the maximum particle size. Additionally, effects of coarse sizes in a specimen were investigated by varying the

percentage of coarse particles in a sample and the authors found that less than thirty per cent of coarse size in a material has no effect on the shear strength. The same friction angle was measured both in small and large scale shear tests.

In conclusion, it can be stated that friction angle is affected by the shear box size normally when the ratio of specimen length to the maximum particle size less than fifty. However, if the ASTM criteria is followed, same values of friction angle would be obtained irrespective of the shear box size.

Regarding density and particle size effect on dilation, Simoni & Houlsby (2006) investigated the effect of varying initial specimen density and also adding coarse materials in a specimen on the friction angle and dilation. The results show that the density and an increase in coarse material affect the friction and dilation (Figure 2-18). By increasing the relative density from 0.22 to 0.54, Figure 2-18 shows that both the shear strength and dilation increase. Moreover, by increasing the granular (G0640-Dr=0.57), Figure 2-18 shows an increase in shear strength and dilation where the density was almost the same.

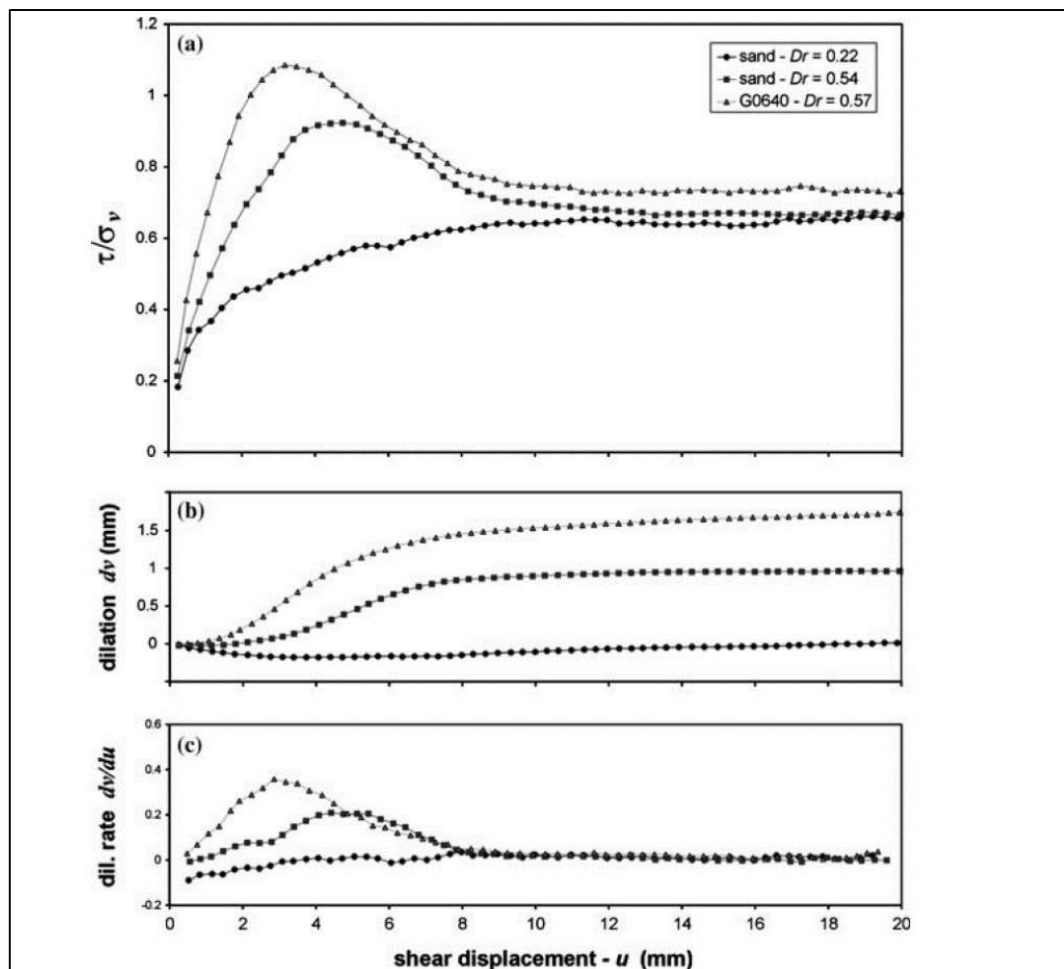


Figure 2-18 Effect of density and particle size on shear strength and dilation (Simoni & Houlsby 2006)

2.7 SHAFT CAPACITY OF PILES

Different methods are used to determine the axial load capacity of piles. These methods are dynamic and static tests, the use of pile driving formulae and analytic methods. This section discusses in situ and analytic methods. In all cases, the capacity of the pile is taken as the sum of shaft and base capacity (Bell & Robinson 2012; Fleming *et al.* 1992).

Shaft resistance is the main factor in determining the resistance of the pile to uplift loads and base resistance of the pile does not come into play. Different parameters have an influence on the ultimate shaft resistance of the pile: soil characteristics, displacement ratio, installation method, and type of loading. Most design methods are based on the radial effective stress, which is a key parameter to estimate the local shaft capacity of a pile. Attention was focused mainly on shaft capacity of driven steel piles in non-cohesive soil.

Many authors have studied the resistance of pile in compression and the concept has been well understood, but the uplift load resistance has been a subject of different conclusion (Meyerhof & Adams 1968). In other words there is still improvement in the subject.

2.7.1 SHAFT CAPACITY EVALUATION BASED ON IN SITU AND EFFECTIVE STRESS ANALYSIS

2.7.1.1 Shaft Capacity Using In Situ Tests

The shaft capacity of piles is estimated by various methods, many of them based on popular in situ tests including the cone penetration (CPT) and standard penetration (SPT). The SPT consists of driving a split-spoon sampler 450mm into the soil by mean of 63.5 kg hammer falling freely through 762mm. In addition, Number of blows is counted for the split-spoon to drive into the soil. The number of blows required to drive the final 300mm is taken as the SPT 'N' value. For CPT, a cone of sixty degree, most of the time combined with a friction sleeve for shaft measurement is pushed into the soil at the rate of 20 mm per second. Measurement of cone penetration resistance and sleeve friction are recorded separately (Byrne & Berry 2008). The cone tip resistance gives the bearing capacity and the friction sleeve measures the shaft capacity. Nonetheless, the cone tip resistance is used to correlate both the base and shaft resistance due to its reliability (Yu & Yang 2012).

Meyerhof (1956) cited in Byrne & Berry (2008) suggested methods for ultimate bearing and shaft capacity for driven piles as:

$$Q_b = 400N'A_b$$

Equation 2-8

Where Q_b = ultimate base capacity in kN

A_b = area of base in m²

N' = average SPT 'N' value above and below base

$$Q_s = 4\bar{N}A_s \quad (\text{Full displacement})$$

Equation 2-9

Equation 2-10

$$Q_s = 2\bar{N}A_s \quad (\text{Low displacement})$$

Where Q_s = ultimate shaft capacity in kN.

A_b = pile shaft area in m²

\bar{N} = average SPT 'N' value over length of shaft

The relationship between CPT point resistance and SPT N' values and shaft resistance is presented in Table 2-2. Table 2-3 gives the relationship with base resistance.

Table 2-2 Shaft resistance per unit area (Byrne & Berry 2008)

| Pile Test | Auger | Auger US | CFA | Oscill. | Precast | Tube | Franki wet shaft | Franki Ram shaft | Forum wet shaft | Forum Ram shaft |
|------------------------------------|-------|-------------|-----|---------|---------|------|------------------------|------------------------|-----------------------|-----------------------|
| Piles in Non-cohesive Soils | | | | | | | | | | |
| CPT q_c | 5 | 5 | 5 | 5 | 8 | 8 | 8 | 12 | 5 | 8 |
| SPT 'N' | 2.5 | 2.5 | 2.5 | 2.5 | 4 | 4 | 4 | 6 | 2.5 | 4 |
| Max (kPa) | 125 | 80 | 125 | 125 | 150 | 150 | 150 | 200 | 125 | 150 |
| Piles in Cohesive Soils | | | | | | | | | | |
| CPT q_c | 10 | 10 | 10 | 10 | 15 | 15 | 15 | 30 | 10 | 8 |
| SPT 'N' | 2.5 | 2.5 | 2.5 | 2.5 | 3 | 3 | 3 | 4.5 | 2.5 | 3.5 |
| α | 0.4 | 0.04 | 0.4 | 0.4 | 0.6 | 0.6 | 0.4 | 0.6 | 0.4 | 0.5 |
| Max (kPa) | 150 | 80 | 150 | 150 | 100 | 100 | 150 | 200 | 150 | 150 |

Table 2-3 Base resistance per unit area (Byrne & Berry 2008)

| Pile Test | Auger | Auger U/S | CFA | Oscill. | Precast | Tube | Franki Wet shaft | Franki Ram Shaft | Forum Wet Shaft | Forum Ram Shaft |
|------------------------------------|-----------|--------------|-----------|-----------|-----------|-----------|------------------------|------------------------|-----------------------|-----------------------|
| Piles in Non-cohesive Soils | | | | | | | | | | |
| CPT q_c | * | * | * | * | | | *** | *** | ** | ** |
| | $0.5q_c$ | $0.5q_c$ | $0.5q_c$ | $0.5q_c$ | $1.0q_c$ | $1.0q_c$ | $1.2q_c$ | $1.2q_c$ | $1.0q_c$ | $1.0q_c$ |
| SPT 'N' | * | * | * | * | | | | | * | * |
| | 300 | 300 | 300 | 300 | 400 | 400 | 500 | 500 | 400 | 400 |
| Max (kPa) | 8000 | 8000 | 8000 | 8000 | 20000 | 15000 | 15000 | 15000 | * | * |
| | | | | | | | | | 15000 | 15000 |
| Piles in Cohesive Soils | | | | | | | | | | |
| CPT q_c | $0.45q_c$ | $0.45q_c$ | $0.45q_c$ | $0.45q_c$ | $0.45q_c$ | $0.45q_c$ | $0.6q_c$ | $0.6q_c$ | $0.5q_c$ | $0.5q_c$ |
| SPT 'N' | 50 | 50 | 50 | 50 | 50 | 50 | 60 | 60 | 50 | 50 |
| N_c | 9 | 9 | 9 | 9 | 9 | 9 | 9-12 | 9-12 | 9-12 | 9-12 |
| Max (kPa) | 4500 | 4500 | 4500 | 4500 | 4500 | 4500 | 6000 | 6000 | 5000 | 5000 |

2.7.1.2 Effective Stress Approach

Three methods of assessing the shaft capacity have been established and popularised for driven piles (API 2000; Gavin & Lehane 2003; Lehane *et al.* 2007). These methods are the American Petroleum Institute (API), Imperial College Pile (ICP), and University of Western Australia (UWA) methods.

- i) American Petroleum Institute (API) has proposed a method to assess the shaft capacity of axial offshore driven pile in cohesiveness soil as:

$$\tau_f = K\sigma'_{vo} \tan \delta = \beta\sigma'_{vo}$$

Equation 2-11

Where

τ_f = the shaft friction capacity in lb/ft² or (kPa)

K = coefficient of lateral earth pressure (ratio of horizontal to vertical effective stress),

σ'_{vo} = vertical effective stress lb/ft² or (kPa) at the point in question,

δ = friction angle between the soil and pile wall.

$$\beta = K \tan \delta$$

The API (2000) recommends values of K of 0.8 for both compression and tension and 1.0 for full displacement (plugged or close ended) pile. Table 2-4 shows guidelines design parameters for non-cohesive soil. This method suggests the shaft capacity to reach a constant value at a certain depth penetration. The reason behind this is, as the coefficient of lateral earth pressure (K) is assumed to be constant along the depth, the effective vertical stress (σ'_{vo}) for long pile is assumed to increase with depth until it reaches a limiting value. However, Poulos & Davis (1980) stated that effective vertical stress adjacent to the pile assumed to be the same in API method as the effective overburden pressure is not necessarily equal but reaches a limit value. Day (2014a) states that there is no consensus on the limiting value of effective vertical stress with depth, with Vesic and Kerisel supporting the limitation and Kulhaway and Fellenius arguing against.

Most practical design methods assume the lateral earth pressure K remains constant with depth, which leads to a linear increase of shaft or skin friction resistance (τ). However, K decreases with depth. This coefficient k depends on the effective vertical stress, which increases with depth as mentioned in previous paragraph (Boulon & Foray 1986).

Table 2-4 Design guideline for non-cohesive soil (API 2000)

| Density | Soil Description | Soil-Pile Friction Angle, Δ Degrees | Limiting Skin Friction Values Kips/ft ² (kPa) | N_q | Limiting Unit End Bearing Values Kips/ft ² (MPa) |
|-------------------------------|-----------------------------|--|--|-------|---|
| Very loose Loose Medium | Sand Sand-Silt** Silt | 15 | 1.0 (47.8) | 8 | 40 (1.9) |
| Very loose Loose Medium | Sand Sand-Silt** Silt | 20 | 1.4 (67.0) | 12 | 60 (2.9) |
| Medium Dense | Sand Sand-Silt** | 25 | 1.7 (81.3) | 20 | 100 (4.8) |
| Dense Very Dense | Sand Sand-Silt** | 30 | 2.0 (95.7) | 40 | 200 (9.6) |
| Dense Very Dense | Gravel Sand | 35 | 2.4 (114.8) | 50 | 250 (12.0) |

- ii) The Imperial College Pile (ICP) approach method proposed by Lehane *et al.* (1993) is based on the Coulomb failure criterion mentioned in Equation 2-4. They conducted experiments to test the compression and tension by using rigid cone piles pushed into medium dense sand up to 6 m and came up with Equation 2-12 and Equation 2-13. The radial effective stress (σ'_{rc}) is controlled by initial soil condition and pile installation processes where as $\Delta\sigma'_{rd}$ is due to the contribution of sand dilation during the loading.

$$\tau_f = \sigma'_{rf} \tan \delta_f = (\sigma'_{rc} + \Delta\sigma'_{rd}) \tan \delta_{cv}$$

Equation 2-12

Where

τ_f = constant volume interface friction angle

σ'_{rf} = radial effective stress at failure

σ'_{rc} = radial effective stress after installation and equalization

$\Delta\sigma'_{rd}$ = change in radial stress due to loading stress path (dilation)

The constant volume friction angle δ_{cv} should be measured in the laboratory for a given pile roughness as a function of mean effective particle diameter (d_{50}) and not of the relative density. The interface friction is independent of initial relative density, but decreases with mean particle size d_{50} (see Figure 2-19) (Jardine *et al.* 1998).

In tension, the shaft capacity method 2005 (ICP-05) also follows the Coulomb failure criteria but with some modifications (Lehane *et al.* 2005):

$$\tau_f = a(0.8\sigma'_{rc} + \Delta\sigma'_{rd}) \tan \delta_{cv}$$

Equation 2-13

Where $a = 1$ for closed ended tube piles and 0.9 for open ended tube piles.

The radial effective stress σ'_{rc} , is considered as a function of CPT tip resistance:

$$\sigma'_{rc} = 0.029 \cdot q_c \left(\frac{\sigma'_{vo}}{P_a} \right)^{0.13} \left[\max \left(\frac{h}{R^*}, 8 \right) \right]^{-0.38}$$

Equation 2-14

Where

h = distance above the pile tip (= pile length – depth)

R^* = equivalent radius = $(R^2 - Ri^2)^{0.5}$, which is R for closed piles

R = outside radius of pile (= $D/2$)

Ri = inside radius of pile (= $Di/2$)

P_a = atmospheric pressure

For non-circular (closed-ended) piles, R^* is considered as the radius of an equivalent circular pile with the same end area.

Lehane *et al.* (1993) suggested $\Delta\sigma_r$ to be quantified using the cavity expansion theory as:

$$\Delta\sigma'_{rd} = 2G \frac{\Delta r}{R}$$

Equation 2-15

Where G =shear modulus and Δr =interface dilation estimate to be approximately 0.02mm for rusted steel pile.

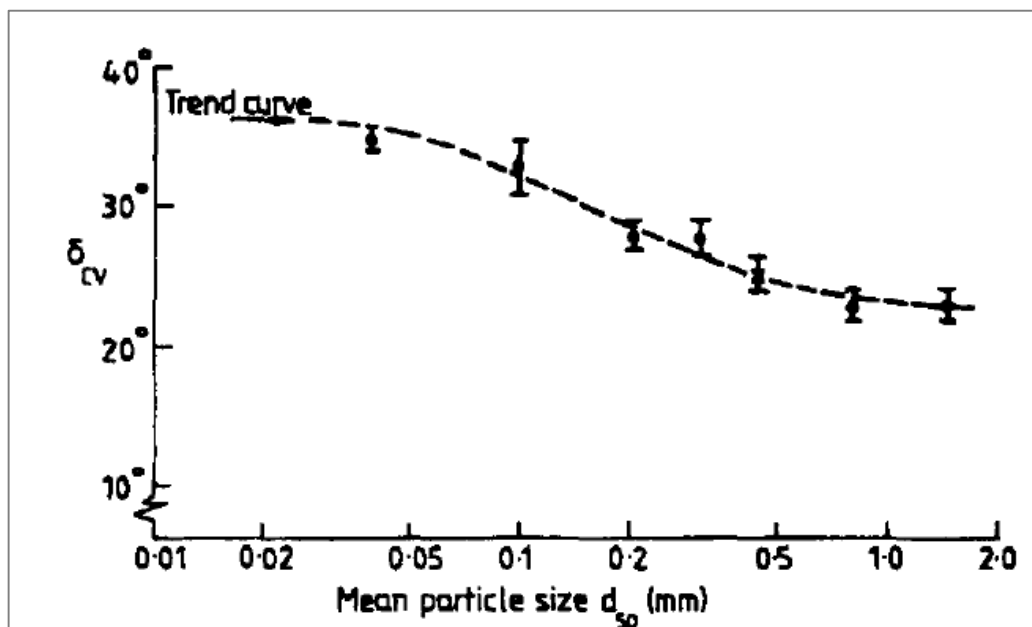


Figure 2-19 Trend of variation of δ_{cv} with grain size of granular soils shearing against a steel interface (Jardine *et al*,1998, after Jardine *et al.*,1992)

iii) University of Western Australia (UWA-05) approach method

Lehane *et al.* (2007) recommended the UWA-05 design method for shaft capacity of open and close ended driven piles in Siliceous sand. This method is the same as the ICP Equation 2-12 but came up with different equations of radial effective stress after installation and equalisation (σ'_{rc}), and change in radial stress due to loading stress path ($\Delta\sigma'_{rd}$) (see Equation 2-17,2-18 and 2-18, 2-20).

$$\tau_f = \sigma'_{rf} \tan \delta_f = \frac{f}{f_c} (\sigma_{rc} + \Delta\sigma'_{rd}) \tan \delta_{cv}$$

Equation 2-16

$$\sigma'_{rc} = 0.03 \cdot q_c (A_{rs}^*)^{0.3} \left[\max \left(\frac{h}{D}, 2 \right) \right]^{-0.5}$$

Equation 2-17

$$A_{rs}^* = 1 - \text{IFR} \left(\frac{D_i^2}{D^2} \right)$$

Equation 2-18

$$\text{IFR}_{\text{mean}} \approx \min \left[\left(\frac{D_i(\text{m})}{1.5} \right)^{0.2} \right]$$

Equation 2-19

$$\Delta\sigma'_{\text{rd}} = 4G \frac{\Delta r}{D}$$

Equation 2-20

Where

τ_f = constant volume interface friction angle

q_c = CPT tip resistance

σ'_{rf} = radial effective stress at failure

σ'_{rc} = radial effective stress after installation and equalization

$\Delta\sigma'_{\text{rd}}$ = change in radial stress due to loading stress path (dilation)

$\frac{f}{f_c} = 1$ for compression and 0.75 for tension

Δr = dilation (assumed for analyses = 0.02mm, the same as for ICP-05)

IFR = incremental filling ratio

D_i = pile inner diameter

D = pile outer diameter

h = relative distance above the pile tip (=pile length - depth)

Figure 2-20 illustrates the trend of interface friction with the average particle size. In order words, this Figure shows the manner in which the interface friction angle is a function of the mean effective particle size D_{50} . The graph is similar to the one employed by ICP-05. The only observable difference was on the limit of interface angle. The $\tan\delta_{\text{cv}}$ is limited by 0.55 due to the potential change of surface roughness during the installation (Lehane *et al.* 2007).

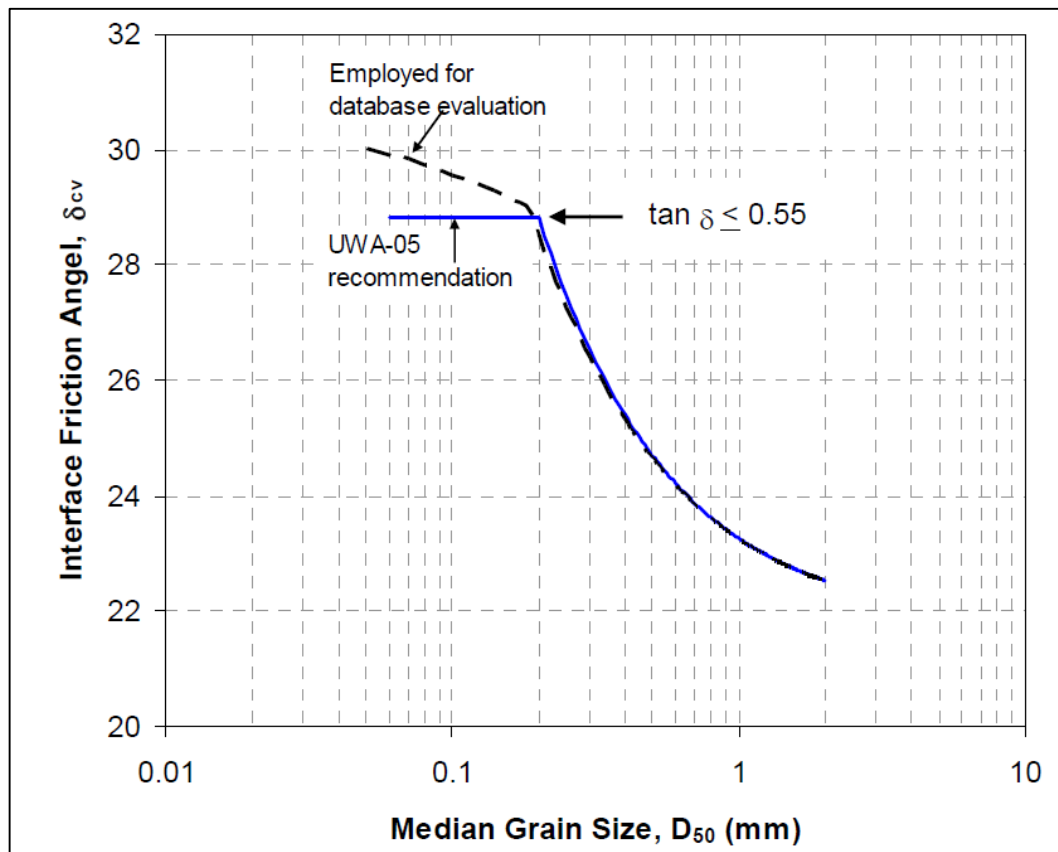


Figure 2-20 Interface friction variation with D_{50} after (Lehane *et al.* 2007)

iv) Conclusion and comparison of methods

- The API (2000) suggests that the shaft capacity τ_f in Equation 2-10 may not increase continuously with depth and proposes to use the value given in Table 2-4. On the other hand, ICP and UWA methods record no critical depth where the shaft capacity becomes constant, but acknowledge the tendency of the shaft to a limiting value due to the ratio of relative depth to pile diameter h/R (see Figure 2-21).
- The UWA method was developed based on the ICP method. They are very similar, except that the UWA is primarily formed for offshore driven piles (Yu & Yang 2012). Lehane *et al.* (2007) compared the prediction of a mean ratio of calculated to measured capacity (Q_o/Q_m) of the three methods using 74 load tests excluding piles data tests from micaceous, calcareous and residuals sands. The performance was classified in four categories: closed-ended piles tested in compression and tension, open-ended piles in compression and tension. The tests were conducted for piles that had a diameter greater than 200mm and length exceeding 5m. For closed ended piles tests in tension, a coefficient of variation 0.29, 0.30, and 0.84 was obtained for UWA, ICP-05 and API respectively. 0.23, 0.27, and 0.76 was obtained for UWA, ICP, and API respectively in driven open-ended piles in tension. The UWA and ICP give close results and more reliable than the API.
- Despite different weighting factors applied to both ICP-05 and UWA-05 methods to open-ended condition and friction fatigue, the University of Western Australia team,

based on the database study done in sand has provided reliable results for these two methods compared to the API method. By the same token, they do not give coincident results when applied to the same piles in the same soil profile (Jardine, R. J. & Chow 2007; Jardine 2009).

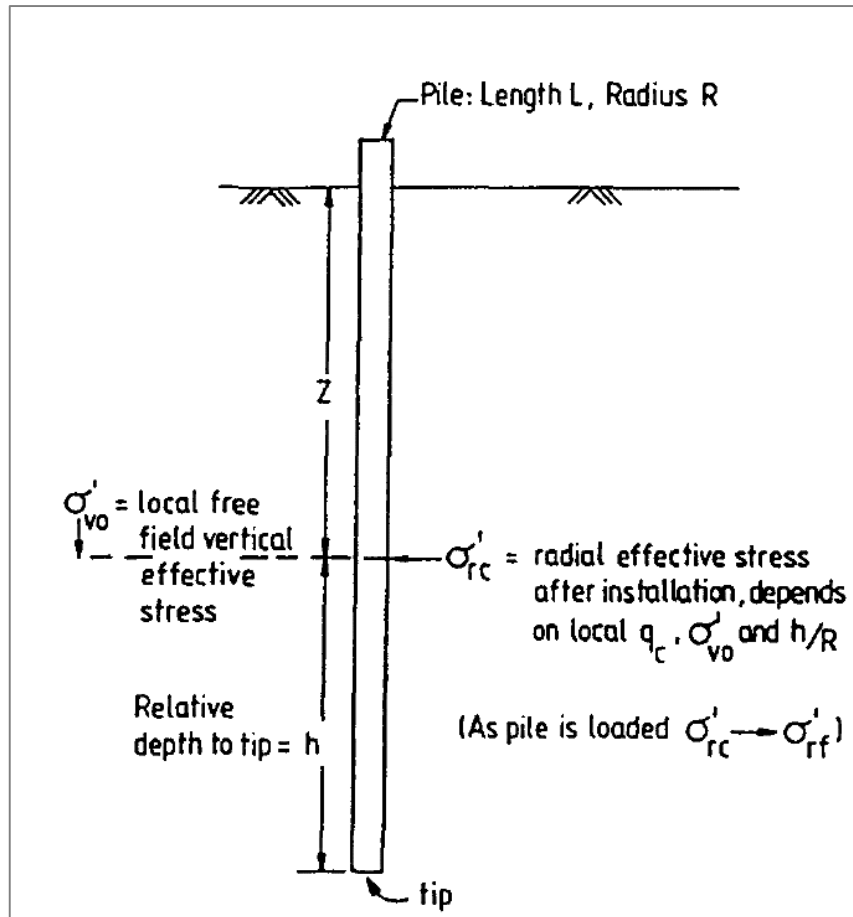


Figure 2-21 Definition of the term used in Equation 2-13 and 2-16 (Jardine *et al.* 1998)

2.7.1.3 Effect of Normal Stress and Initial Density on Dilation and Shaft Capacity

The primary factor that influences the dilation is the initial density. A granular soil expands or contracts on shear depending on the density initial condition. The higher the density of a granular soil the higher the dilation will be. However, the normal effective stress tends to prevent the soil from dilating. An increase in normal effective stress decreases dilation in soil. The higher the normal effective stress and the lower the density, then there is likelihood that the soil will compress. The lower the effective stress and the higher the density, then the soil will likely dilate (Duncan & Wright 2005; Houlsby 1991).

Alawneh *et al.* (1999) investigated the uplift capacity of model piles using pile placement method, smooth and rough interface piles and varying the initial relative density conditions. The pull-out tests were conducted using a hydraulic actuator. They found that by varying the initial relative density from 45% to 70%, there was an increase in capacity of 70 % for the driven model piles and of 100 % for the jacked model piles. The values 1.33 and 1.52

were the mean ratio shaft capacity of driven model pile to jacked model pile for dense and medium sand respectively. The dilation of the sand has contributed to the shaft capacity.

Alexson (2000) illustrates the effect the dilation has on the shaft capacity. Figure 2-22 shows when the pile has been loaded, the particles 1, 2, 3 move from the rest position to loading position causing shear zone to expand and increase the radial stress due to dilation of materials. Therefore, the shaft capacity increases.

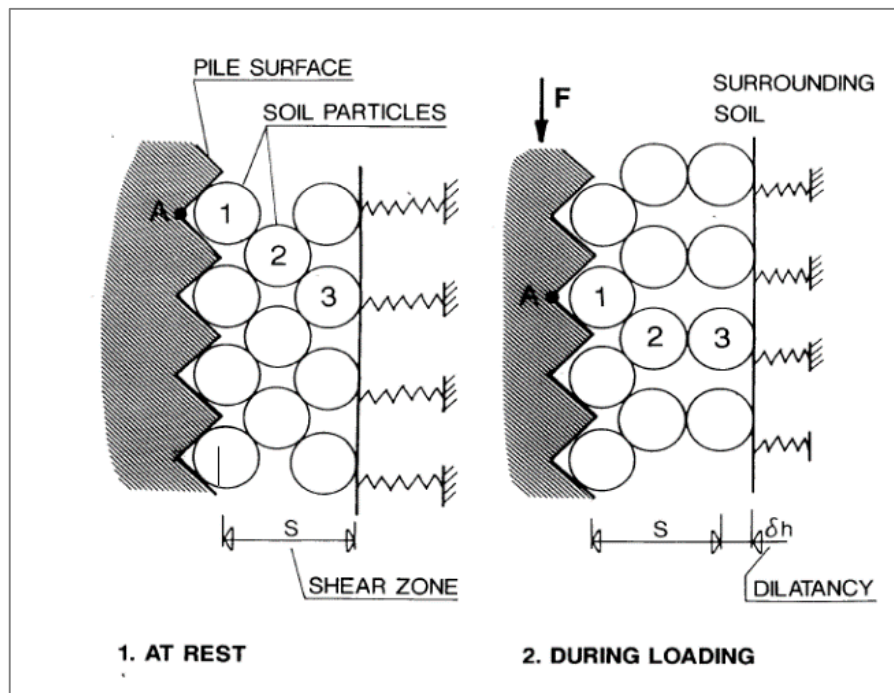


Figure 2-22 Behaviour of particles during loading causing dilation (Axelsson 2000)

2.7.1.4 Effect of Soil Characteristics on Shaft Capacity

Ultimate shaft capacity is expected to increase with an increase in friction and interface friction angle between soil and pile. In addition to these strength parameters, stress-strain parameters also influence the shaft resistance as well as the deformation caused by application of load on the piles. For instance, calcareous sands, despite their higher angle of friction even in loose conditions, develop a fraction of shaft resistance that can record in medium siliceous sands which develop less friction angle (Kraft 1991). This behaviour is due to crushing of calcareous soil particles, which contracts the volume increase in the shear zone. Compressibility is a key factor in the performance of shaft capacity. Nicola & Randolph (1993) also corroborated the compressibility factor on shaft capacity.

Furthermore, Uesugi & Kishida (1986) investigated the influence of soil type, surface roughness of the steel and grain size on the coefficient of friction (interface friction angle). Based on the results for roughness (equal to $1.5\text{--}3\mu\text{m}$ and $10\text{--}15\mu\text{m}$), they found that material types and surface roughness of steel have profound influence while the average grain size ($0.55\text{--}0.62$ and $0.15\text{--}0.19$) has less significance influence.

Regarding the particle grain size, installation and loading of pile lead to crush of the materials. The coarser the material the higher is the crushing and the finer the materials the lower is the crushing. Moreover, the more the tip base of piles is thicker the more important is the crushing for driven pile. Less crushing is observed for lower displacement than for full displacement piles and the shear zone along the shaft is also depend on the wall thickness at the toe of the open-ended piles (Kraft 1991). Figure 2-23 illustrates the shear zone behaviour during installation and loading. Soil compresses during driving and dilates during static loading.

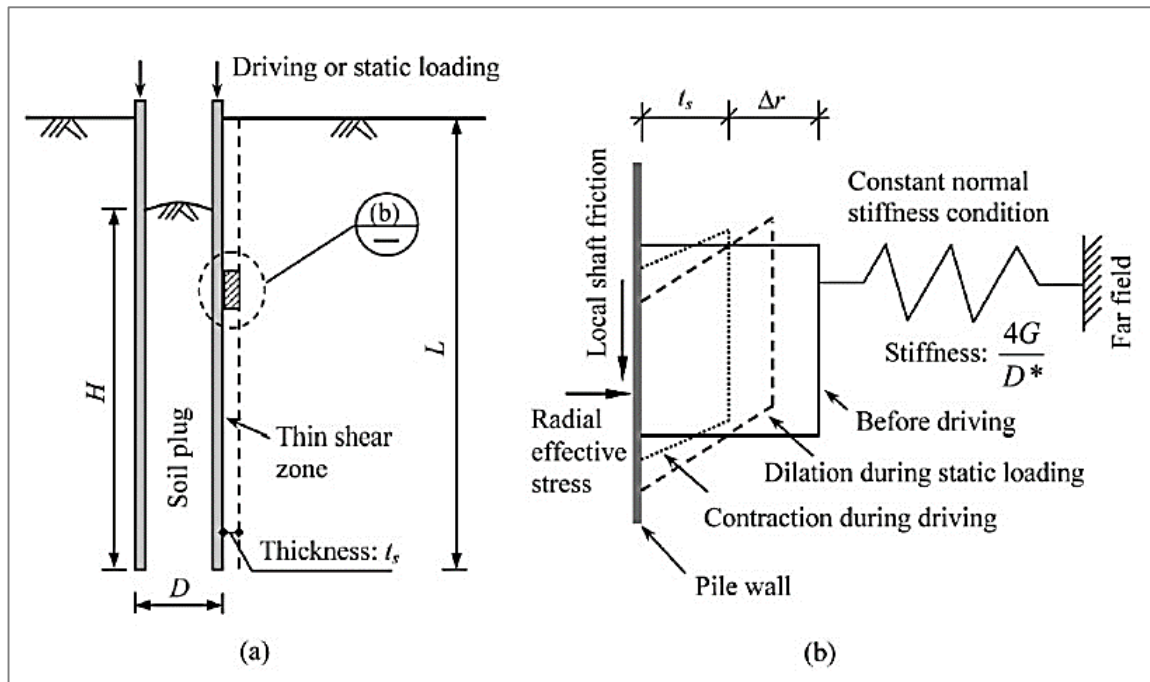


Figure 2-23 Behaviour of the shear zone during installation and static loading: (a) schematic diagram of the shear zone; (b) variation in the shear zone (Yu & Yang 2012)

2.7.1.5 Installation Methods, Loading Type and the Effect of Time on Shaft Capacity

Various installation methods are used for driven piles such as, hydraulic hammer, drop hammer, and hydraulic jack. These methods influence the shaft capacity of the piles. Alawneh *et al.* (1999) compared hydraulic jack and driving installation methods. The driving method was made of cylindrical hammer of 7.14 kg with a mass falling freely from 300mm. The results showed that the shaft capacity for driven method was 1.33 times the jack methods in a dense condition and 1.52 times in a medium sand condition. They suggested that the reason for the higher shaft resistance for the driven method might be due to the densification of the sand during the driving, which is usually associated with vibration.

The method of loading also affects the performance of the shaft capacity. Loading can be static loading, dynamic or cyclic (wave and wind) loading (see Figure 2-24). Igwe *et al.* (2011) stated that the radial effective stress decreases with an increase of loading cycle. This has also been acknowledged by Yu & Yang (2012).

The effect of time has been proved to increase the capacity of the shaft friction of the driven pile (Chow & Jardine 1998; Gavin *et al.* 2013; Axelsson 1998; Axelsson 2000). They have concluded that the increase in shaft capacity is due to stress relaxation causing arch deterioration with time, creeping, increase of the stiffness due to the soil ageing. Lim & Lehane (2015) stated in addition that the effect of the increase in shaft capacity over time triggering set-up is due to constraint dilation caused by the increase in shear stiffness and dilatancy surrounding the pile. With age, the particles surrounding the pile (see Figure 2-25) change their position leading to interlocking and increase the dilation (shear zone).

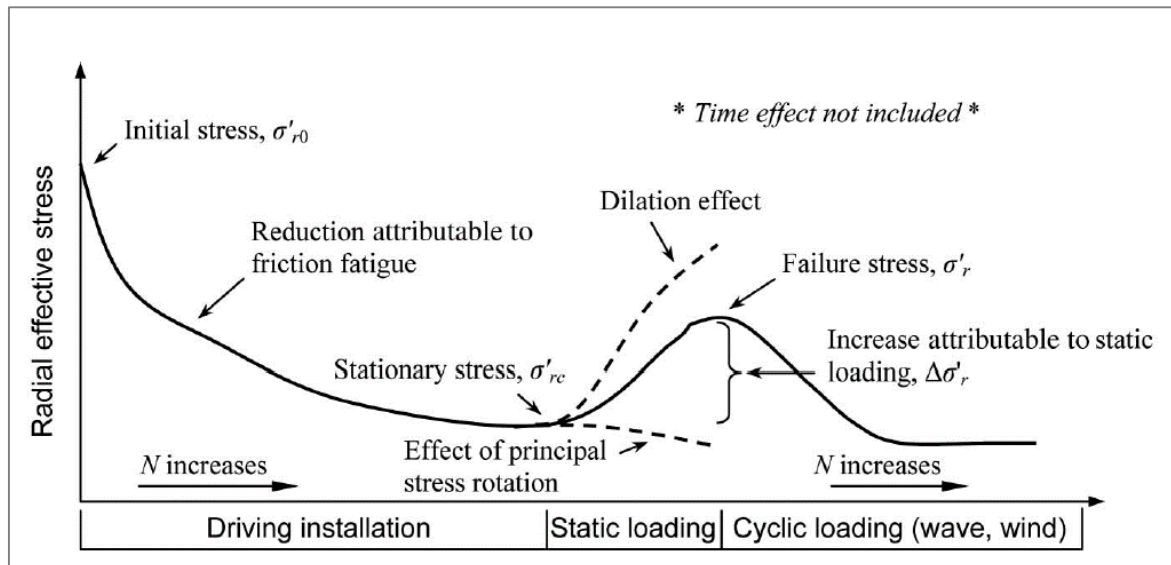


Figure 2-24 Effect of dilation and loading type on radial effective stress (Yu & Yang 2012)

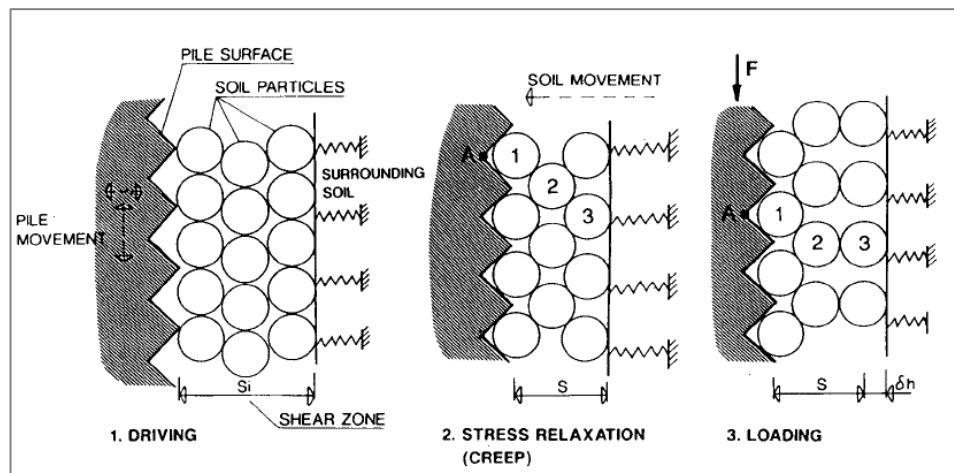


Figure 2-25 Reorientation of particles increasing shear zone (Axelsson 2000)

2.7.2 OBLIQUE PULL-OUT CAPACITY OF THE PILE

The application of an oblique pull-out force on the piles mobilises a combination of axial and lateral load resistances. The axial load capacity has been discussed in section 2.6 and was shown to be a function of lateral (or radial) stress acting normally on the side of the pile.

When a lateral load is applied to the pile, the stress normal to the pile shaft increased on one side of the pile. High lateral pressure will occur near the top and tip of the pile (Poulos & Davis 1980). Brown (1965) cited in Poulos & Davis (1980) gives equations of axial and lateral failure in function of inclined load capacity as:

$$P_u = P_{uo} + \Delta P_u \quad \text{Equation 2-21}$$

Where:

P_{uo} = axial capacity when the applied load acts along the pile axis

ΔP_u =increase in pull-out resistance caused by two lateral forces, T and R, in Figure 2-26

P_u = ultimate axial load capacity of pile

The ultimate inclined load capacity becomes:

$$Q_u = P_u \sec \delta \quad \text{Equation 2-22}$$

It can be seen in Equation 2-21 that the lateral load influences the axial load contributing in its increase by an increase in T and R.

Poulos & Davis (1980) assumed that the vertical load in inclined load has no influence on the lateral capacity and come up with the following inclined load equation:

$$Q_u = H_u \csc \delta \quad \text{Equation 2-23}$$

Where

H_u is ultimate lateral load capacity of pile

Q_u is the ultimate inclined load capacity of pile

In other words, the axial load mobilised in oblique pull-out is affected by the lateral load. However, the lateral load mobilised during the oblique pull-out is not affected by the axial load. This thus explains the rationale behind Equation 2-21.

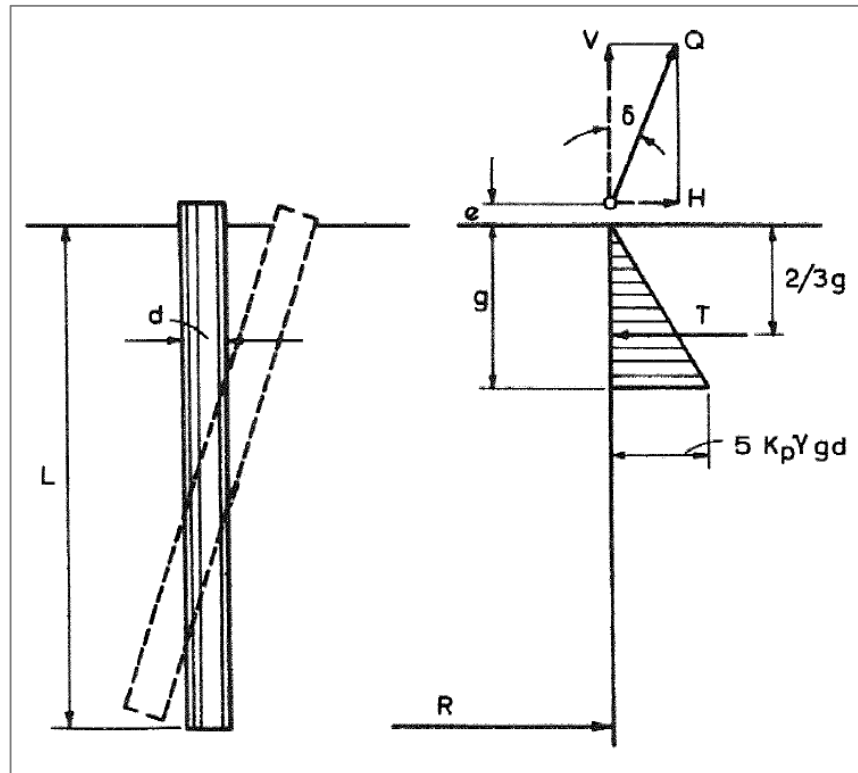


Figure 2-26 Earth pressure distribution (Poulos & Davis 1980)

The increase of uplift resistance of piles due to the lateral load has also been acknowledged by (Reddy & Ayothiraman 2015). They conducted experiments on the behaviour of piles under uplift and lateral loading independently and under combined uplift and lateral loading. They found out that the load-displacement is non-linear under both independent uplift and combined lateral-uplift loading. The behaviour of the pile under combined loading and independent loading was different. The combined loading increased considerably.

When a load displacement curve exhibits an elasto-plasticity behaviour during oblique pull-out test, a two tangents method has been used. This is due to the difficulty of finding the ultimate capacity because the curve keeps increasing.

Bhardwaj & Singh (2013) conducted experiment on model auger pile of 25 diameter and 600 mm of length using the two tangent methods illustrated in Figure 2-27. Nine different degrees (from 0° to 90°) were used to observe the influence of inclination degree on the oblique pull-out capacity. By measuring separately the vertical and horizontal displacement, they found that the vertical displacement for 0° and 5° govern the pull-out capacity, while from 10° to 90° ; the horizontal displacement curve governs the pull-out capacity.

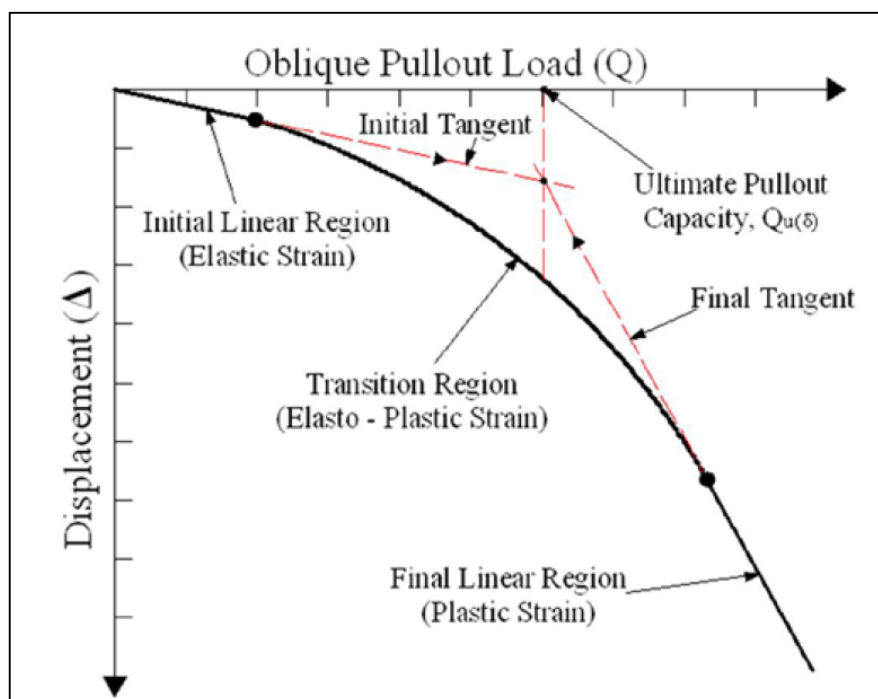


Figure 2-27 Two tangent methods of load capacity (Bhardwaj & Singh 2013)

2.8 SOUTH AFRICAN CLIMATIC CONDITIONS

South Africa is situated in the subtropical zone within latitudes 22° to 35° S and longitudes from 17° to 33° E. Oceans and the altitude plateau moderate the climates of the three coastal sides and the internal country respectively. Compared to the world average rainfall, South Africa is a relatively dry country.

Variations of climates are observed along the country. Except for the Western Cape which has a wet winter and dry summer, the rest of the country experiences cold and dry winters as well as hot and wet summers. The coastal regions of South Africa experience a warm climate.

However, there is a striking temperature difference between the east coast and the west coast due to the warm current along the east coast and cold along the west coast. South Africa has four climate seasons in a year: summer, autumn (fall), winter and spring (South African Government 2015).

Solar panel farms are usually installed where the solar radiation is high. As it can be observed in Figure 2-28, South Africa is a country with high solar resources. This has been corroborated by the Department of Energy of South Africa (2014) reporting that South Africa is one of the leading countries in the world in terms of the best solar resources in the world.

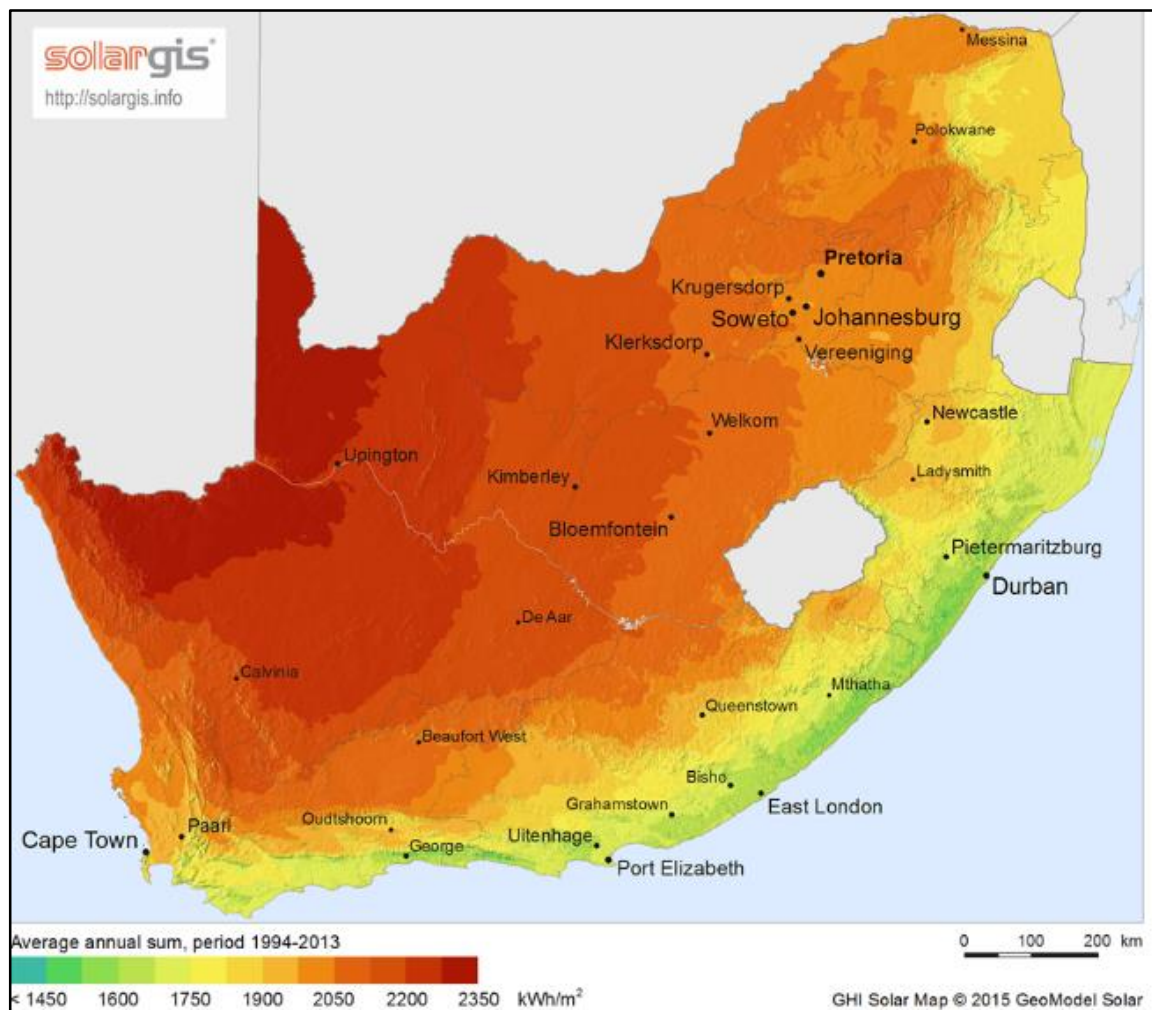


Figure 2-28 Solar resource map of South Africa (Solargis 2015)

However, South Africa experiences high wind intensity. This makes the wind load to represent a dominant environmental action to be considered during the structure design as highlighted by Kruger *et al.* (2013). Kruger *et al.* (2010) and Kruger *et al.* (2013) underlined six causes of the wind gusts in South Africa. These wind gusts are caused dominantly by thunderstorms and extratropical low pressure systems, which can be related to the passage of cold fronts over the Southern African subcontinent. SANS10160-3 (2011) specifies the wind load actions to be considered in structural design. This wind load actions specified in SANS 10160 do not take into account the effect high intensity wind caused by wind gusts. The reason is the lower probability of such wind to occur at a specific geographical location. Figure 2-29 shows the representation of wind speed all over South Africa and it can be seen that the high values of wind speed are between the Northern and Western Cape in Beaufort West, Victoria West Brandvlei and Calvinia. Comparing Figure 2-28 and Figure 2-29, it can be seen that regions that experience high wind speeds overlap the region of high solar radiation.

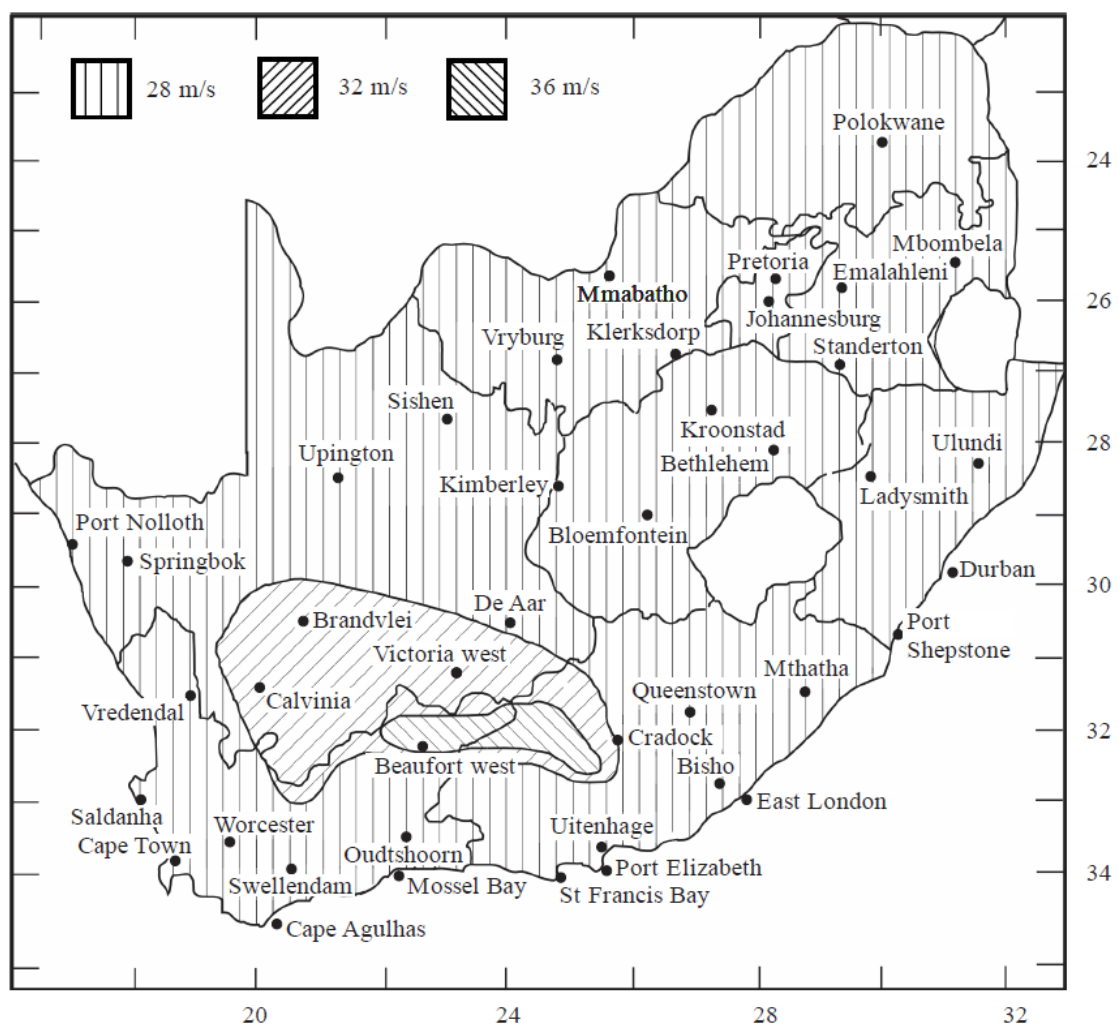


Figure 2-29 Map of basic wind speeds (SANS10160-3 2011)

2.9 SUMMARY OF LITERATURE REVIEW

The review of existing scholarship provides necessary knowledge on the performance of the driven piles in non-cohesive materials. Physical and mechanical properties play a significant role in the capacity of driven piles as well as the loading type.

Well graded material is likely to have a better performance than gap or poorly graded materials. Particle shapes influence the strength of materials. Materials which have lower roundness use high energy to be compacted compared to higher roundness ones.

High compaction effort is required for well graded non-cohesive materials and lower compaction effort for poorly graded materials. The more the compaction effort, the higher the densification, and the higher the strength the materials become. Nevertheless, depending on the types of material, crushing will occur for weak material. The grading modulus, coefficient of uniformity and curvature are additionally used to check the quality of the material.

Dilation governs the compression and the uplift capacity of piles. It is a function of physical and mechanical properties mentioned above. Densification of materials increases their dilation depending again on strength and type of materials. The shaft capacity of piles increases as material dilates during loading and uplifting. However, loose material and poor quality material decrease the shaft capacity by compressing and crushing respectively.

In addition, water content, confinement in driven piles and the repetition of loading- unloading of the piles (cyclic loading), are additional factors affecting the shaft capacity of the driven pile.

Concerning the climatic conditions of South Africa, available literature shows that high wind speeds occur in the regions of high radiation where solar panels would ideally be installed.

This study, investigates the capacity of solar panel posts shaft driven into non-cohesive material. Backfill material type, compaction effort, displacement ratio, water content, load inclination, and aging are identified as having an effect on the shaft capacity of the driven piles.

CHAPTER 3 METHODOLOGY AND EXPERIMENT DESIGN

3.1 INTRODUCTION

This chapter describes the different types of materials and tests used for the purposes of the present study. The chapter consists of three parts. The first part deals with the origin of materials as well as their classification. The second part deals with shear strength and dilation of materials using the direct shear test and the last part is the methodology used to conduct the model tests (axial and oblique pull-out tests) using the Instron 2000 machine.

Various standards were used to classify, characterise, and simulate model experiments of the materials. Materials preparation, apparatus description and the test procedures are included in this chapter for the direct shear strength tests and the pull-out tests. Chapters 4, 5 and 6 present the results.

3.1 MATERIALS, TEST METHODS AND STANDARDS

Three types of materials were used for the study: crusher dust (CD) derived from hornfels, Malmesbury sand (MS) and Philippi sand (PS). The crusher dust was collected at Lafarge quarry located in Tygerberg Valley, Western Cape, South Africa. Malmesbury and Philipp sands were collected from quarries near the towns of Malmesbury and Philippi, both in the Western Cape.

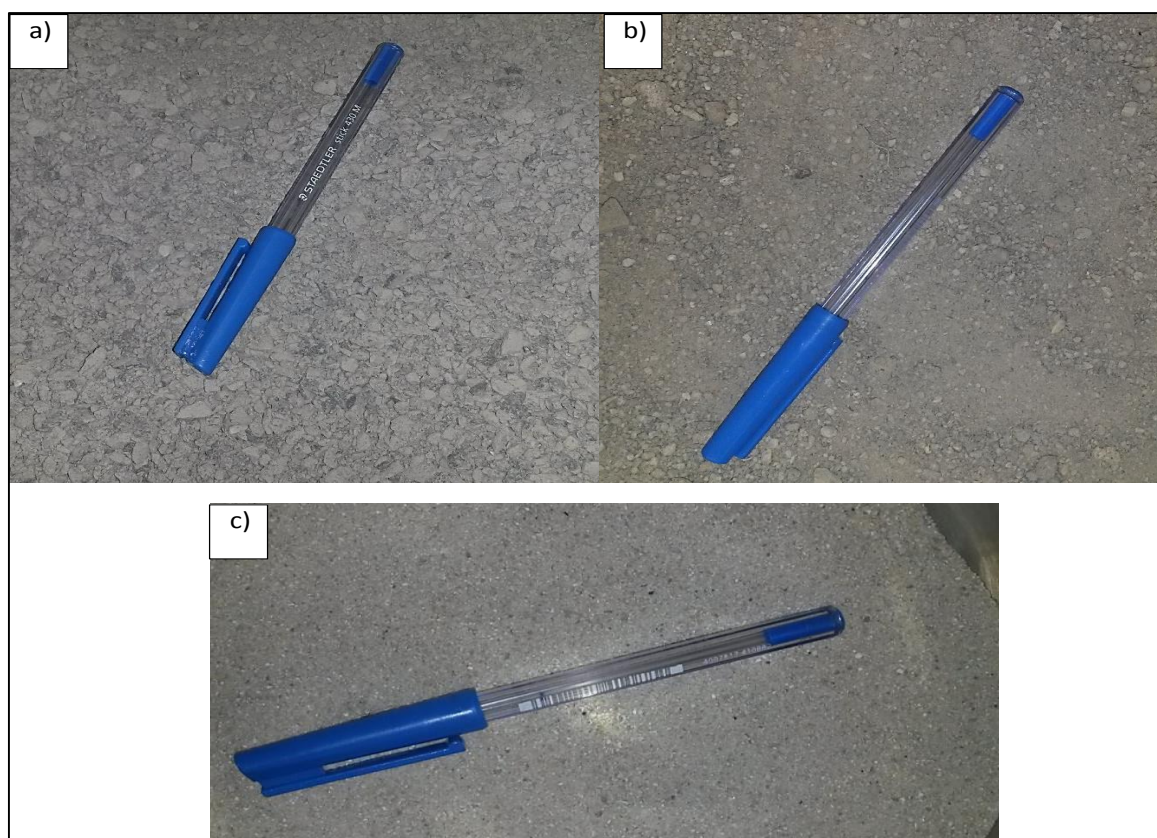


Figure 3-1 Research materials a) Crusher dust, b) Malmesbury sand, c) Philippi sand

3.1.1 GRADING

Grading is a process of determining the particle size distribution of a soil. This offers an understanding related to the packing of particles. This packing of materials influences its density. Sieve analysis of the materials was conducted according to Method A1 (b) of South African Standard Methods of Testing Road Construction Materials (TMH1 1986). Figure 3-2 shows the particle size distribution of the three materials used in the research. The dry sieving method was used. Firstly, dry materials were quartered in order to get representative samples. Thereafter, an average of 1000g was passed through a deck of sieves.

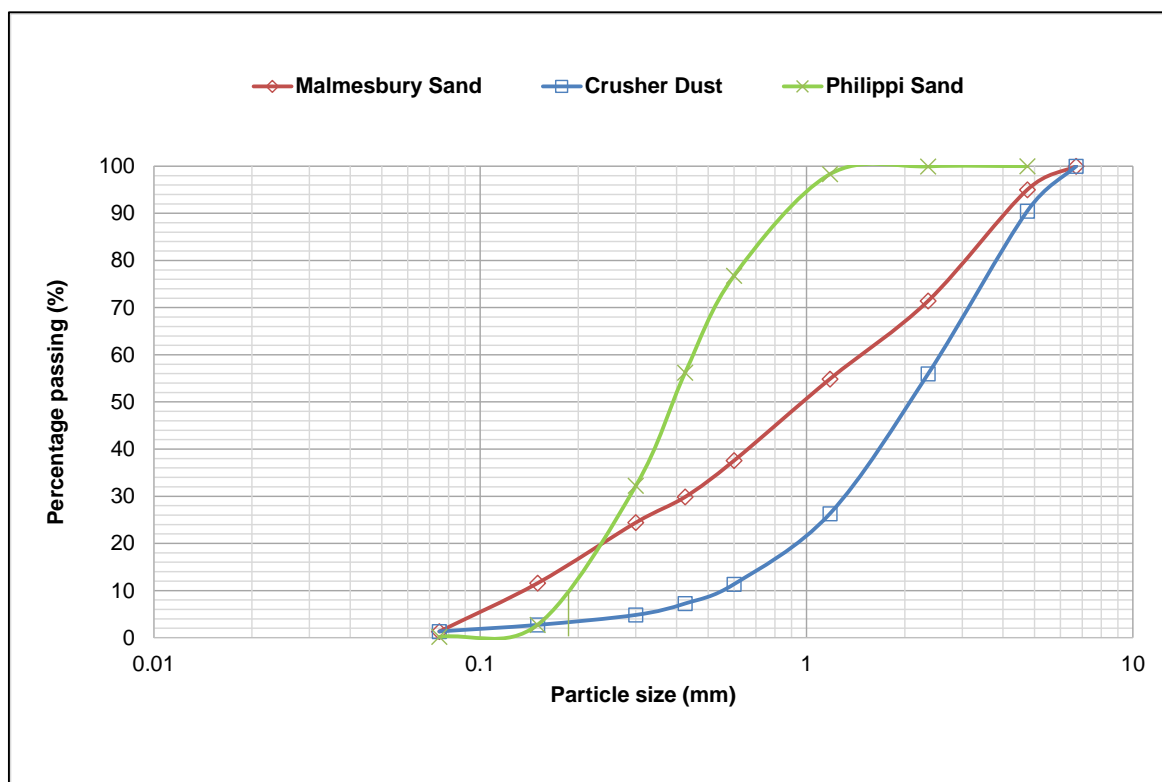


Figure 3-2 Particle size distribution curves of the research materials

3.1.2 ATTERBERG LIMITS

The Atterberg limits tests were conducted to observe the change of the behaviour of materials as they are moistened. Materials containing clay usually have high plasticity index. Good quality fill materials are normally non-plastic. The Atterberg limit tests comprise Liquid Limit (LL), Plastic Limit (PL), and Shrinkage Limit (SL). The Plastic Index (PI) is used to measure the plasticity and it is the difference between of Plastic Limit and the Liquid Limit (LL-PL). Method A2 and A3 of TMH1 were followed to determine the Liquid Limit and Plastic Limit respectively.

3.1.3 PARTICLE SHAPE

Particle shape was characterised by roundness. Visual assessment of images from an optical microscope (Figure 3-3) and chart developed by Krumbein (1941) were used for interpretation. Krumbein (1941) recommended the measuring of at least 25 particles of the whole sample. For this study, roundness was determined for each size fraction, 20 particles were analysed for each particle size from the sieve analysis and then the average of roundness was calculated by considering the percentage each fraction has in the sample. Finally, the roundness categories were determined using Figure 3-4.

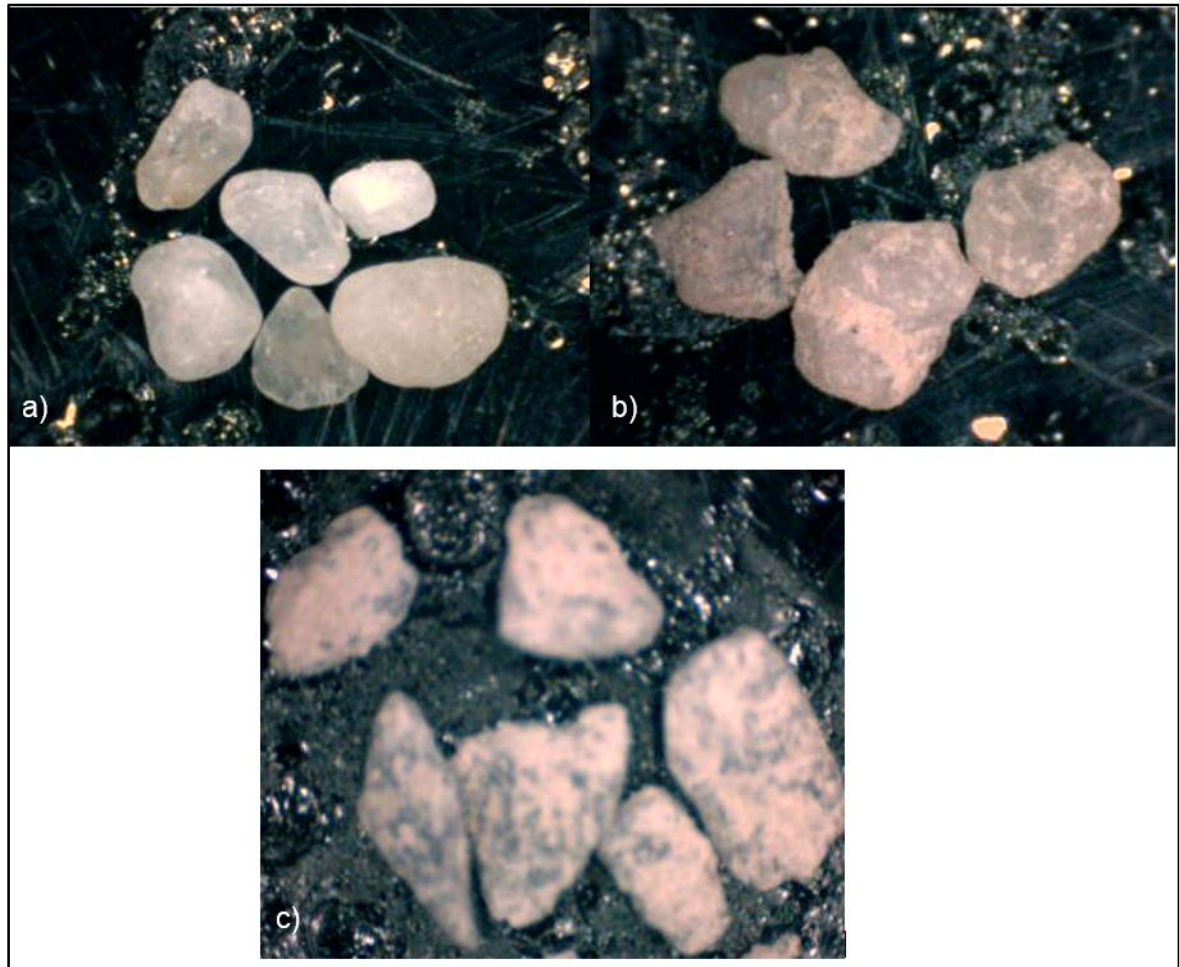


Figure 3-3 Particle shape of research materials a) Philippi sand b) Malmesbury sand c) crusher dust

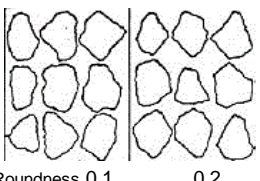
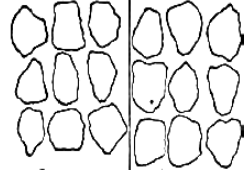

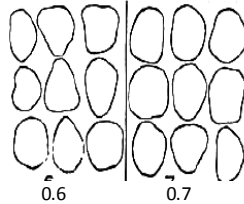
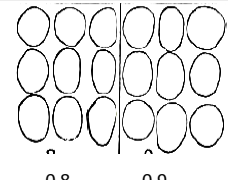
| Roundness | Krumbein image | Range | Average |
|--------------|---|-----------|---------|
| Angular |  Roundness 0.1 0.2 | 0.1-0.26 | 0.18 |
| Subangular |  0.3 0.4 | 0.26-0.42 | 0.34 |
| Subrounded |  0.5 | 0.42-0.58 | 0.5 |
| Rounded |  0.6 0.7 | 0.58-.74 | 0.66 |
| Well Rounded |  0.8 0.9 | 0.74-0.9 | 0.82 |

Figure 3-4 Roundness categories, Krumbein images and range of roundness modified from Krumbein (1941) (Edil *et al.* 2007)

3.1.4 MODIFIED AASHTO COMPACTION TESTS

Modified AASHTO Compaction tests were carried out to determine the Maximum dry density (MDD) and the Optimum moisture content (OMC) of crusher dust, Malmesbury and Philippi sands. Method A7 (TMH1 1986) was followed to determine the MDD and OMC. The MDD and OMC obtained were used as a reference for compaction of specimens used in the direct shear tests and for the axial and oblique pull-out tests. Figure 3-5 shows the automatic Modified AASHTO compaction machine used for testing.



Figure 3-5 Modified AASHTO compactor machine

3.2 SHEAR STRENGTH TESTING

Direct Shear testing was conducted using 100x100 mm shear box on all three research materials. The effect of three factors on shear strength and dilation were investigated, namely moisture content, density and normal stress level.

The crusher Dust was used as a reference material and testing was undertaken at three compaction effort (80%, 85% and 90% Mod AASHTO MDD) and two moisture conditions (saturated and unsaturated).

Tests on the Malmesbury and Philippi sands were conducted at unsaturated and saturated conditions using one compaction effort namely 85% Mod AASHTO MDD.

Three normal pressures (50 kPa, 100 kPa and 150 kPa) were used in all tests. The purpose was to measure the friction angle and observe the influence of normal pressure on dilation. Two tests were conducted for each combination in order to check the reliability of the results, but a third test was conducted when there was divergence in result of the first two tests. Figure 3-6 shows a summary of tests conducted.

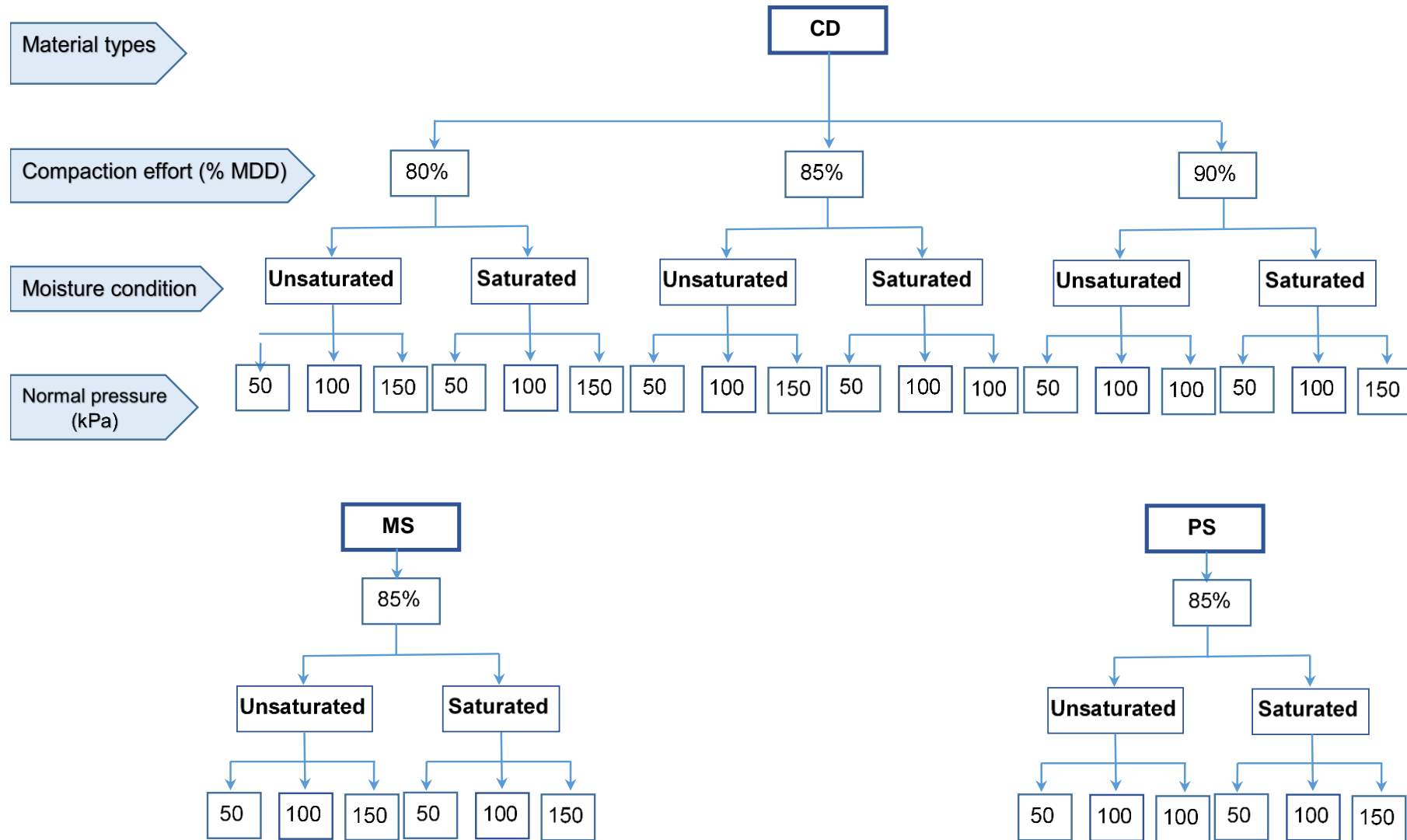


Figure 3-6 Flowchart of shear test experimental design

3.1.5 SPECIMEN PREPARATION

Preparation of samples was almost the same for the three materials, except the number of layers used for compaction. Specimen preparation was according to ASTM (2003) and compaction was performed inside the 100x100mm direct shear box. The following steps represent in detail the preparation procedure.

- As mentioned before crusher dust (CD) was used as a reference material. Therefore, three compaction efforts were used. Compaction of the CD was done using a compactor hammer (see Figure 3-7). The total mass of the hammer and platter was 3029g, 2097 g for the hammer alone. The hammer was dropped from 25 cm. Two layers were used (see Table 3-1) to compact the specimen. This is due to higher compaction efforts required for well graded material such as CD. Attention was paid to ensure that the interface between layers did not coincide with the shear plane in the shear box. As recommended by ASTM (2003), the top of the first layer was scarified (see Figure 3-8) prior to the addition of the second layer to allow a full adhesion. 6, 16, and 22 number of blows per layer were obtained after attempting various trials.

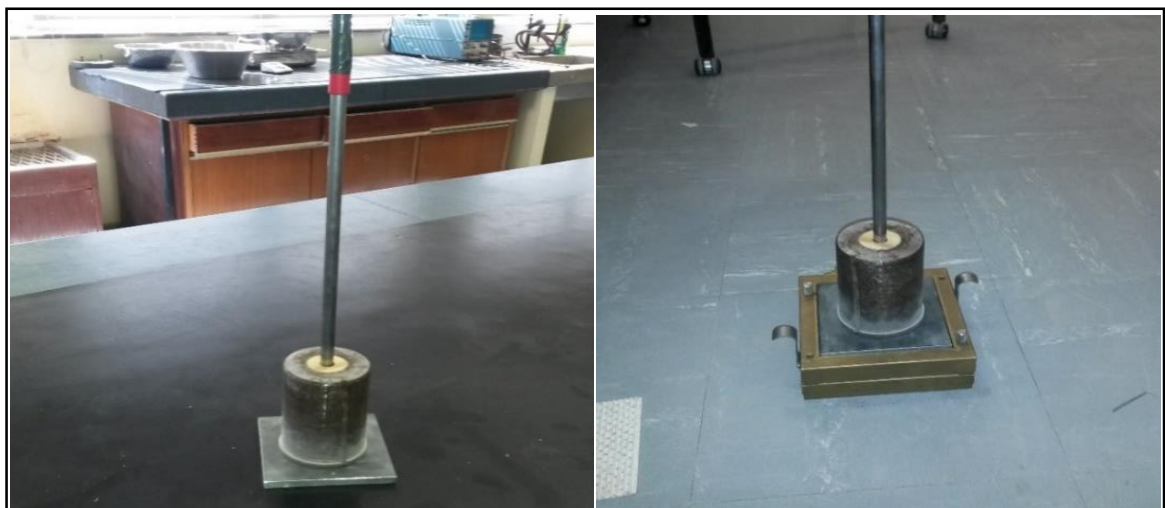


Figure 3-7 Shear box compactor



Figure 3-8 Illustration of sample preparation

Table 3-1 Compactor hammer and layer details of CD

| Types of material | CD | | | MS | PS |
|--------------------------------------|------|-----|-----|-----|-----|
| Compaction effort (% Mod AASHTO MDD) | 80% | 85% | 90% | 85% | 85% |
| Sample prepared (g) | 500 | 500 | 500 | 500 | 500 |
| Mass of first layer (g) | 300 | | | - | - |
| Mass of second layer (g) | 150 | | | - | - |
| Total mass (g) | 450 | | | 450 | 450 |
| Number of blows per layer | 7 | 16 | 22 | - | - |
| Number of layer | 2 | | | 1 | 1 |
| Weight of hammer (g) | 2097 | | | | |
| Weight of hammer and the platen (g) | 3029 | | | | |
| Height of drop (cm) | 25 | | | - | |

- Due to the lower compaction effort required for Malmesbury and Philippi sand, the height of the specimen was measured to obtain 85% MDD Mod AASHTO rather than applying a predetermined number of blows. The compactor was used to compress the sample in order to get a required height. Dry material of 500g was mixed with water to achieve the optimum moisture content of each material for preparation of unsaturated and saturated samples.

Appendix B-1 shows details of test data and worksheet of the test.

3.1.6 SHEAR BOX AND MACHINE CONFIGURATION

Figure 3-9 and Figure 3-10 show elements of shear box and testing machine configuration.

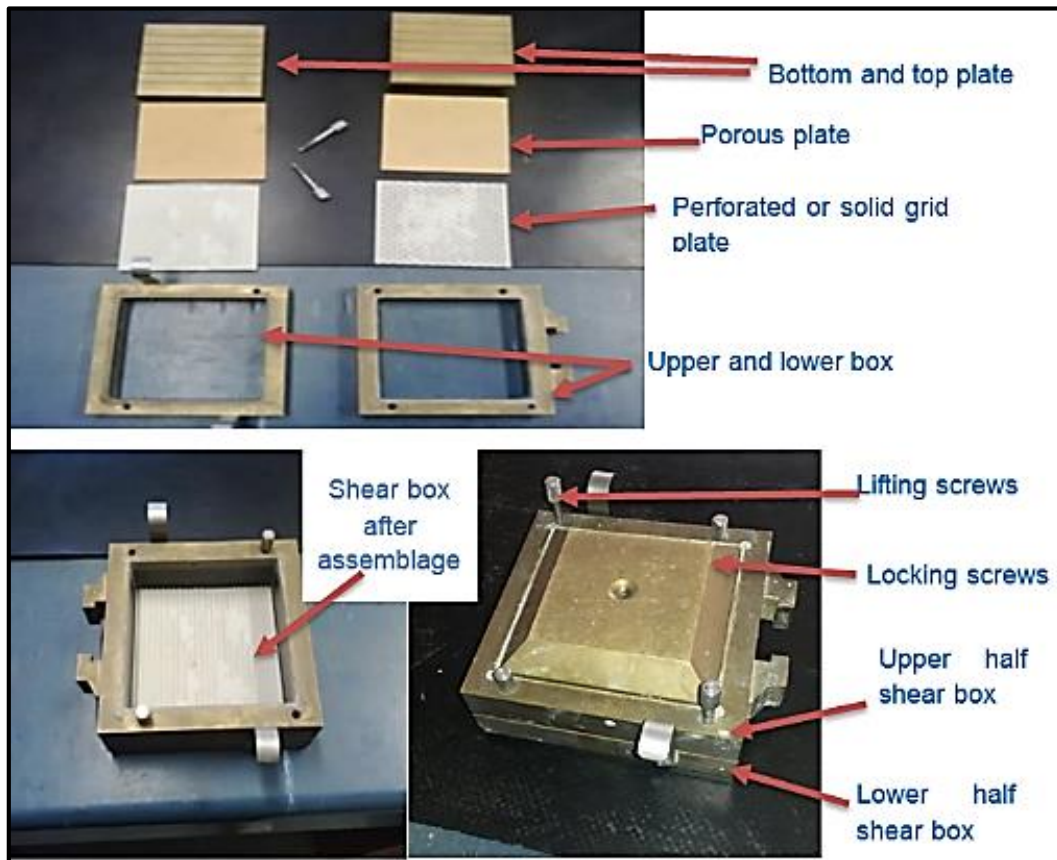


Figure 3-9 Shear box apparatus set up



Figure 3-10 Shear box apparatus for 60x60 and 100x100 mm

3.1.7 TESTING PROCEDURE

ASTM (2003) recommends that the specimen height must be at least six times greater than the maximum particle size as mentioned in the literature review, section 2.5. Therefore, particles retained by the sieve number (N^o) 4 (4.75 mm) were removed (scalped) to meet the specification. The crusher dust and Malmesbury sand were affected by the requirement. Figure 3-11 shows the distribution curve of materials after scalping.

Using studies done by Bareither et al. (2008) and Cerato & Lutenecker (2006), strain rates of 0.25 and 0.24 mm/min were calculated for saturated tests. Based on these studies, a strain rate of 0.2 mm/min was adopted for saturated tests and 0.8 mm/min for unsaturated tests.

Prior to the test, the specimen was soaked in water for 30 minutes. This was enough for 100x100 mm specimen to be fully saturated. Additionally, the specimen was kept fully submerged before and during the test in order for the specimen to stay saturated. Before starting the test, the gap screws were lifted up by half a rotation in other words, to approximately 0.5-0.64 mm to avoid the metal-metal friction between the upper and lower halves of the shear box. For unsaturated test, the specimen was shear immediately after compaction without being soaked. Readings were recorded every six seconds, which is every 0.08 mm and 0.02 mm for unsaturated and saturated respectively.

At least two tests were performed for each variable test, and then the average of the two was taken.

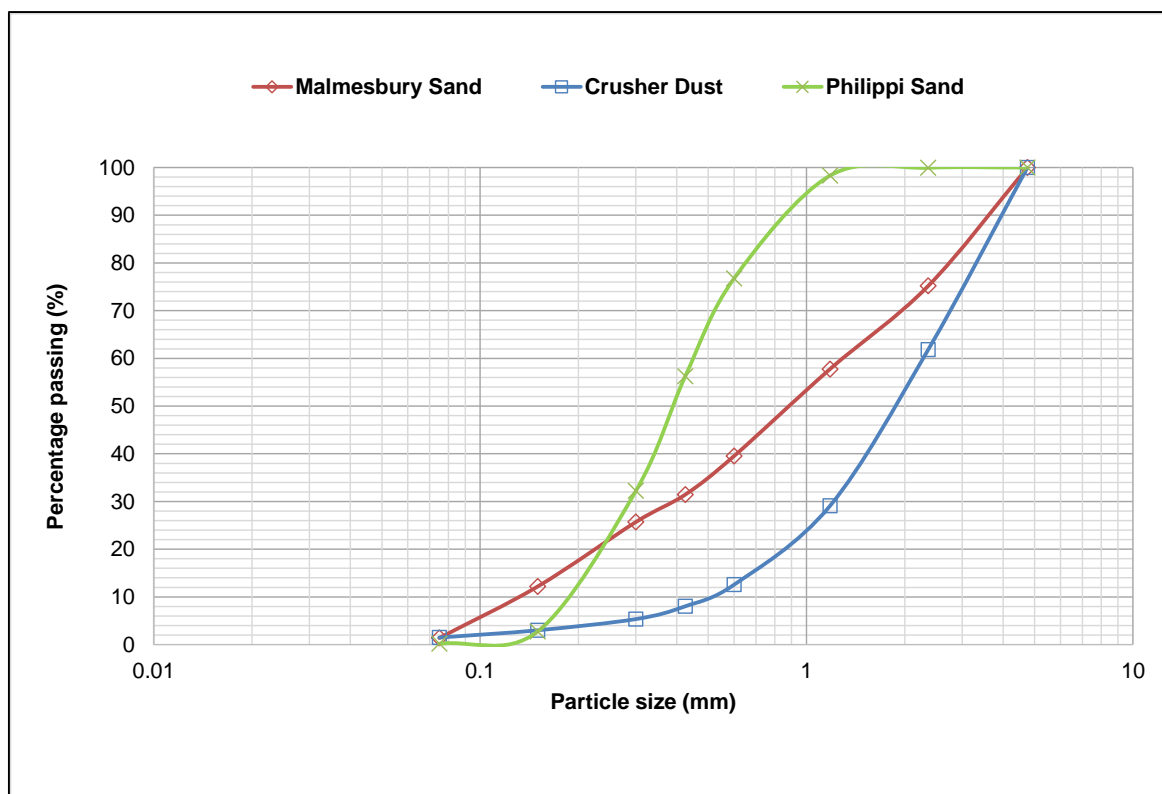


Figure 3-11 Distribution curve of the research material after scalping

3.3 LOAD EXPERIMENT DESIGN

In order to evaluate the performance of pull-out capacity (vertical and oblique) of solar panel posts for different materials, an experimental plan was developed as shown in Figure 3-12. The aim was to evaluate the influence of the following variables on uplift load capacity:

- Material type: crusher duster (passing 6.7 mm sieve), Malmesbury sand (passing 6.7 mm sieve) and Philippi sand (passing 4.75 mm sieve).
- Density: three compaction efforts for crusher dust (CD), one for Malmesbury sand (MS), and one for Philippi sand (PS).
- Displacement ratio: Three compaction efforts for CD were used, one for MS, and one for PS.
- Testing conditions: CD: at dry, unsaturated and saturated, MS: at unsaturated and saturated, PS: at unsaturated and saturated.

Vertical pull-out tests at lower and higher compactions under dry conditions were run additionally to the tests in Figure 3-12. More details of the experimental program of both axial and oblique tests are shown in Figure 3-21 and Figure 3-22 respectively.

An Instron 2000 testing machine was used for the axial load and oblique pull-out test. It is important to acknowledge that the push in and pull-out were conducted using the static load.

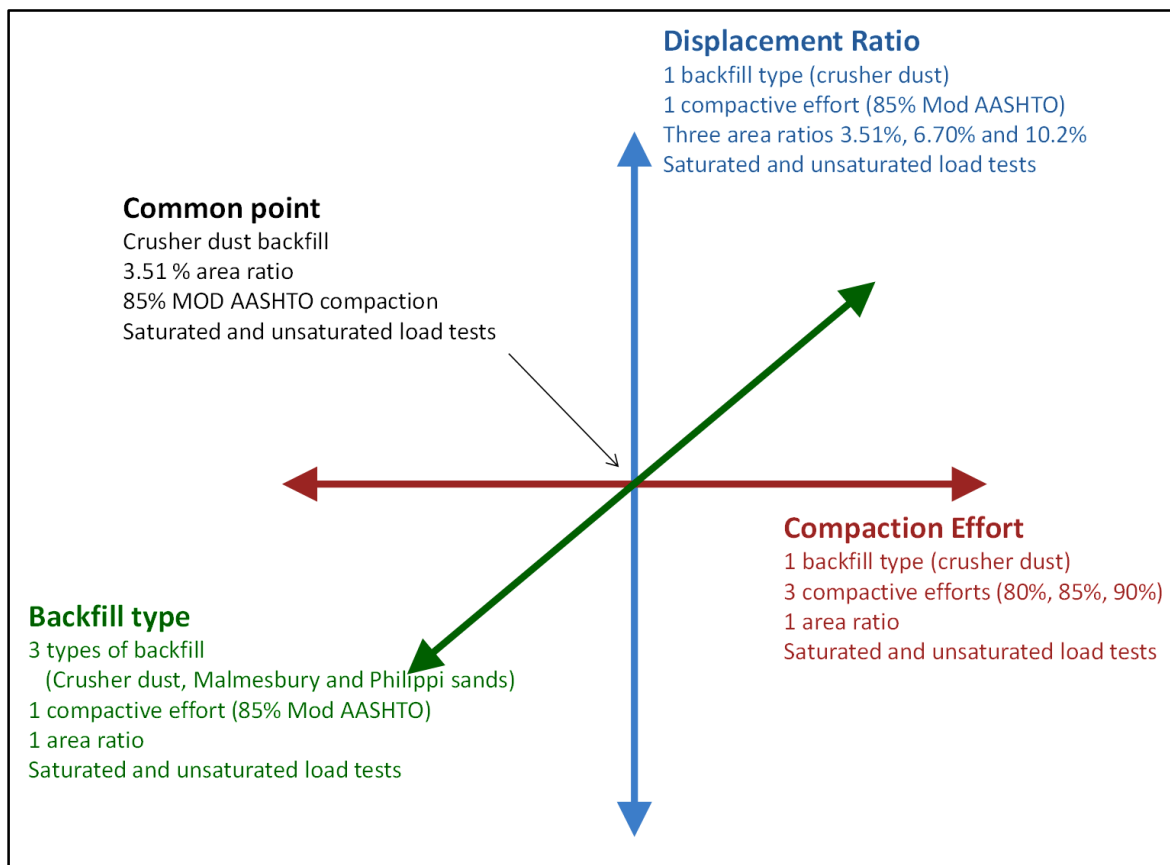


Figure 3-12 Summary of experimental program

3.1.8 DIMENSION AND PROPOSED SIZES FOR EXPERIMENTAL WORK

On a typical solar power project, the diameter of the drilled hole is approximately 200 mm and the hole is drilled to a depth of about 1.3 m. After placement and compaction of the backfill material in the hole, the post is driven to a nominal depth of 1.15, i.e. 150 mm above the bottom of the hole (Day 2014b). This post is “top-hat” section with the dimensions shown in Figure 3-13 a). For the purposes of this research, it was assumed that the hole has been drilled into rock over its entire depth. As such, a steel pipe (see Figure 3-14) was used to represent the hole.

For the purposes of the experimental research, half scale was adopted. In other words, the pile hole was modelled using a 104 mm diameter pipe (representing the 200 mm diameter (hole), 650 mm long (Figure 3-14). Regarding the post, 700 mm iron sections were used (see Figure 3-13 b)) due to its availability from many steel merchants.

The area ratios (area of post divided by area of the hole), with the above dimensions, are 3.51 % (50x50x3 mm), 6.7% (50x50x6 mm) and 10.21% (50x50x9mm) (Figure 3-13 b). It is important to mention that the post platens (in Figure 3-14) were designed and welded so that their center of area coincided with the center of area of the post to avoid eccentricity loading

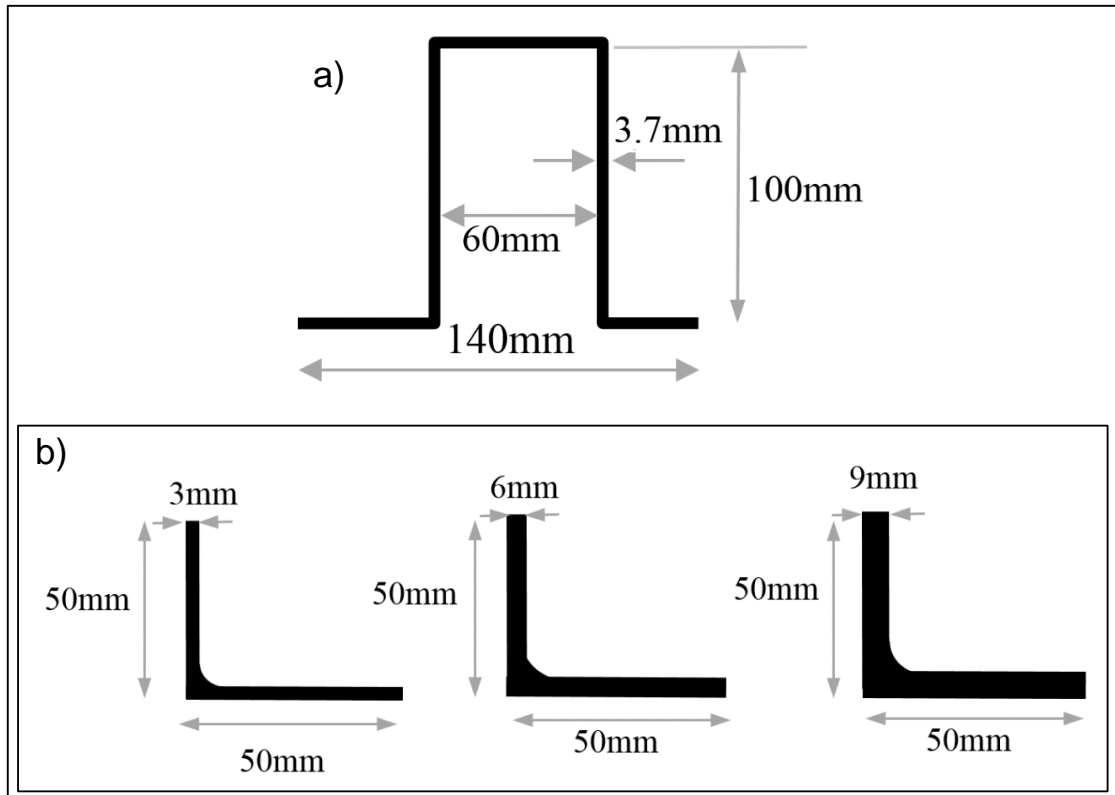
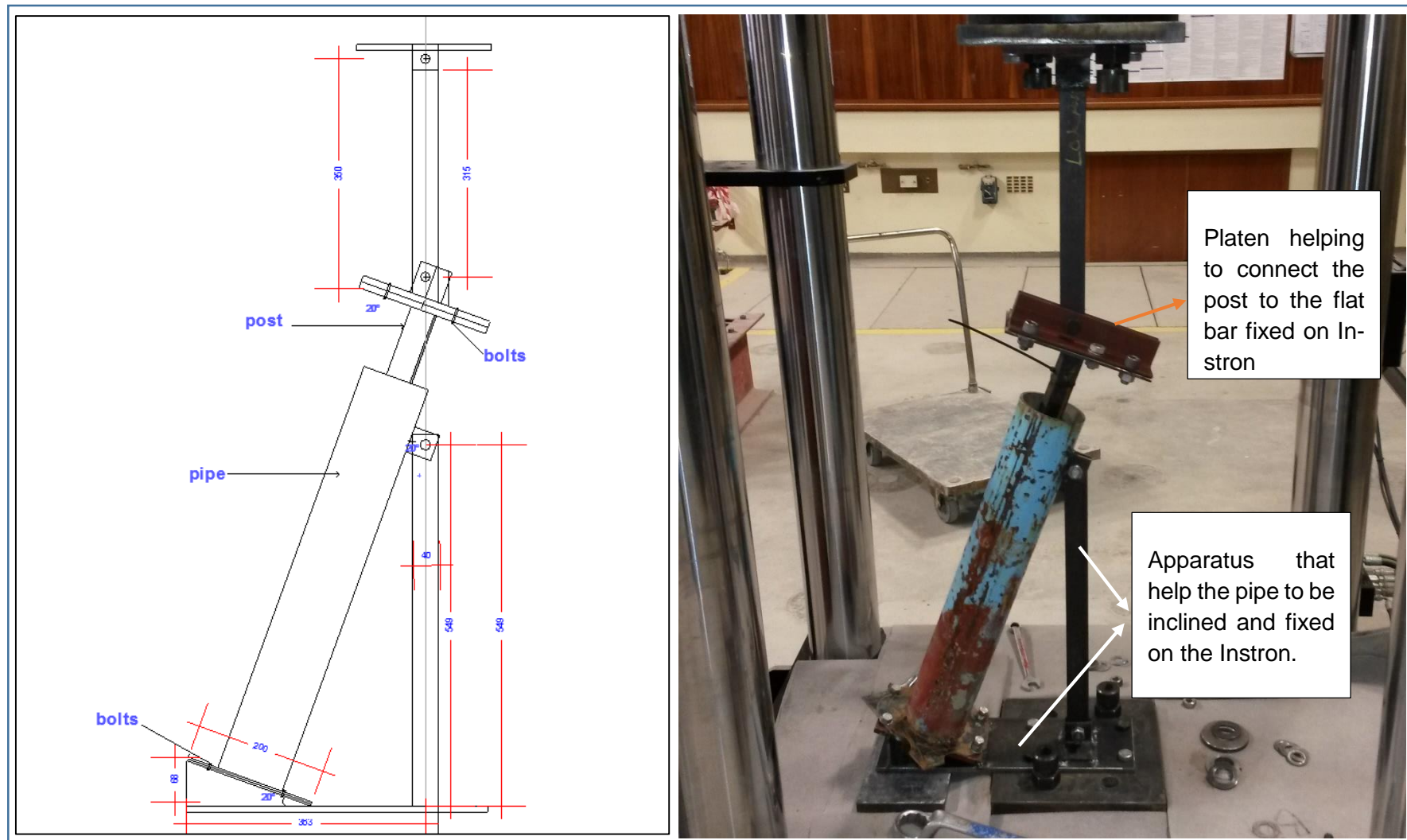


Figure 3-13 a) Top-hat section of a typical solar project and b) L base section of the research experimental work



Figure 3-14 Experimental pipe and post

Furthermore, a setup design for oblique pull-out testing was conceived. Usually, the solar panels are tilted about 20 degrees from horizontal. The wind forces act mainly perpendicularly to the plane of the panel. To simulate this inclined loading, the pipe was inclined to 20 degrees to the vertical in the testing frame so that the forces are applied at 20 degrees of the pipe. Figure 3-15 shows schematic design and picture of the pull-out test. The bottom flat bar (see Figure 3-15) fixed at the Instron base and the second flat bar fixed on the Instron ram were designed to be aligned to avoid any moment caused by the eccentricity. The load applied by the testing machine was transmitted to the top of the post using a tie that was pinned at both ends to allow the top of the post to move laterally and rotate in response to the load.



3.1.9 SPECIMEN PREPARATION

All the three materials were compacted to specified compaction density based on the MDD values from Mod AASHTO test. Each sample used for load tests was a representative of the research sample and this was achieved using quartering method described in TMH1 (1986 A1(a)). The laboratory mixer shown in Figure 3-17 was used to mix the sample of 10.5 kg and water to achieve a proper mixing. Four blows around the sides of the pipe and one blow in the middle were adopted to compact the materials (see Figure 3-16) compared to 8 blows around and three in the middle of the mould used in TMH1 (1986). The reason is due to the small pipe diameter of 104 mm compared to the 152.5 mm of TMH1 (1986). To obtain a specified compaction degree, materials were compacted in several layers depending on the materials and compaction degree required. Appendix B-2 shows the procedure of measuring the compaction density and worksheet data. The details of compaction for each material are described in the following steps:

- Crusher dust: 7 to 8 layers were used to compact the material in the pipe. TMH1 (1986) manual rammer compaction was used for compaction. 5, 10, and 20 blows per layer were used to obtain 80%, 85% and 90% MDD Mod ASSHTO respectively.
- Malmesbury sand: Proctor compaction rammer was used to compact material in 5 layers to obtain the target value 85% MDD Mod AASHTO.
- Philippi sand: No compaction was needed to obtain 85% MDD Mod AASHTO for Philippi sand. After mixing, the sample was poured into the pipe and shaken 5 times, to obtain the 85% MDD compaction. Due to the uniform and fine particle sizes of PS, the 85% compaction degree was achieved without additional compacting.

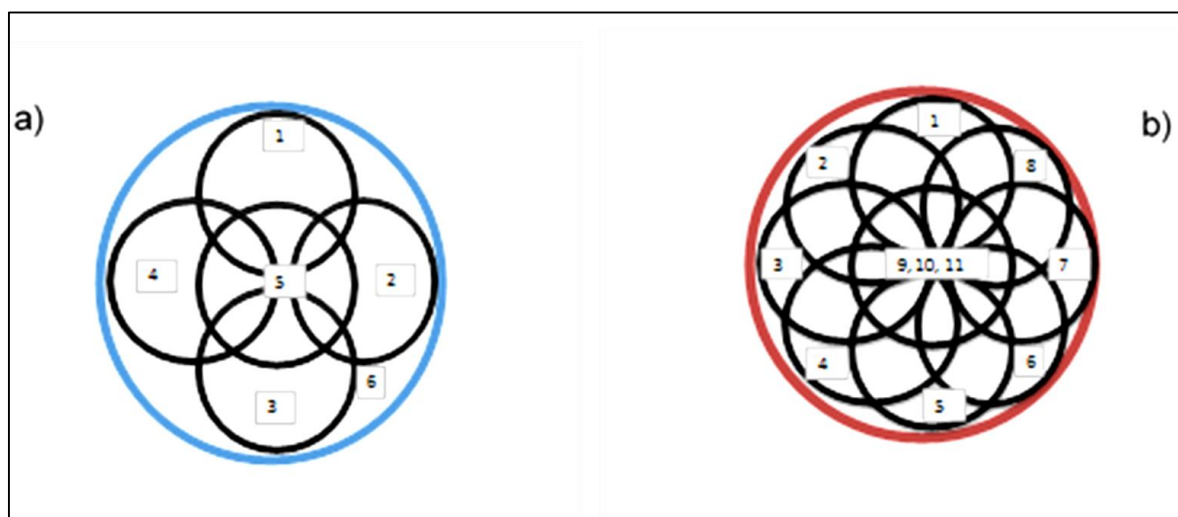


Figure 3-16 Rammer pattern for compaction: a) the one adopted b) TMH1



Figure 3-17 Laboratory mixer

The specimen preparation was the same for both axial and oblique tests. The material was placed to within 40 to 70 mm of the top of the pipe i.e. the specimen did not entirely fill the pipe.

3.1.10 GENERAL CONFIGURATION OF INSTRON 2000

Figure 3-18 shows the photograph of Instron 2000 machine. The system is automatic and consists of load frame with the capacity of 250 KN and a computer control system.

The Instron load frame consists of:

- compression and tension testing methods
- manual control over ram position: jog up and down together with fine adjustment
- computer system: maximum load and end of displacement setting for specimen protection.
- high precision load and displacement of 0.00001 N and 0.00001 mm respectively.



Figure 3-18 Photograph of Instron 2000

3.1.11 TESTING PROCEDURE

3.3.1.1 Push-in Procedure

The push in procedure was conducted under dry and unsaturated conditions. Figure 3-19 illustrates the test configuration for push-in tests. The steps that were followed are outline below:

1. The specimen was placed and fixed on the Instron machine using bolts
2. The post was then fixed on the instron ram using bolts
3. After, the position of the post was adjusted using the jog down and fine positioning for the post to touch slightly the top of the sample prior for testing.
4. Finally, the post was pushed into the compacted soil until it was 60 mm from the bottom of the pipe.

The push in test was run at 50 mm per minutes. After the completion of the push-in test, the specimen was rested overnight before the pull-out test, in order for the soil to relax. For case of the saturated pull-out test discussed in the following section, the specimen was removed from Instron and soaked overnight in water tank for the specimen to be saturated.



Figure 3-19 Positioning and push in of the post

3.3.1.2 Pull-out Procedure

Axial pull-out and oblique pull-out tests were conducted in different ways. For the former, the specimen after push in and relaxing overnight (and saturation, if required), was positioned vertically on the Instron and then pull-out test was performed. In addition to the axial pull-out test configuration shown in Figure 3-21, one specimen, compacted at 90% MDD Mod ASSHTO was tested under unsaturated conditions after 21 days to evaluate the effect of time (aging) on the pull-out capacity. A period of at least 20 days was recommended by Chow & Jardine (1998) for the implication of setup (effect of time) on piles. Therefore, 21 days was opted. Both axial pull-out and oblique pull-out tests were run at 10mm per minute as pull-out rate displacement.

For oblique pull-out, the specimen (pipe) was inclined and fixed on the step up frame (see Figure 3-15). Unsaturated and saturated tests were conducted. The following steps describe the test configuration and the pull-out test procedures for the oblique tests:

1. First, the set up apparatus was fixed on the Instron base (see Figure 3-15)
2. The specimen (pipe and post) was then positioned and fixed on the set up using bolts

3. The flat bar was fixed on the Instron ram, then positioned by means of Jogging and fine positioning to allow the flat bar to be connected to the platen on the post (Figure 3-15)
4. Finally, the test was run

The following are Figure 3-20 showing the behaviour of soil during the pull-out test. It can be observed in Figure 3-20 that some the soil inside the angle iron of the post was pulled upwards with the post. In addition, Figure 3-21 and Figure 3-22 showing the summary of axial and oblique pull-out tests conducted respectively.



Figure 3-20 Soil behaviour and condition when a post is been pulled-out

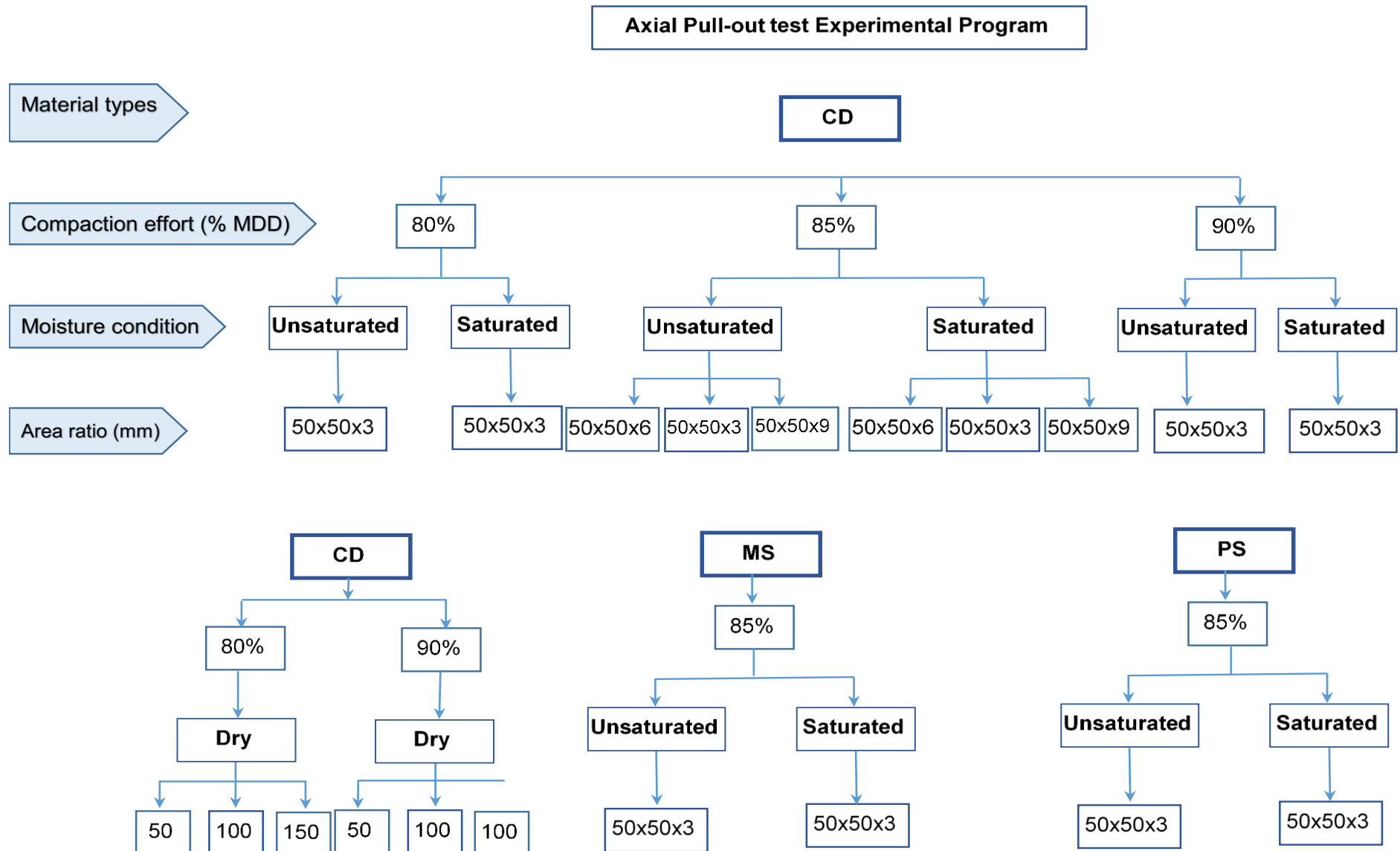


Figure 3-21 Axial pull-out test experimental program

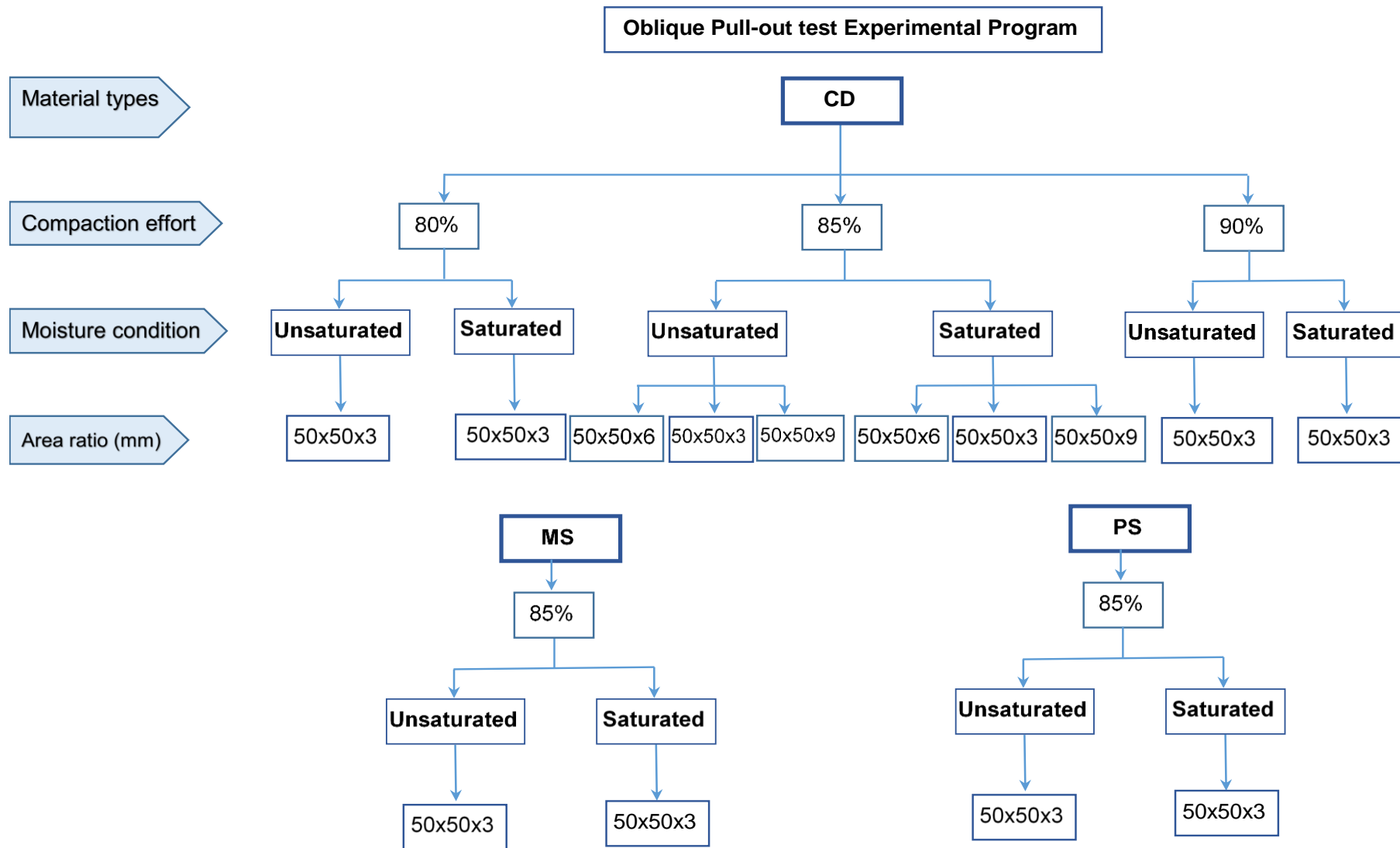


Figure 3-22 Oblique pull-out test experimental program

CHAPTER 4 LABORATORY TEST RESULTS AND DISCUSSION

This chapter presents the summary of the classification test results of crusher dust (CD), Malmesbury sand (MS), and Philippi sand (PS). The analysis of shear strength and dilation of materials compacted at different percentage of Mod AASHTO MDD are also included. Tabulations and graphical presentations were used to analyse the test results.

4.1 CLASSIFICATION TEST RESULTS

Table 4-1 is a summary of the classification of the CD, MS, and PS materials. This classification includes sieve analysis, Atterberg Limits, particle shape, and compaction test results. The description of the materials was based on unified classification system (UCS).

4.1.1 SIEVE ANALYSIS

The maximum aggregate size of CD and MS materials is 6.7mm while that of PS is 4.75mm. The coefficient of curvature (C_z) and grading modulus (GM) in Table 4-1 indicate that crusher dust (CD) is a better material than Malmesbury sand (MS) and Philippi sand (PS). A C_z of 1.18 and GM of 2.35 classify the CD as a well graded. On the other hand, a coefficient of curvature and grading modulus of 0.75 and 1.97 respectively for MS, 0.97 and 1.44 for PS classifies the materials as poorly graded and poor quality materials. In addition, MS has a large range of particle sizes compared to CD and PS. The coefficient of uniformity (C_u) of MS, CD, and PS is 10.67, 4.73, and 2.5.

4.1.2 ATTERBERG LIMITS

The Atterberg Limits of the three material types, CD, MS, and PS indicate that the materials are non-plastic. The Atterberg Limit tests were conducted on materials passing the 0.425 mm sieve. Given that the moist samples are non-cohesive, the testing of the plastic limit by rolling the sample could not be carried out. Therefore, materials were considered as non-plastic.

4.1.3 PARTICLE SHAPE

The particle shape was determined by its roundness. Table 4-1 presents the roundness of CD, MS, and PS. CD was found to be subangular whereas MS and PS are subrounded and rounded respectively. Crusher dust is a processed material formed by crushing hornfels rock. On the other hand, Malmesbury and Philippi sand are natural soil.

4.1.4 COMPACTION TESTS

The Maximum Dry Density (MDD) of CD is higher than that of MS and PS. This is indicative of the fact that the CD is better graded, and the amount of fines is lower than in MS and PS. In addition, the Optimum Moisture Content (OMC) is considerably higher in PS than in CD and MS due to the amount of fines. Figure 4-1 illustrates compaction curves of CD, MS, and PS, while Table 4-1 presents the MDD and OMC results of CD, MS, and PS.

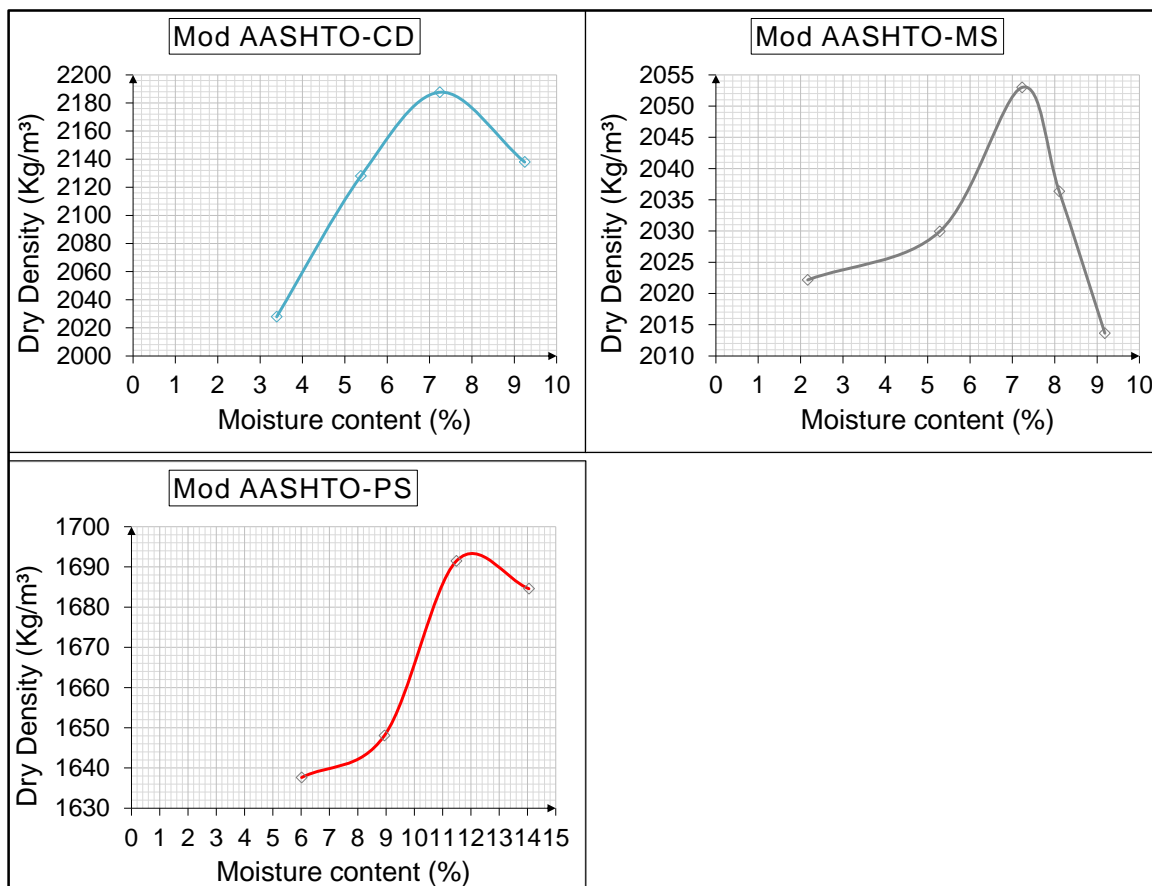


Figure 4-1 Compaction curves a) crusher dust b) Malmesbury sand c) Philippi sand

Table 4-1 Summary of research materials characteristics

| Particle size [mm] | CD Cumulative Passing [%] | MS Cumulative Passing [%] | PS Cumulative Passing [%] |
|--|---------------------------|---------------------------|---------------------------|
| 6.7 | 100.0 | 100.0 | 100.0 |
| 4.75 | 90.5 | 95.0 | 100.00 |
| 2.36 | 56.0 | 71.4 | 99.95 |
| 1.18 | 26.3 | 54.9 | 98.30 |
| 0.6 | 11.4 | 37.6 | 76.76 |
| 0.425 | 7.3 | 29.9 | 56.23 |
| 0.3 | 4.8 | 24.4 | 32.22 |
| 0.15 | 2.7 | 11.6 | 2.75 |
| 0.075 | 1.3 | 1.3 | 0.18 |
| Property | CD | MS | PS |
| Cu | 4.73 | 10.67 | 2.5 |
| Cz | 1.18 | 0.75 | 0.97 |
| d ₅₀ | 2.1 | 1 | 0.28 |
| GM | 2.35 | 1.97 | 1.44 |
| UCS | Well graded | Poor graded | Poor graded |
| Liquid Limit (%) | Non-Plastic | Non-Plastic | Non-Plastic |
| Plastic Limit (%) | Non-Plastic | Non-Plastic | Non-Plastic |
| Roundness values | 0.28 | 0.44 | 0.59 |
| Roundness Category | Subangular | Subrounded | Rounded |
| Maximum Dry Density (MDD) (Kg/m ³) | 2187.63 | 2053 | 1693 |
| Optimum Moisture Content (OMC) (%) | 7.24 | 7.3 | 12 |

4.2 DIRECT SHEAR STRENGTH TESTS

This section presents and discusses the results of the direct shear strength testing described in Chapter 3. For each test, the force required to shear the material, the relative horizontal displacement between the upper and lower boxes, and the vertical displacement, which indicates changes of volume were recorded. It is important to mention that the compaction densities achieved were not exactly the same values as the ones proposed in experimental design in Chapter 3. 82% Mod AASHTO MDD was achieved instead of the target value of 80% whereas an average of 86%, and 89% were recorded for 85% and 90% target values respectively. This does not materially affect the objective of the research as a sufficiently wide range of densities was achieved to assess the effect of this parameter. All tests were fully drained and the materials were tested in an unsaturated and saturated conditions.

4.2.1 CRUSHER DUST

4.2.1.1 Shear Stress and Horizontal Displacement Relationship

Figure 4-2 illustrates the relationship of shear stress to the horizontal displacement of crusher dust (CD). Each test was conducted at three normal pressure (50, 100 and 150 kPa) and three compaction degrees (nominally 80%, 85% and 90% Mod AASHTO MDD) under unsaturated and saturated conditions.

As expected, the application of higher compaction efforts and normal stresses resulted in general increase in shear resistance. The shear resistance decreased with specimen saturation.

In Figure 4-2 a), b) and c), CD compacted at 90% exhibited higher shear stress than the ones compacted at 80% and 85%. For instance, at constant normal pressure 150 kPa-unsaturated, the maximum value of shear stress increases from 145.96 at 80% to 180.16kPa at 90%. This implies an increase of 18.98%. Likewise, a reduction in maximum shear stress was observed when the specimen was saturated. For instance, at 50 kPa normal pressure and 85% Mod AASHTO MDD, the maximum shear stress was reduced from 104.90kPa to 92.17kPa. This represents a 12.14% reduction.

The summary of the maximum shear stress results is presented in Table 4-2.

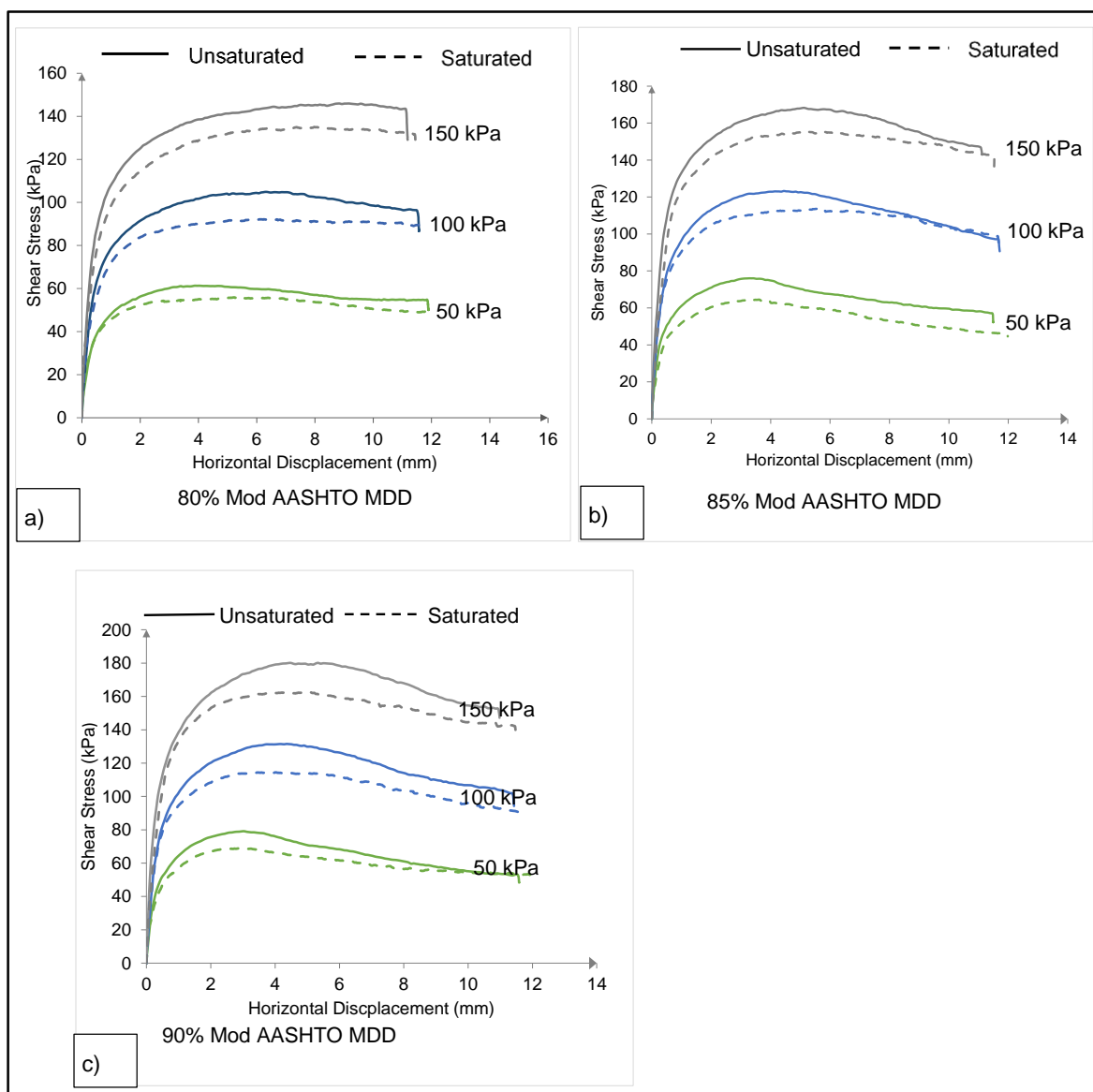


Figure 4-2 Shear stress versus horizontal displacement of crusher dust (CD)

4.2.1.2 Shear Stress and Normal Stress Relationship

Figure 4-3 presents the Mohr-Coulomb failure envelope for the CD at three different compaction degrees (80%, 85%, and 90% Mod AASHTO MDD) under unsaturated and saturated conditions. Solid lines and dashed lines represent unsaturated and saturated conditions respectively.

The Mohr-Coulomb envelope was obtained by plotting the shear stresses at failure from the graph in Figure 4-2, against their corresponding normal pressures. Thereafter, a linear regression was carried out to determine the equation of the line of best fit through the three points representing the Mohr-Coulomb envelope. The cohesion c is the constant value in the equation (intercept on vertical axis) whereas friction coefficient ($\tan\phi$) is the regression coefficient (slope of line).

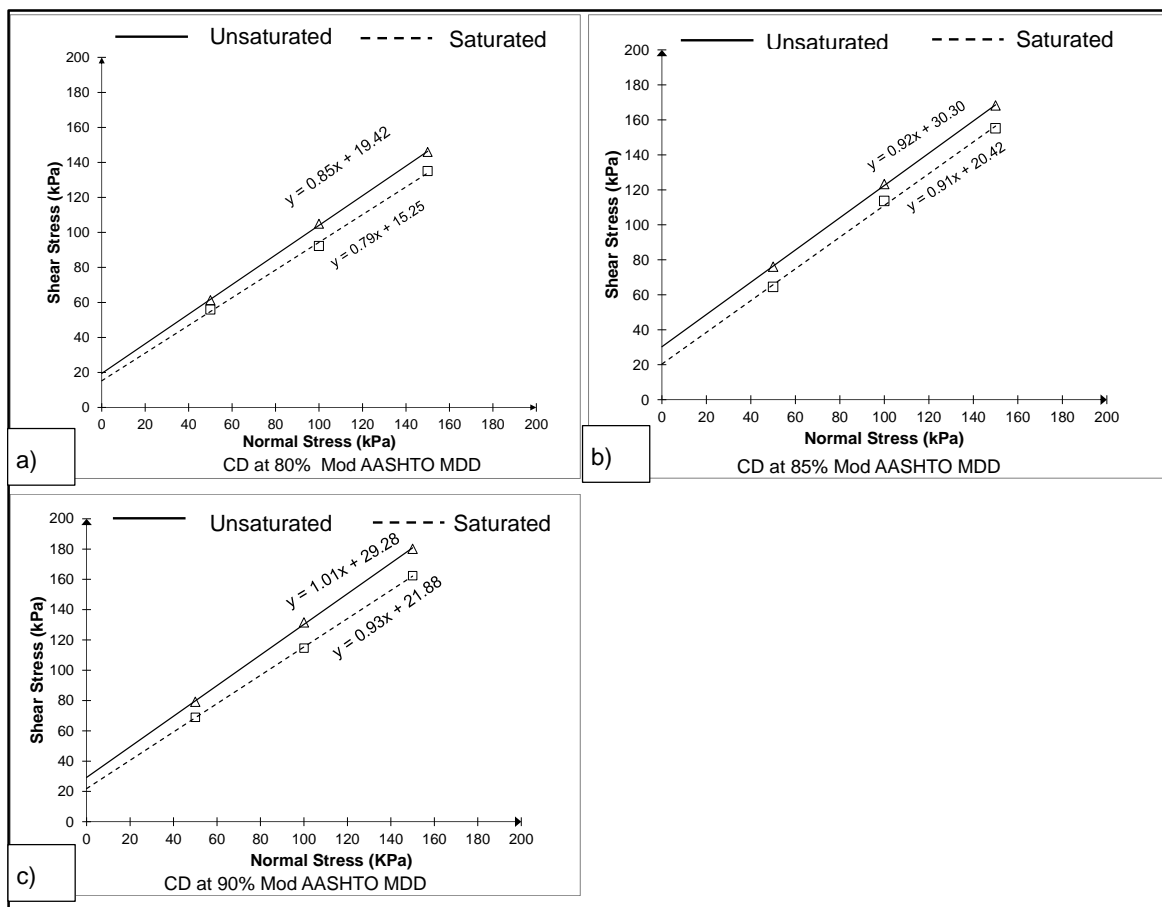


Figure 4-3 Relationship of shear stress to normal stress of crusher dust (CD)

Figure 4-3 illustrates the effects of compaction degree and saturation on the coefficient $\tan\phi$. This coefficient $\tan\phi$ increases with compaction degree for both the saturated and unsaturated tests. Saturation of the material decreases the value of $\tan\phi$.

Table 4-2 and Figure 4-4 summarise the results of the coefficient friction and the cohesion of CD material compacted at different Mod AASHTO MDD degree under unsaturated and saturated conditions. From the results, the following interpretations are made:

- The compaction degrees affected the friction coefficient and cohesion. At unsaturated conditions, the friction coefficient $\tan\phi$, increases about 8% from 80% to 85% compaction degree and 9% from 85% to 90% compaction degree. An increase of approximately of 36% was observed for the cohesion from 80% to 90% compaction degree. This increase in friction coefficient can be explained by the parking of particles. This thus causes an increase in particles resistance to the shear force.
- The addition of water decreases both the friction coefficient and the cohesion. For instance at 80% Mod AASHTO MDD, the friction coefficient reduces about 7%. This reduction can be explained by the concept presented in Section 2.5.2 of Chapter 2, which is that the shear strength reduces with addition of water caused by the removal of stabilised force at contact point of particles. This reduction thus allowed particles to slide over one another easily when a shear force is applied. Moreover, the cohesion c reduced with saturation. At 80%, the cohesion c reduced about 22%.

Table 4-2 Summary of Maximum shear stress and horizontal displacement at failure of crusher dust (CD)

| Material type | Maximum size of aggregate (mm) | Testing moisture condition | Mod AASHTO MDD average(%) | Normal Stress (kPa) | Maximum Shear Stress (kPa) | Horizontal Displacement at Failure (mm) | $\mu=\tan\phi$ | ϕ (°) | C (kPa) |
|---------------|--------------------------------|----------------------------|---------------------------|---------------------|----------------------------|---|----------------|------------|---------|
| CD | 4.75 | Unsaturated | 82.1 | 50 | 61.3 | 3.87 | 0.85 | 40.24 | 19.42 |
| | | | 82.1 | 100 | 104.9 | 6.30 | | | |
| | | | 82.4 | 150 | 146.0 | 9.16 | | | |
| | | Saturated | 81.9 | 50 | 55.9 | 5.23 | 0.79 | 38.35 | 15.25 |
| | | | 81.8 | 100 | 92.2 | 6.11 | | | |
| | | | 82.5 | 150 | 135.0 | 7.98 | | | |
| | | Unsaturated | 86.6 | 50 | 76.0 | 3.29 | 0.92 | 42.68 | 30.30 |
| | | | 86.5 | 100 | 123.3 | 4.44 | | | |
| | | | 86.7 | 150 | 168.3 | 5.13 | | | |
| | | Saturated | 85.7 | 50 | 64.5 | 3.61 | 0.91 | 42.20 | 20.42 |
| | | | 85.7 | 100 | 113.6 | 5.70 | | | |
| | | | 85.6 | 150 | 155.2 | 5.29 | | | |
| | | Unsaturated | 89.8 | 50 | 79.2 | 3.03 | 1.01 | 45.29 | 29.28 |
| | | | 88.5 | 100 | 131.5 | 4.35 | | | |
| | | | 89.8 | 150 | 180.2 | 5.34 | | | |
| | | Saturated | 88.7 | 50 | 69.0 | 2.89 | 0.93 | 43.07 | 21.88 |
| | | | 89.1 | 100 | 114.6 | 3.84 | | | |
| | | | 87.2 | 150 | 162.5 | 5.11 | | | |

4.2.1.3 Effects of Normal Pressure and Compaction Degrees on Shear stress

Figure 4-4 summarises the shear strength test of CD. A linear regression typifies the effect of normal stress at different compaction degree to the maximum shear stress. The maximum shear stress increases with both normal pressure and compaction effort, it decreases with saturation.

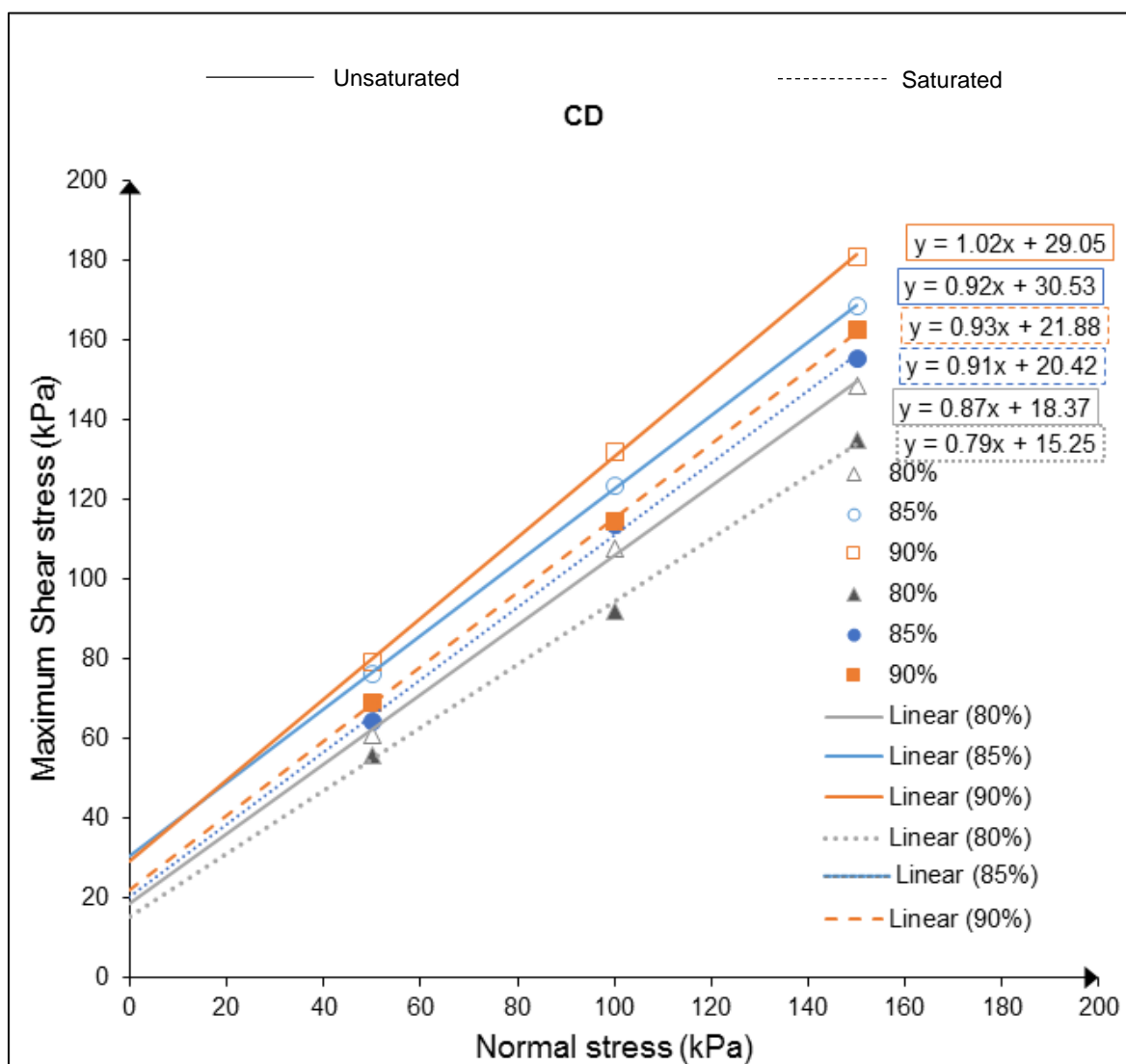


Figure 4-4 The effect of normal pressure and compaction effort on maximum shear stress of CD

4.2.1.4 The Effect of Compaction Degree on Angle of Friction

Figure 4-5 illustrates the relationship between friction angles and various compaction degrees. The relationship of friction angle to compaction degree provides insight into the influence of compaction in altering the mechanical properties of the material. The relationship follows a linear trend. Figure 4-5 shows that the friction angle increases with an increase of compaction degree whereas it reduces with saturation, which supports the literature review.

At unsaturated condition, the friction angle of crusher dust increased about 11% from 80% to 90% Mod AASHTO MDD compaction degree. However, at constant compaction effort, the friction angle was reduced with saturation. A reduction of 5% was observed at 80% and 90% Mod AASHTO MDD compaction degree. This is an indicative of the influence of densification and saturation of material on friction angle.

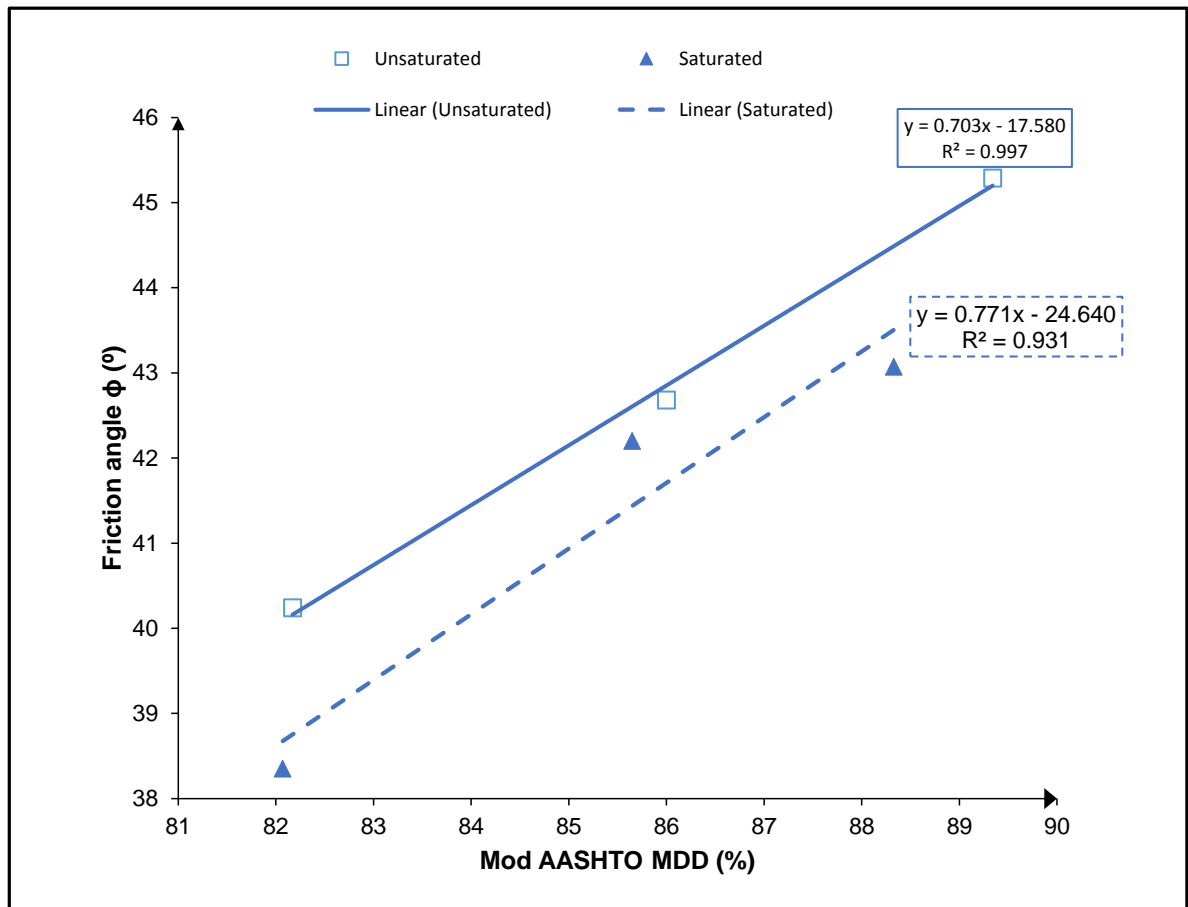


Figure 4-5 The effect of compaction on the friction angle of CD

4.2.1.5 Horizontal Displacement and Vertical Displacement Relationship

Figure 4-6 illustrates the relationship between horizontal and vertical displacements of CD compacted at different compaction degrees. The compaction degree, normal pressure, and water content influence the volume change in material. In general, vertical displacement increases with an increase in the compaction degree and reduces with an increase of normal pressure. Moreover, the vertical displacement reduces with saturation.

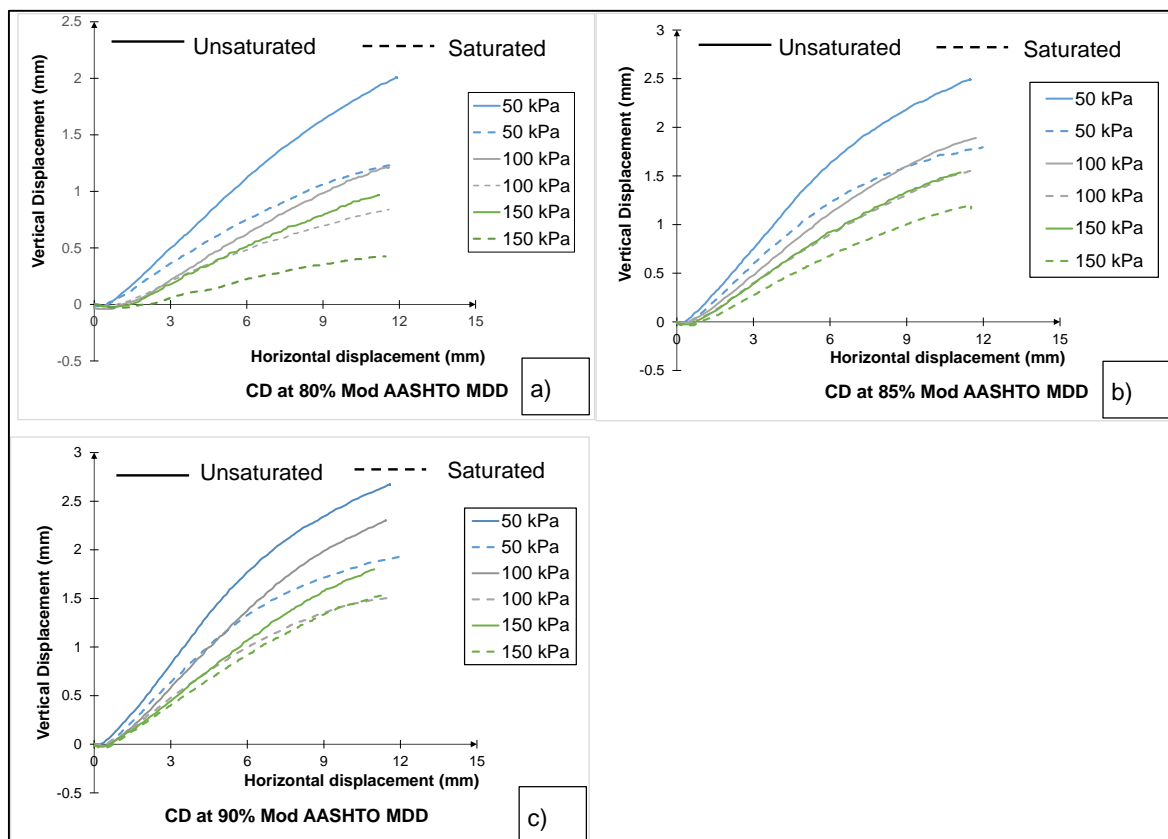


Figure 4-6 Horizontal versus vertical displacement of crusher dust(CD)

Table 4-3 presents the maximum vertical displacement and maximum volume change (dilation angle Ψ_{max}) plotted in Figure 4-6. The followings are the findings observed:

- The vertical displacement increased with compaction degree. For instance, at unsaturated conditions, the vertical displacement of crusher dust increases about 19%, 6.7% from 80% to 85%, and 85% to 90% Mod AASHTO MDD compaction degree. However, the vertical displacement of crusher dust reduced with saturation. When 100kPa applied, the reduction was about 17.5% at 85% Mod AASHTO MDD. Therefore, maximum dilation angle of crusher dust increased with an increase in compaction but decreased with saturation.
- The vertical displacement decreased with an increase in normal stress. For instance at nominally 80% Mod ASSHTO MDD, a reduction of about 52% was observed from 50kPa to 150kPa normal stress. Therefore, maximum dilation angle reduced.

Table 4-3 Summary of maximum vertical displacement of crusher dust (CD)

| Material type | Maximum size of aggregate (mm) | Testing moisture condition | Relative Compaction (%) | Normal pressure (kPa) | Maximum vertical displacement (mm) | Maximum dilation angle ($\Psi^{\circ}\text{max}$) |
|---------------|--------------------------------|----------------------------|-------------------------|-----------------------|------------------------------------|---|
| CD | 4.75 | Unsaturated | 82.17 | 50 | 2.01 | 10.61 |
| | | | | 100 | 1.21 | 6.28 |
| | | | | 150 | 0.97 | 5.16 |
| | | Saturated | 82.07 | 50 | 1.24 | 7.23 |
| | | | | 100 | 0.84 | 4.70 |
| | | | | 150 | 0.42 | 2.29 |
| | | Unsaturated | 86.60 | 50 | 2.49 | 15.36 |
| | | | | 100 | 1.89 | 10.56 |
| | | | | 150 | 1.53 | 8.83 |
| | | Saturated | 85.65 | 50 | 1.79 | 11.85 |
| | | | | 100 | 1.56 | 8.55 |
| | | | | 150 | 1.21 | 6.54 |
| | | Unsaturated | 89.34 | 50 | 2.67 | 16.71 |
| | | | | 100 | 2.30 | 13.02 |
| | | | | 150 | 1.80 | 10.25 |
| | | Saturated | 88.33 | 50 | 1.95 | 12.77 |
| | | | | 100 | 1.51 | 9.58 |
| | | | | 150 | 1.55 | 8.79 |

4.2.2 MALMESBURY SAND

4.2.2.1 Shear Stress and Horizontal Displacement Relationship

The Malmesbury sand was tested at 85% Mod AASHTO MDD only.

Figure 4-7 shows the stress-displacement curve of MS under unsaturated and saturated conditions. Three normal pressures were also applied on each of the test. The general trend shows an increase in shear stress with normal pressure and a reduction of shear stress with saturation.

The shear stress increased steadily until 2 mm of shearing, then became almost constant until the end of testing. The shear stress of Malmesbury material increased about 42% and 30.4% from 50kPa to 100kPa and from 100kPa to 150kPa normal stress. However, shear stress reduced about 13% with saturation when applied 100kPa normal stress.

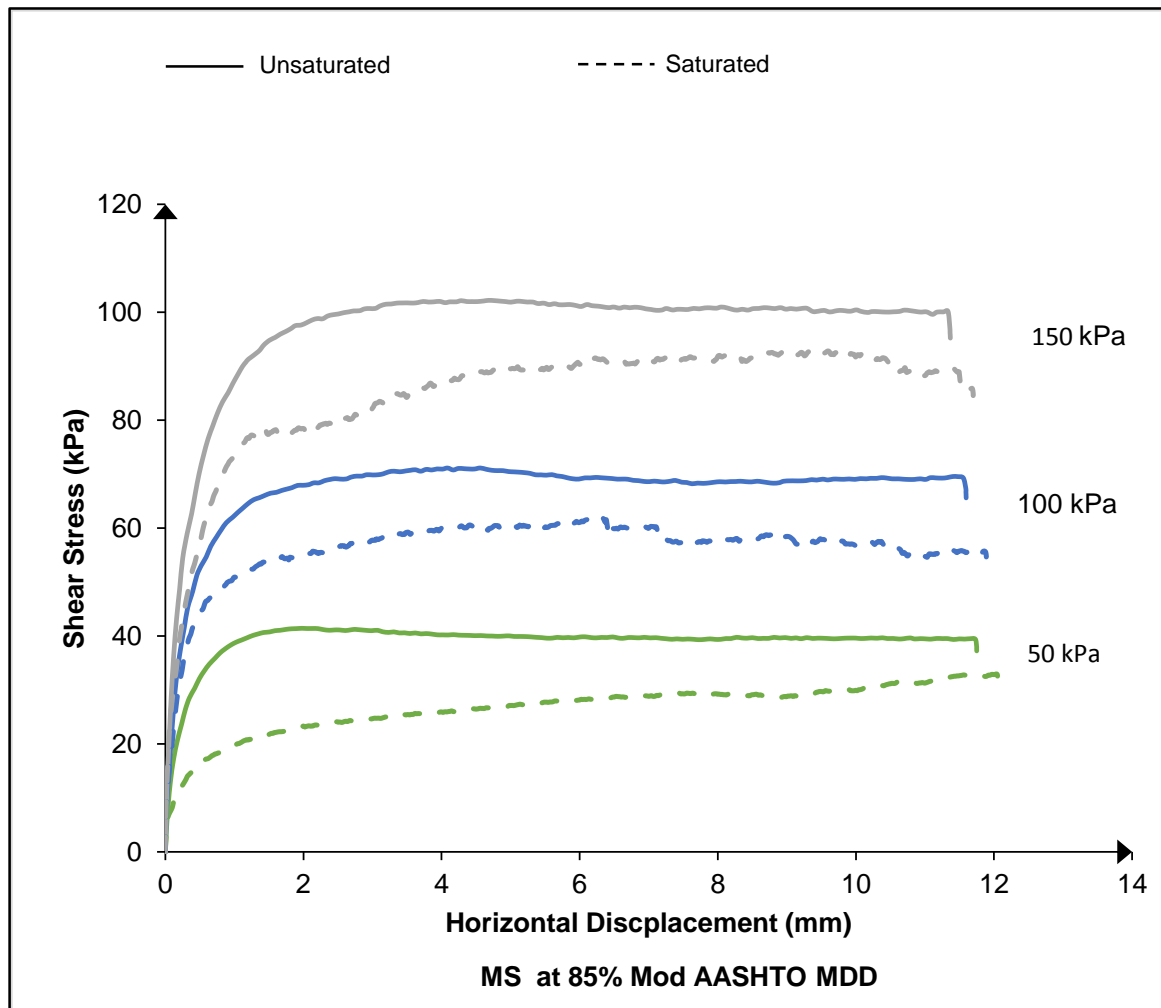


Figure 4-7 Shear stress versus horizontal displacement for MS

4.2.2.2 Shear Stress and Normal Stress Relationship

Figure 4-8 illustrates the relationship between maximum shear stress and normal stress. A linear regression represents the effect of normal stress on the maximum shear stress. The friction coefficient $\tan\phi$ in Figure 4-8 reduces with addition of water. The friction coefficient reduced slightly from 0.61 to 0.60 whereas a higher reduction of cohesion was registered i.e. 10.83 to 2.67, which is about 4 times.

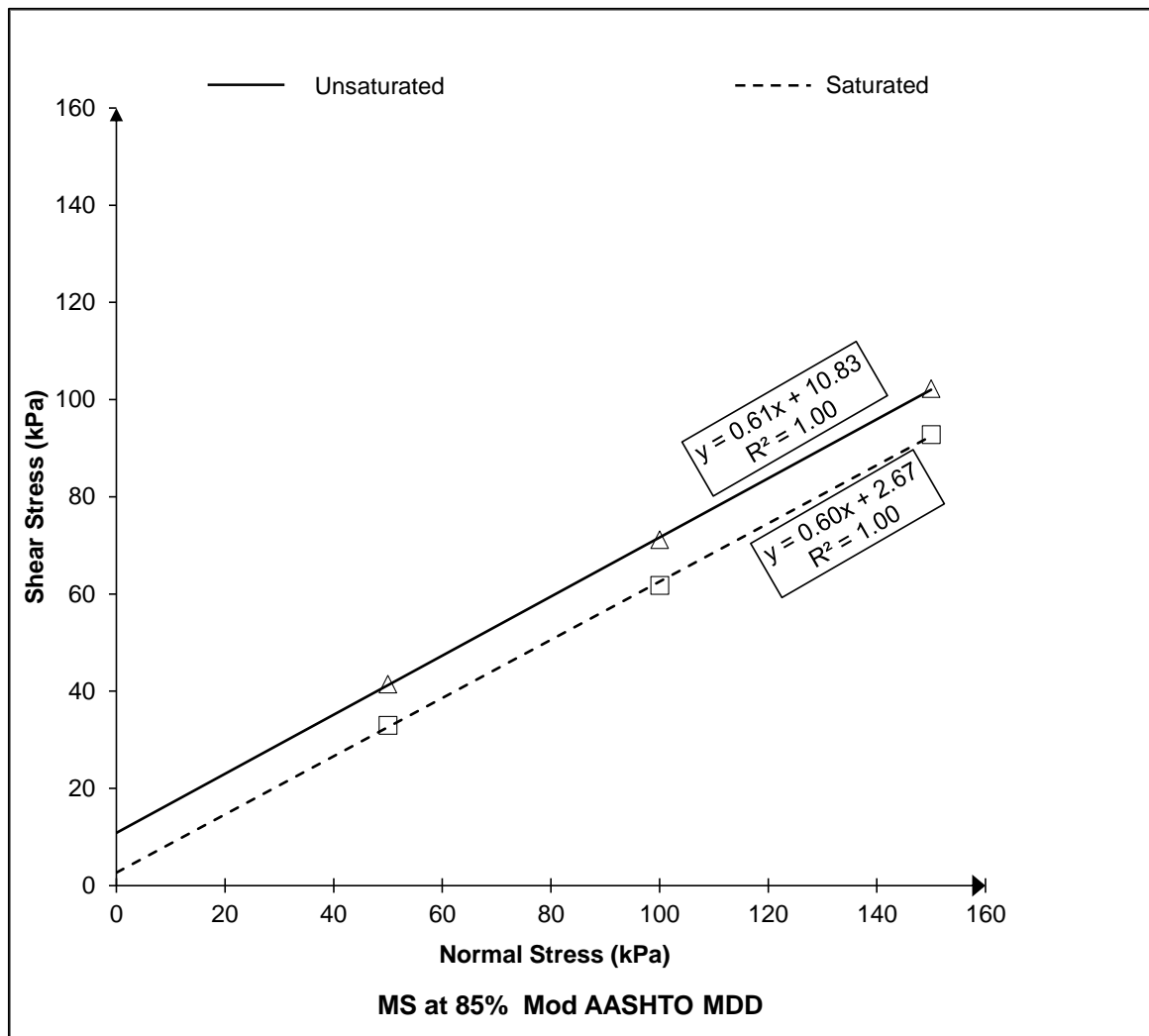


Figure 4-8 Shear stress versus normal pressure for MS

4.2.2.3 Horizontal and Vertical Displacement Relationship

Figure 4-9 shows the relationship of vertical displacement to horizontal displacement of MS when normal stresses are applied. A significant effect on vertical displacement is observed when varying the normal pressure. MS dilates at lower normal pressure under unsaturated conditions however compresses with both the increase of normal pressure and saturation. It should be noted that a positive sign (+) in Table 4-4 means material dilates and negative sign (-) material compresses.

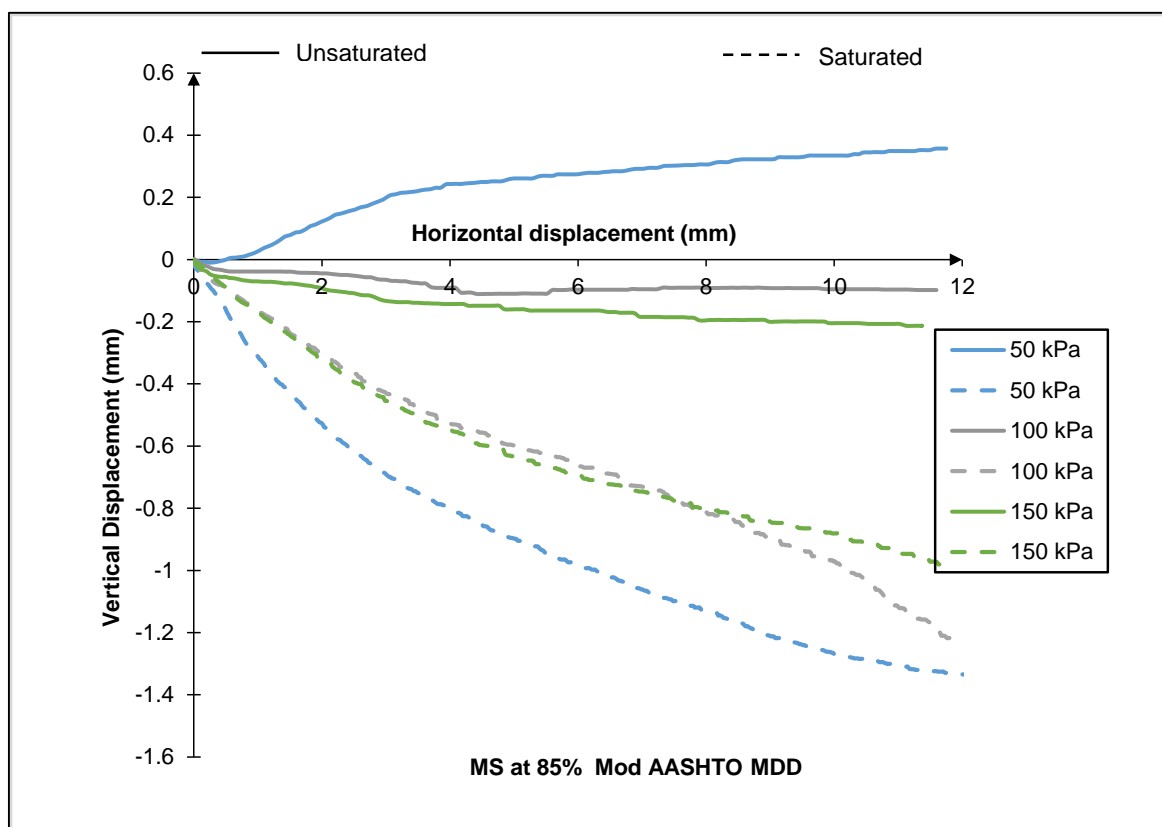


Figure 4-9 Vertical displacement versus horizontal displacement

Table 4-4 Summary of maximum vertical displacement and maximum dilation angle of MS

| Material type | Maximum size of aggregate (mm) | Testing moisture condition | Mod AASHTO MDD (%) | Normal pressure (kPa) | Maximum vertical displacement (mm) | Maximum dilation angle ($\Psi^{\circ}\text{max}$) |
|---------------|--------------------------------|----------------------------|--------------------|-----------------------|------------------------------------|---|
| MS | 4.75 | Unsaturated | 86.31 | 50 | 0.36 | 3.86 |
| | | | | 100 | -0.10 | -0.48 |
| | | | | 150 | -0.21 | -1.07 |
| | | Saturated | 86.26 | 50 | -1.33 | -6.32 |
| | | | | 100 | -1.23 | -5.53 |
| | | | | 150 | -0.98 | -4.79 |

4.2.3 PHILIPPI SAND

4.2.3.1 Shear Stress and Horizontal Displacement Relationship

The Philippi sand was also tested at 85% Mod AASHTO MDD compaction only. Figure 4-10 illustrates the relationship between shear stress and horizontal displacement of PS under unsaturated and saturated conditions by applying three normal pressures for each test. The shear stress continued to increase with horizontal displacement. Failure was thus taken as occurring at 10% strain. The shear stress increased about 2.7 times from applying 50kPa to 150kPa at unsaturated condition as it is shown in Table 4-5. By adding water, the shear

stress was reduced from 62.15kPa to 58.32kPa when a normal pressure of 100kPa was applied.

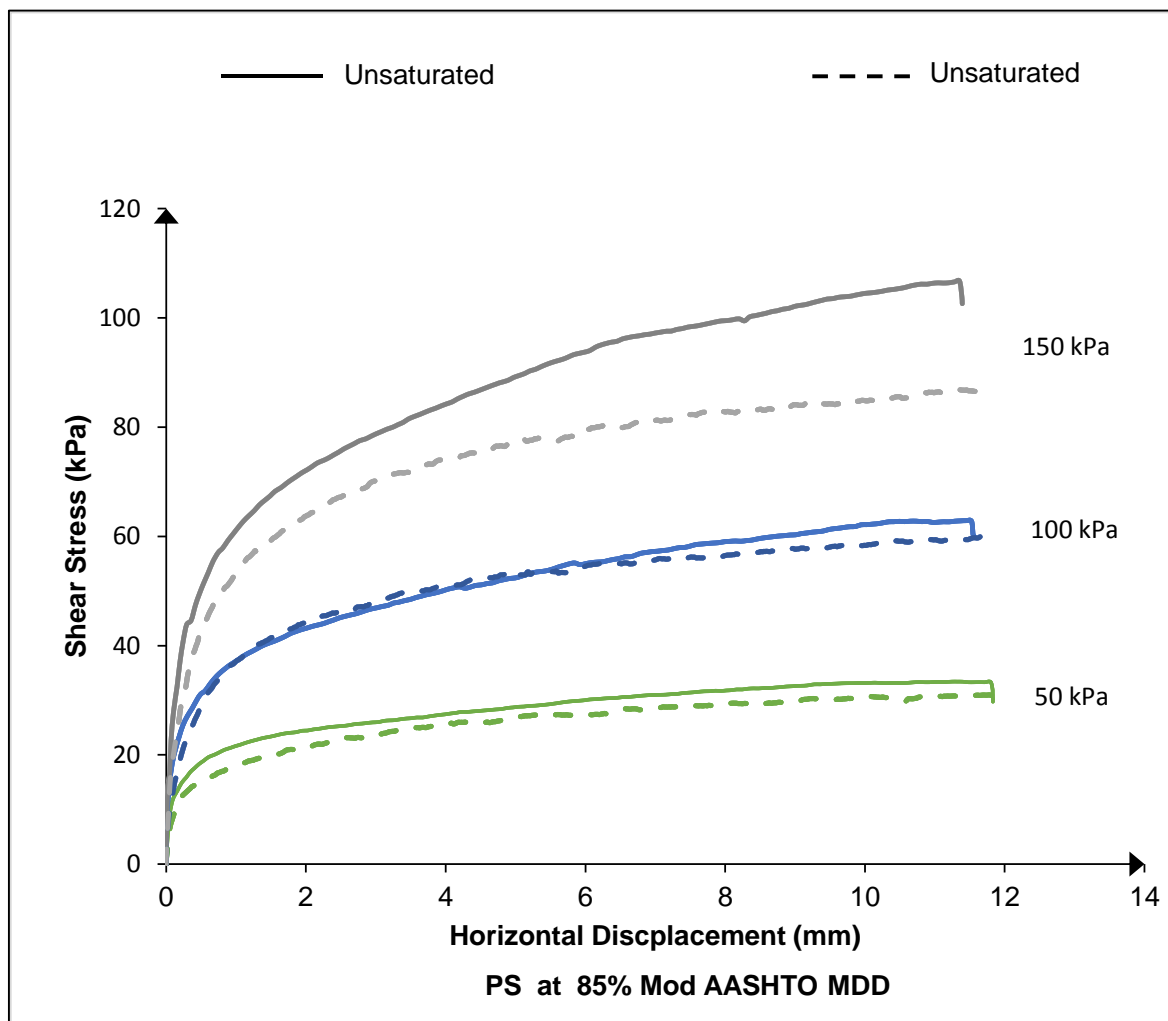


Figure 4-10 Shear stress versus horizontal displacement for PS

Table 4-5 Summary of shear stress, friction angle, vertical displacement and dilation angle of PS

| Material type | Maximum size of aggregate (mm) | Testing moisture contidion | Mod AASHTO MDD average(%) | Normal Stress (kPa) | Maximum Shear Stress (kPa) | Horixontal Displacement at Failure (mm) | $\mu=\tan\phi'$ | ϕ' (°) | C' (kPa) |
|---------------|--------------------------------|----------------------------|---------------------------|---------------------|----------------------------|---|-----------------|-------------|------------|
| PS | 2.3 | Unsaturated | 85.75 | 50 | 33.18 | 10.00 | 0.57 | 31.00 | 4.96 |
| | | | 85.64 | 100 | 62.15 | 10.00 | | | |
| | | | 86.38 | 150 | 90.00 | 10.00 | | | |
| | | Saturated | 85.8 | 50 | 30.68 | 10.00 | 0.54 | 28.37 | 3.82 |
| | | | 85.51 | 100 | 58.32 | 10.00 | | | |
| | | | 86.36 | 150 | 84.78 | 10.00 | | | |

| Material type | Maximum size of aggregate (mm) | Testing moisture contidion | Mod AASHTO MDD (%) | Normal pressure (kPa) | Maximum vertical displacement (mm) | Maximum dilation angle ($\Psi^{\circ}\max$) |
|---------------|--------------------------------|----------------------------|--------------------|-----------------------|------------------------------------|---|
| PS | 2.3 | Unsaturated | 85.92 | 50 | -0.71 | -3.42 |
| | | | | 100 | -0.86 | -4.24 |
| | | | | 150 | -0.88 | -4.43 |
| | | Saturated | 85.89 | 50 | -0.74 | -3.51 |
| | | | | 100 | -0.79 | -3.79 |
| | | | | 150 | -0.78 | -3.80 |

4.2.3.2 Shear Stress and Normal Stress Relationship

Figure 4-11 illustrates the relationship between shear stress and normal stress. This thus provides the friction coefficient obtained by means of the linear regression equation shown. The friction coefficient reduced slightly with saturation from 0.57 to 0.54, which is a reduction of about 5.3 %. Table 4-5 provides a summary of friction coefficient of each variable.

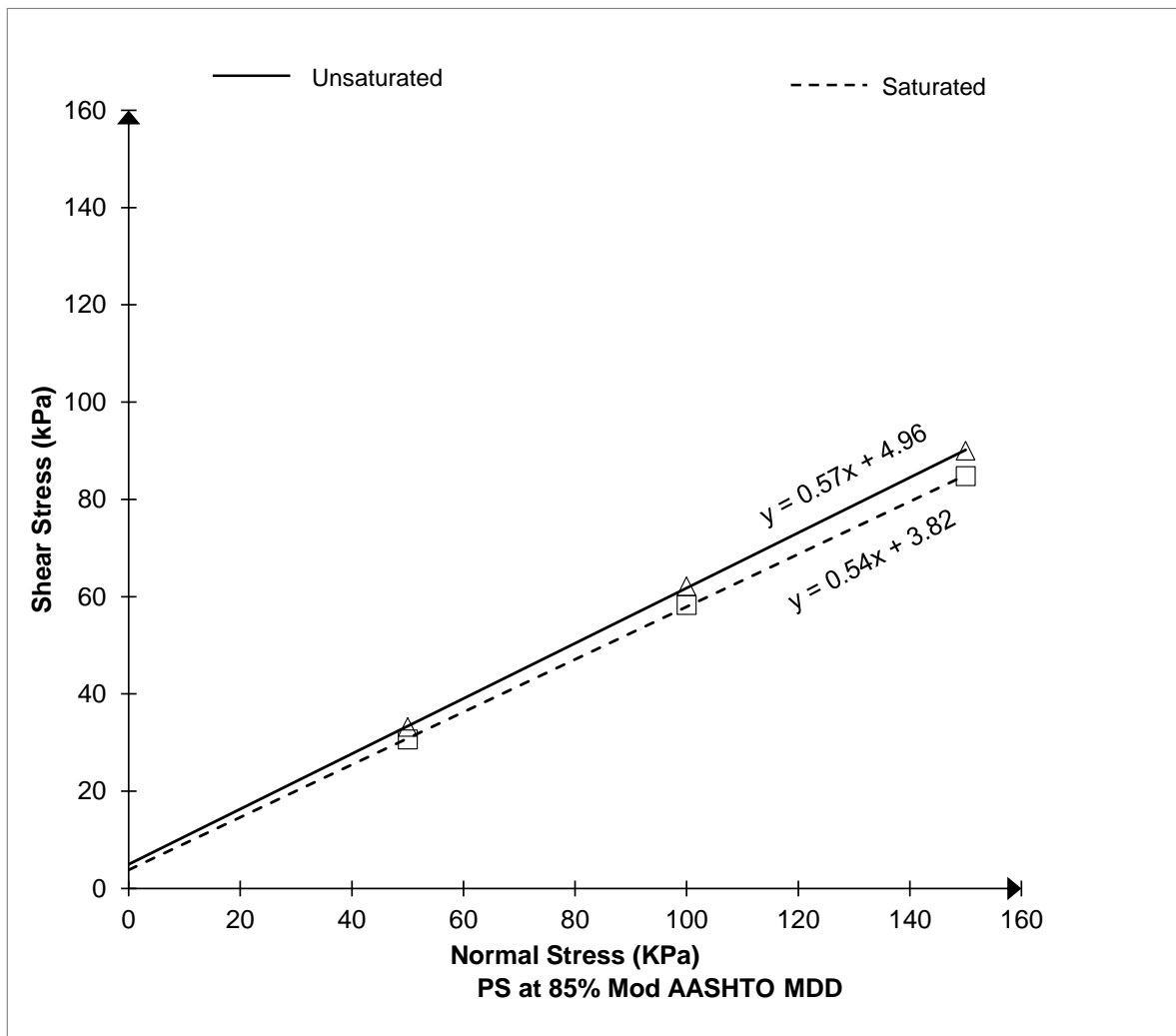


Figure 4-11 Shear stress versus normal pressure of PS

4.2.3.3 Horizontal Stress and Vertical Stress Relationship

Figure 4-12 shows the relationship of vertical displacement to horizontal displacement. PS compressed at all normal stresses and at both moisture conditions. The vertical displacement is higher in saturated conditions than in unsaturated conditions for both 100kPa and 150kPa normal pressures. Briefly, the PS does not dilate on shear.

Table 4-5 summarises the values of the maximum vertical displacement and dilation angle of Philippi sand. A small increment of compression with normal stress was observed when applied 100kPa and 150kPa.

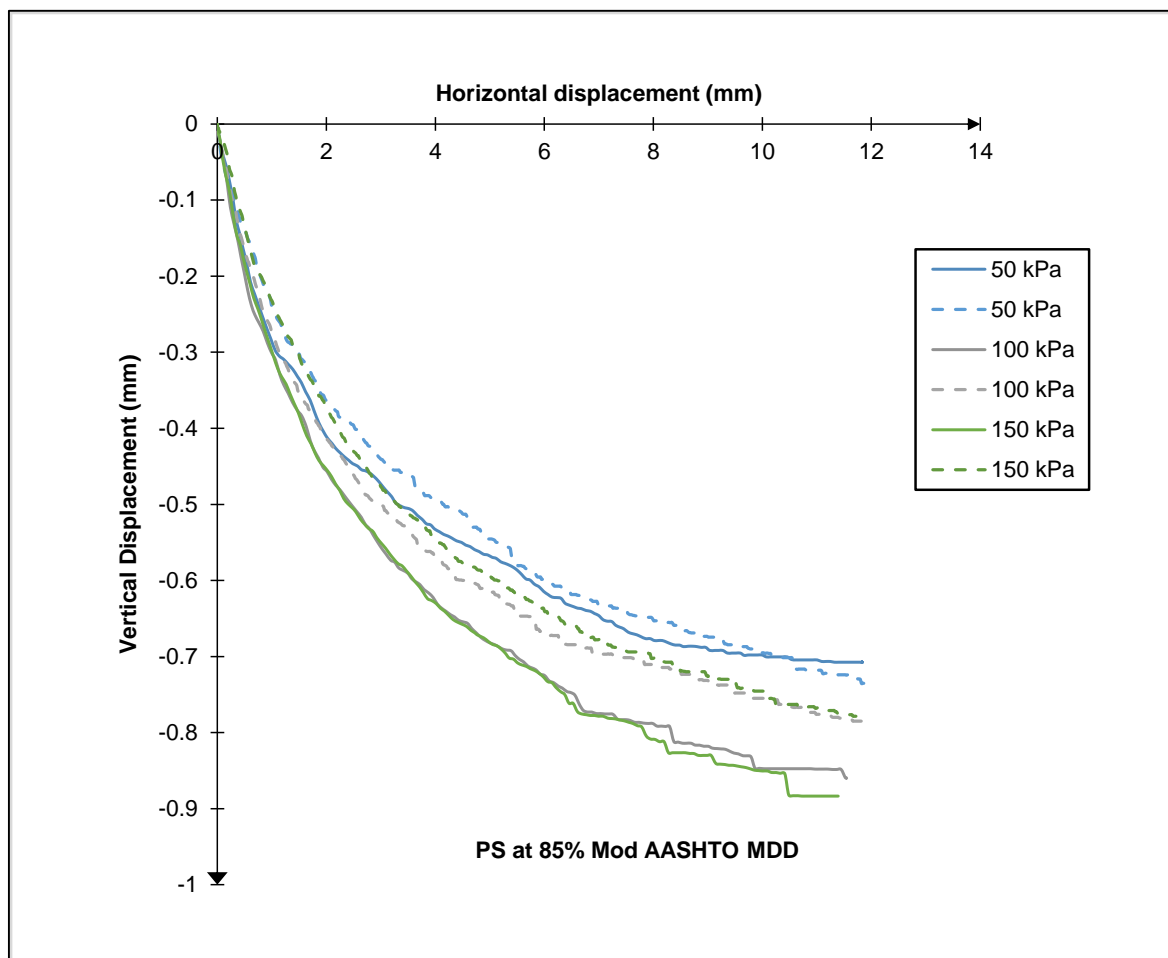


Figure 4-12 Vertical displacement versus horizontal displacement of PS

4.2.4 COMPARISON OF DIFFERENT MATERIAL TYPES

In this section, maximum stress, dilation angle, and friction angle of CD, MS, and PS were analysed and compared in order to get an insight into the effect of material types. The compaction degree was maintained at 85% for all three materials.

4.2.4.1 Maximum Shear Stress versus Normal Stress

Figure 4-13 illustrates the effect of material type on maximum shear stress and normal stress at 85% Mod AASHTO MDD. The slope of the trend lines indicates the effect of normal stress on maximum shear stress. Generally, the CD exhibited higher shear stress than MS and PS. The following are the findings observed:

- The maximum shear stress increases with increased in normal stress for all the three materials. However, it reduces with saturation.
- CD exhibited a higher friction coefficient $\tan\phi$ than MS and PS. At unsaturated conditions, a difference in friction coefficient of 33.7% and 38% were observed between CD-MS and CD-PS. In terms of angle friction, CD exhibited 26.7% and 30.4% more than MS and PS respectively. Table 4-6 shows friction coefficient and angles of

crusher dust (CD), Malmesbury sand (MS) and Philippi sand (PS). This shows that the quality and types of materials influence strength properties

- The intercept term (cohesion) shows a similar trend. CD exhibited higher cohesion c than MS and PS.

Table 4-6 gives the summary of the maximum shear stress, friction coefficient as well as the angle of internal friction.

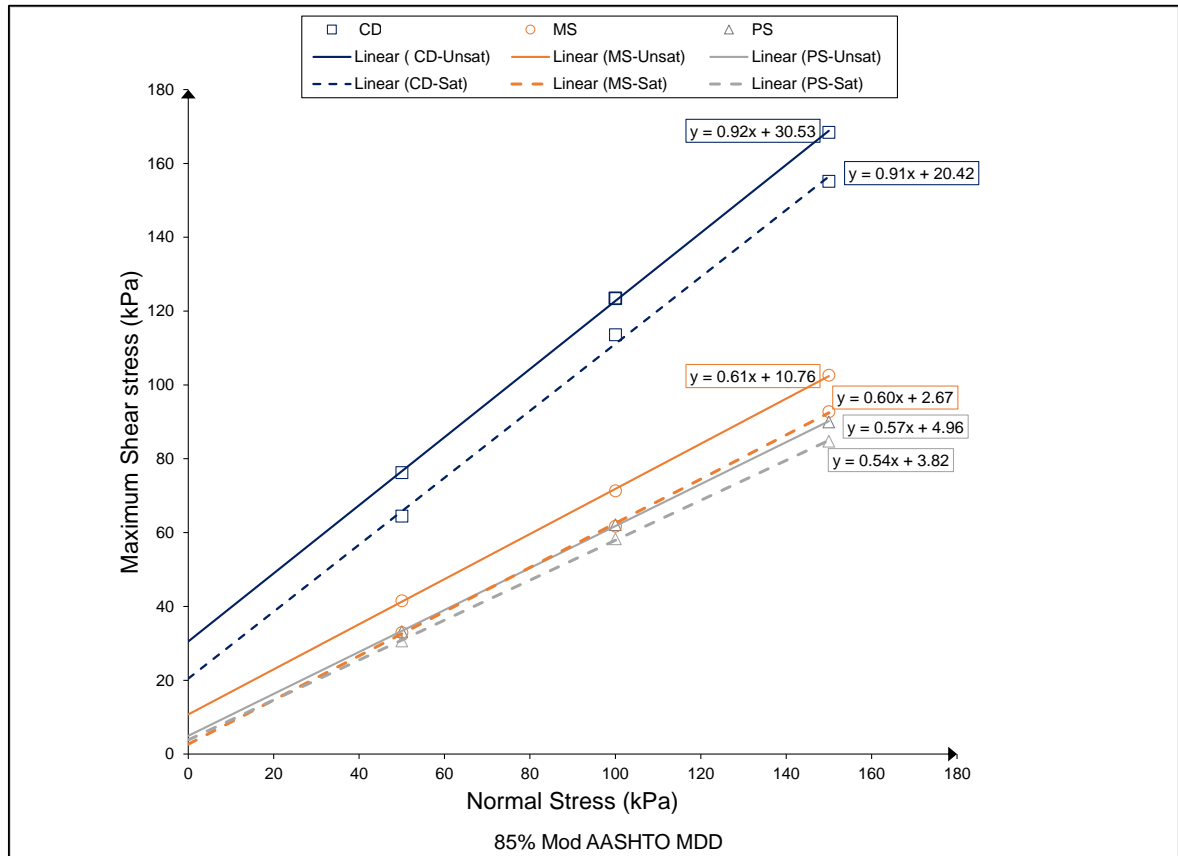


Figure 4-13 Maximum shear stress versus normal stress of research materials

Table 4-6 A summary of shear maximum shear stress, horizontal displacement, friction angle and cohesion of research materials

| Material type | Maximum size of aggregate (mm) | Testing moisture condition | Mod AASHTO MDD average(%) | Normal Stress (kPa) | Maximum Shear Stress (kPa) | Horizontal Displacement at Failure (mm) | $\mu=\tan\phi$ | ϕ (°) | C (kPa) |
|---------------|--------------------------------|----------------------------|---------------------------|---------------------|----------------------------|---|----------------|------------|---------|
| CD | 4.75 | Unsaturated | 86.6 | 50 | 76.0 | 3.29 | 0.92 | 42.68 | 30.30 |
| | | | 86.5 | 100 | 123.3 | 4.44 | | | |
| | | | 86.7 | 150 | 168.3 | 5.13 | | | |
| | | Saturated | 85.7 | 50 | 64.5 | 3.61 | 0.91 | 42.20 | 20.42 |
| | | | 85.66 | 100 | 113.6 | 5.70 | | | |
| | | | 85.6 | 150 | 155.2 | 5.29 | | | |
| MS | 4.75 | Unsaturated | 85.97 | 50 | 41.4 | 1.98 | 0.61 | 31.29 | 10.89 |
| | | | 86.21 | 100 | 71.2 | 4.56 | | | |
| | | | 86.76 | 150 | 102.2 | 4.68 | | | |
| | | Saturated | 86.11 | 50 | 31.0 | 12.00+ | 0.60 | 30.90 | 2.67 |
| | | | 85.98 | 100 | 61.8 | 6.34 | | | |
| | | | 86.68 | 150 | 92.8 | 9.60 | | | |
| PS | 2.3 | Unsaturated | 85.75 | 50 | 33.2 | 10.00 | 0.57 | 31.00 | 4.96 |
| | | | 85.64 | 100 | 62.2 | 10.00 | | | |
| | | | 86.38 | 150 | 90.0 | 10.00 | | | |
| | | Saturated | 85.8 | 50 | 30.7 | 10.00 | 0.54 | 28.37 | 3.82 |
| | | | 85.51 | 100 | 58.3 | 10.00 | | | |
| | | | 86.36 | 150 | 84.8 | 10.00 | | | |

4.2.4.2 Maximum Vertical Displacement and Dilation Angle

Table 4-7 presents a summary of maximum vertical displacement and dilation angle. This is a summary of results plotted in Figure 4-6, Figure 4-9, and Figure 4-12. Figures of dilation rate curves of all materials are presented in Appendix A. Maximum vertical displacement as well as maximum dilation angle are higher for CD than for MS and PS. Generally, the CD dilates whereas MS and PS compress when sheared. The following are the results of maximum vertical displacement and maximum dilation observations presented in Table 4-7:

- At unsaturated conditions, the crusher dust (CD) dilates at all normal pressures, Malmesbury sand (MS) dilates at low normal stresses (50kPa) but compresses at 100kPa and 150kPa and Philippi sand (PS) does not dilate at all. However, the Malmesbury sand (MS) compresses at all normal stresses in saturated conditions.

Table 4-7 Summary of vertical displacement and dilation angle of the research material

| Material type | Maximum size of aggregate (mm) | Testing moisture condition | Mod AASHTO MDD (%) | Normal pressure (kPa) | Maximum vertical displacement (mm) | Maximum dilation angle ($\Psi^{\circ}\text{max}$) |
|---------------|--------------------------------|----------------------------|--------------------|-----------------------|------------------------------------|---|
| CD | 4.75 | Unsaturated | 86.60 | 50 | 2.49 | 15.36 |
| | | | | 100 | 1.89 | 10.56 |
| | | | | 150 | 1.53 | 8.83 |
| | | Saturated | 85.65 | 50 | 1.79 | 11.85 |
| | | | | 100 | 1.56 | 8.55 |
| | | | | 150 | 1.21 | 6.54 |
| MS | 4.75 | Unsaturated | 86.31 | 50 | 0.36 | 3.86 |
| | | | | 100 | -0.10 | -0.48 |
| | | | | 150 | -0.21 | -1.07 |
| | | Saturated | 86.26 | 50 | -1.33 | -6.32 |
| | | | | 100 | -1.23 | -5.53 |
| | | | | 150 | -0.98 | -4.79 |
| PS | 2.3 | Unsaturated | 85.92 | 50 | -0.71 | -3.42 |
| | | | | 100 | -0.86 | -4.24 |
| | | | | 150 | -0.88 | -4.43 |
| | | Saturated | 85.89 | 50 | -0.74 | -3.51 |
| | | | | 100 | -0.79 | -3.79 |
| | | | | 150 | -0.78 | -3.80 |

4.3 DISCUSSION OF RESULTS

Results from classification and shear investigation provide valuable insight relating to the evaluation of physical and mechanical properties of the materials used in the research. The shear strength and dilation or compression of the research materials are influenced by different factors include compaction effort, water content, type of materials and normal pressure.

The research assessment of the strength and dilation of research materials are summarised as follows:

- An increase in the compaction density of the crusher dust (CD) from 80%, 85% to 90% Mod AASHTO MDD leads to an increase in shear strength and dilation.
- An increase in normal stress leads to a decrease in dilation or an increase in compression. This thus shows the effect of confinement on dilation.
- Saturation reduces the shear strength and dilation.
- Material types influence the shear strength and dilation. CD exhibited higher shear strength than MS and PS. This is due to CD particle shape (subangular), particle size distribution (well graded) compared to poorly graded, subrounded and rounded of MS and PS respectively.
- CD material dilates at all normal stress whereas MS material generally dilates at low normal stress and PS material compresses at all normal stresses.

CHAPTER 5 PULL-OUT TEST RESULTS AND DISCUSSION

5.1 INTRODUCTION

This chapter provides the results of the pull-out test and an analysis of these results. The tests conducted include axial and oblique pull-out results on posts driven into the research materials. Note that the compaction densities presented in figures are the target densities (80%, 85%, and 90% Mod AASHTO MDD). The actual densities achieved differ from these target densities by $\pm 1\%$ in general except the drive-in at dry condition where lower compaction density were obtained.

5.2 AXIAL PULL-OUT TEST

Table 5-1 presents the area ratio (area of the post divided by the area of the pipe expressed as a percentage) of the posts used for the pull-out tests.

Table 5-1 Area ratio of posts to pipe section

| Description | Post section Area A mm² | Pipe section area A (mm²) | Area ratio A/Ap (%) |
|--------------------|---|---|--------------------------------|
| Post 50x50x3 | 298 | 8494.87 | 3.51 |
| Post 50x50x6 | 569 | 8494.87 | 6.70 |
| Post 50x50x9 | 867 | 8494.87 | 10.21 |

5.2.1 CRUSHER DUST

5.2.1.1 Drive-in Force

a) Unsaturated Condition at Different Compaction Density

Figure 5-1 illustrates the relationship of drive-in force to penetration of crusher dust (CD). An increase in compaction density increases the resistance to penetration. Compaction densities of nominally 80%, 85%, and 90% Mod AASHTO MDD were used at near moisture content.

In general, as Figure 5-1 shows, the drive-in force increased rapidly during the first 100-150mm of penetration, then became constant with depth until the toe of the post approached the pipe bottom. This could be the result of end bearing contributing significantly more than skin friction. After a certain depth of penetration, the end bearing would be fully mobilised and does not increase much further with increased penetration. The skin friction continues to increase as the area over which it acts increases with penetration but this is only a minor component of the total resistance. As expected, the drive in force increased with increasing compaction density.

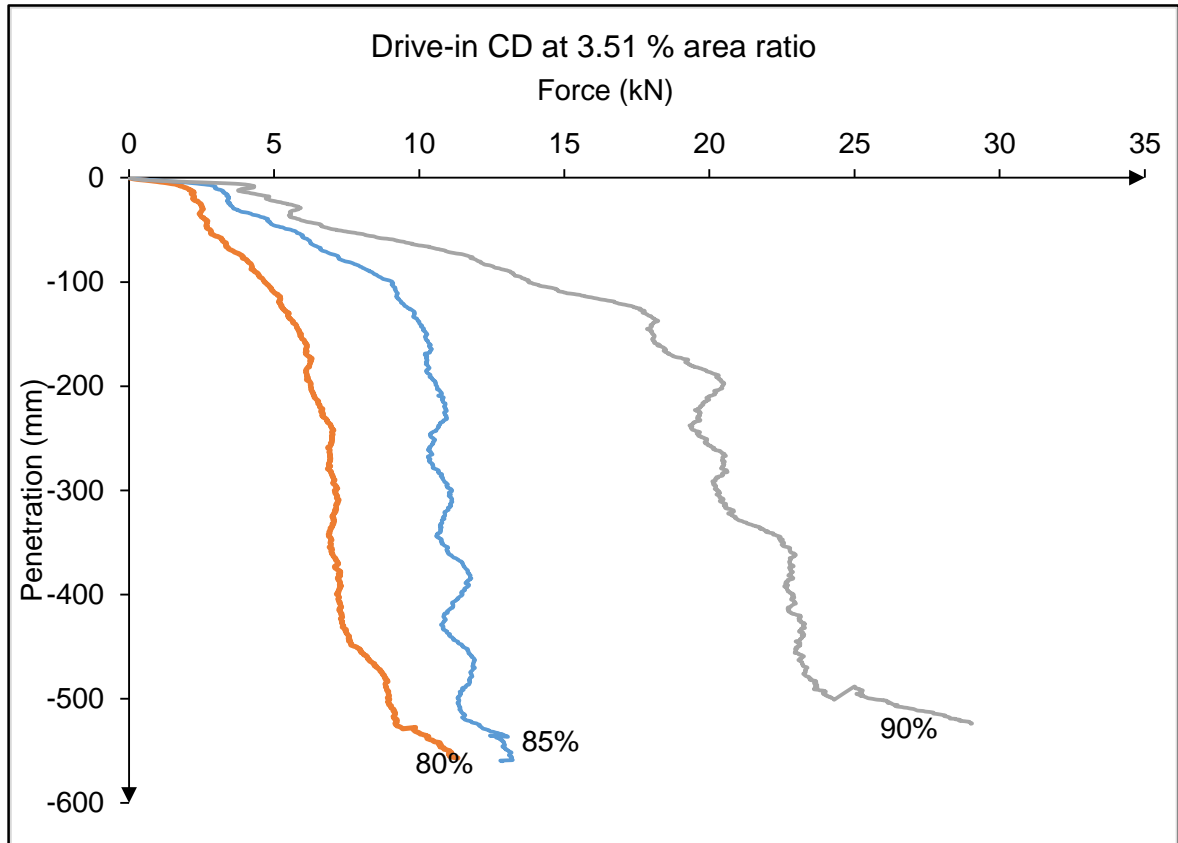


Figure 5-1 Drive-in force at different Mod AASHTO MDD degrees of CD

b) Unsaturated Conditions at Different Post Area Ratios

Figure 5-2 shows the effect of area ratio of the post on the drive-in force. Area ratios of 3.51%, 6.7%, and 10.21% were used. Higher drive-in forces were required for higher area ratios. It is likely that more crushing of materials occurred as the area ratio increased. Despite this, the insertion of the post would have displaced the soil resulting in an increase in the density of the fill during driving of the post.

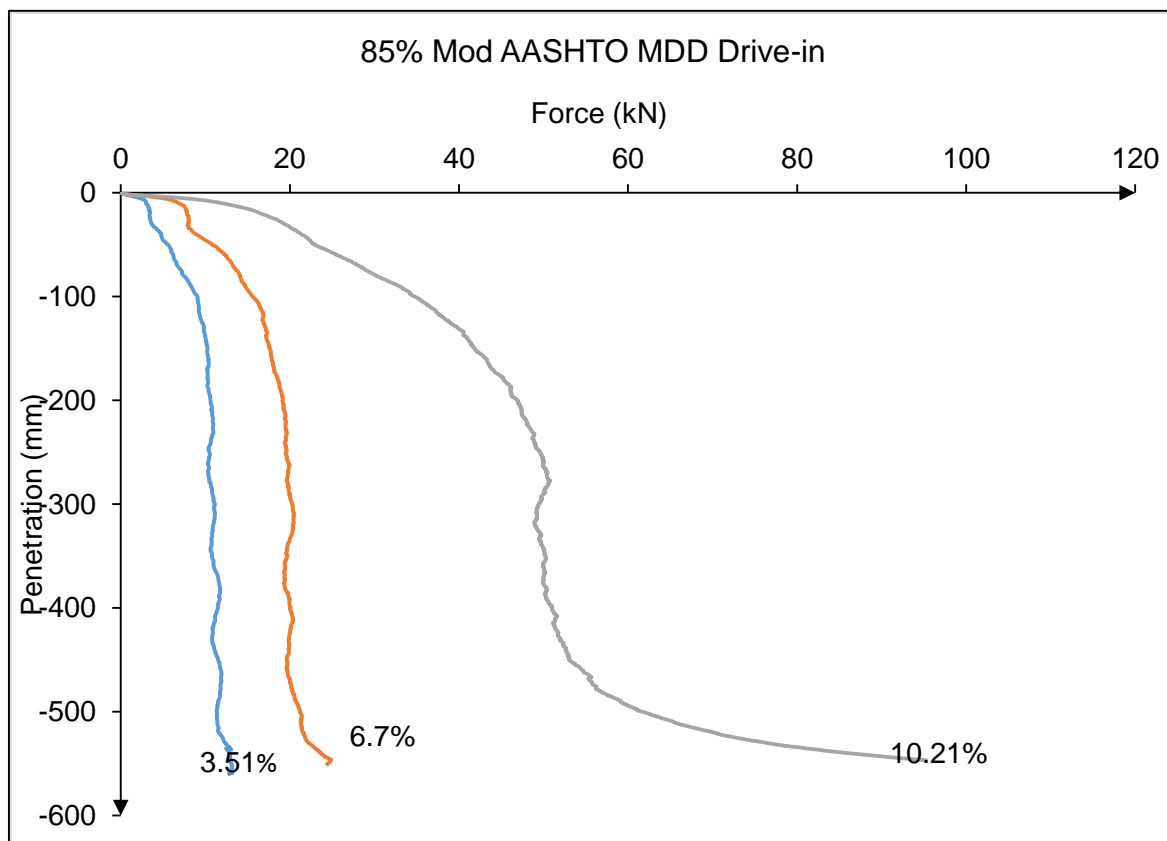


Figure 5-2 Drive in force versus displacement at different area ratio of CD

c) Comparison of Drive-in Force between Dry and OMC Conditions

During preparation for the tests, the fill was compacted into the pipe either “dry” (i.e. at the moisture content of the material after storage in the lab without addition of water) or close to Optimum Moisture Content (OMC) using a pre-determined compaction effort. The effect of driving the post when sample was compacted dry or at OMC is shown in Figure 5-3 for compaction densities of 80% and 90% Mod AASHTO MDD.

For compaction under dry conditions, as it is shown in Table 5-2, the target densities of 80% and 90% MDD were not achieved and the measured densities were 74.61% and 81.92% MDD. For the same compaction effort, densities of 79.89% and 90.18 % were achieved when the backfill was compacted near optimum moisture content. The higher drive-in forces recorded for the OMC condition shown in Figure 5-3 reflect this difference in density of the backfill.

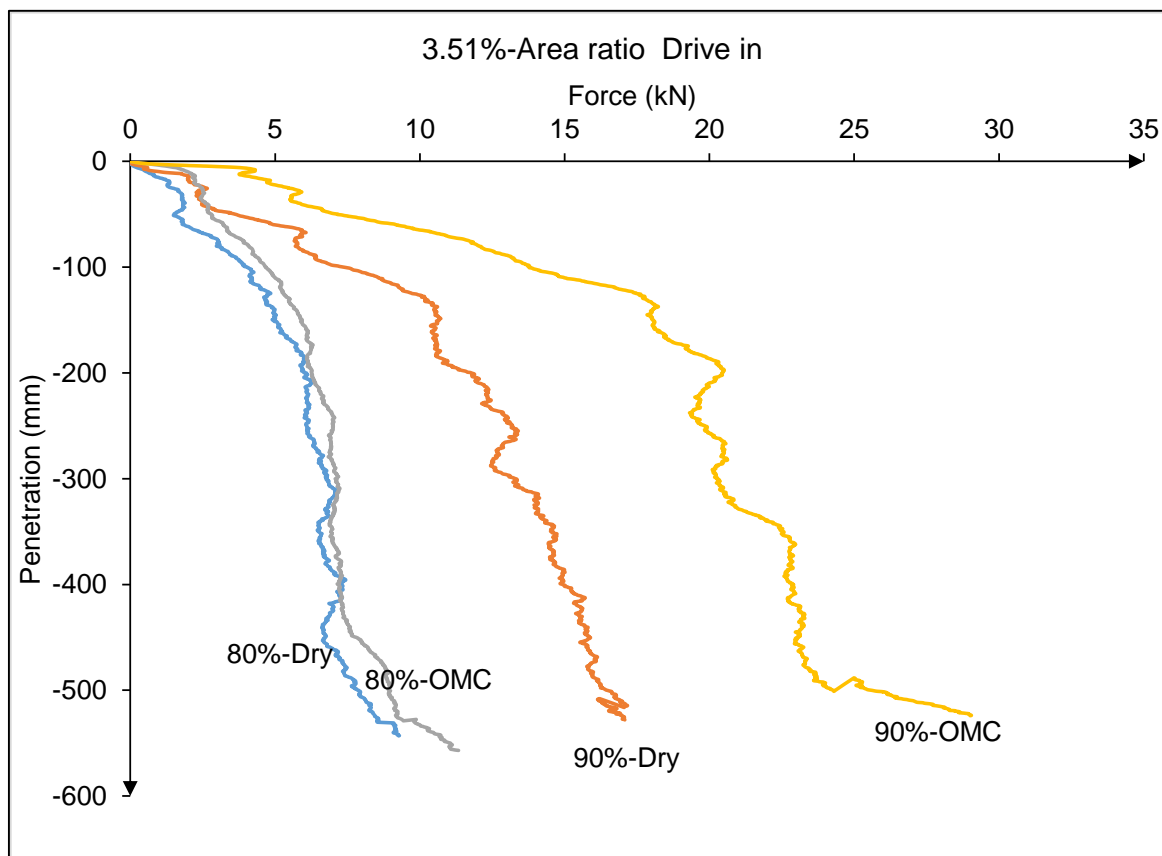


Figure 5-3 Drive-in force compacted at dry and OMC conditions

5.2.1.2 Axial Pull-out Capacity

a) Unsaturated and Saturated Test Conditions at Different Compaction Densities

The pull-out tests were carried out with and without soaking of the backfill prior to testing. These conditions are referred to as “saturated” and “unsaturated” conditions respectively.

Figure 5-14 illustrates the relationship of axial pull-out force to displacement of CD at different Mod AASHTO compaction densities and in unsaturated and saturated conditions. The pull-out resistance increased with the compaction density in both the saturated and unsaturated conditions. Saturation of the backfill decreased the pull-out resistance in all cases.

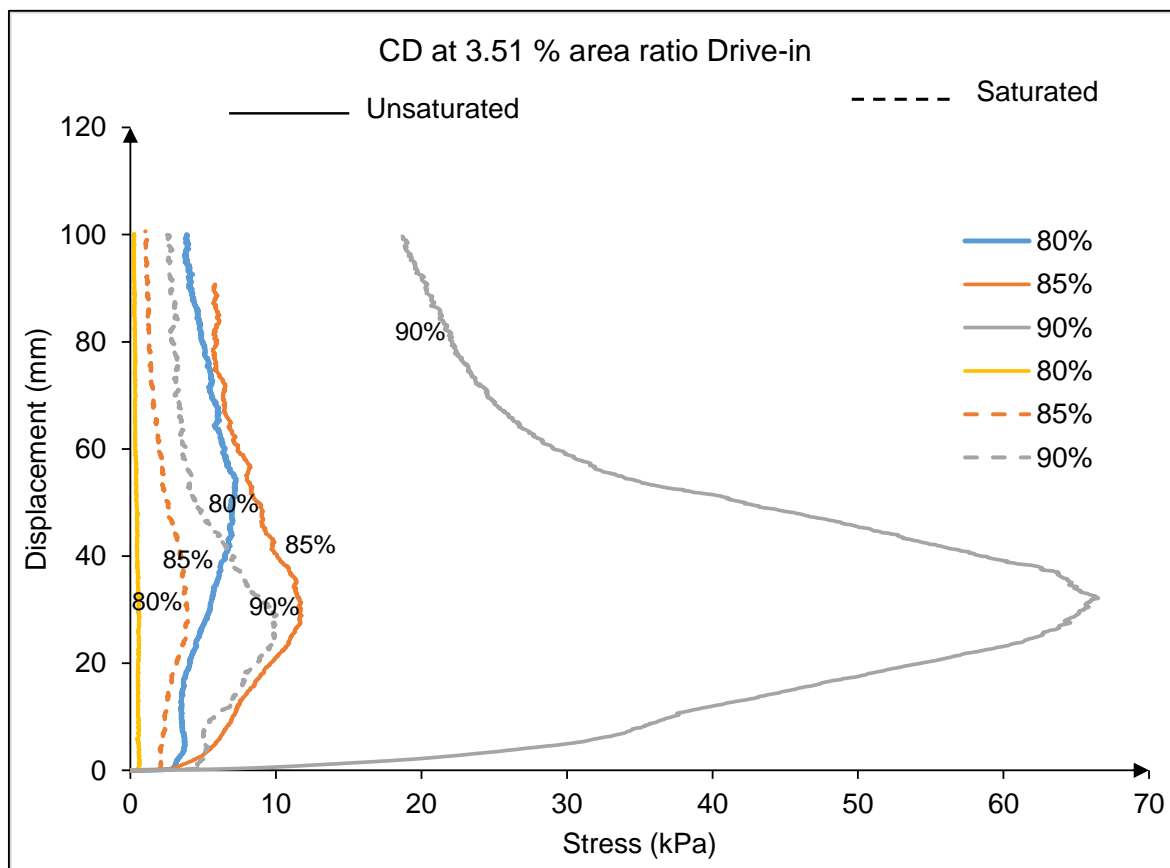


Figure 5-4 Pull-out resistance versus displacement of Crusher Dust (CD) at different compaction densities for an area ratio of 3.51%

b) Unsaturated and Saturated Test Conditions at Different Post Area Ratios

Different post sections with area ratios of 3.51%, 6.7%, and 10.21 % were used to investigate the effect of the area ratio on the axial pull-out resistance. Each of the tests was performed at a compaction density of 85% Mod AASHTO MDD using CD material.

Figure 5-5 illustrates the relationship between axial pull-out stress and area ratio for unsaturated and saturated test conditions. An increase in the area ratio increases the axial pull-out force. Conversely, the axial pull-out force reduced with saturation.

In the unsaturated condition, the axial pull-out force value using 10.21% area ratio was higher than for the 6.7% and 3.51% area ratios. This is due to the densification of CD material caused during the driving of the post. Table 5-2 shows details of maximum axial pull-out force of CD observed at different post area ratios. An area ratio of 10.21% exhibited 20.03kPa of axial pull-out resistance while 6.7% and 3.51% of area ratio exhibited 12.94kPa and 11.79kPa respectively.

The axial pull-out force reduced considerable when the tests were conducted after soaking of the backfill (saturated condition). An axial pull-out resistances of 3.98kPa, 2.90kPa and 7.54kPa were recorded for area ratios of 3.51%, 6.7% and 10.21% respectively. Although the variation in axial pull-out force recorded was not consistent with the variation in area

ratio (resistance at for an area ratio of 3.51% being higher than that for 6.7%), the reduction in pull-out resistance due to soaking of the backfill is clearly evident. This may be due to the lubricating effect of water on the interface between the pile and the soil, allowing shear to take place locally on the interface without significant dilation of the material as a whole.

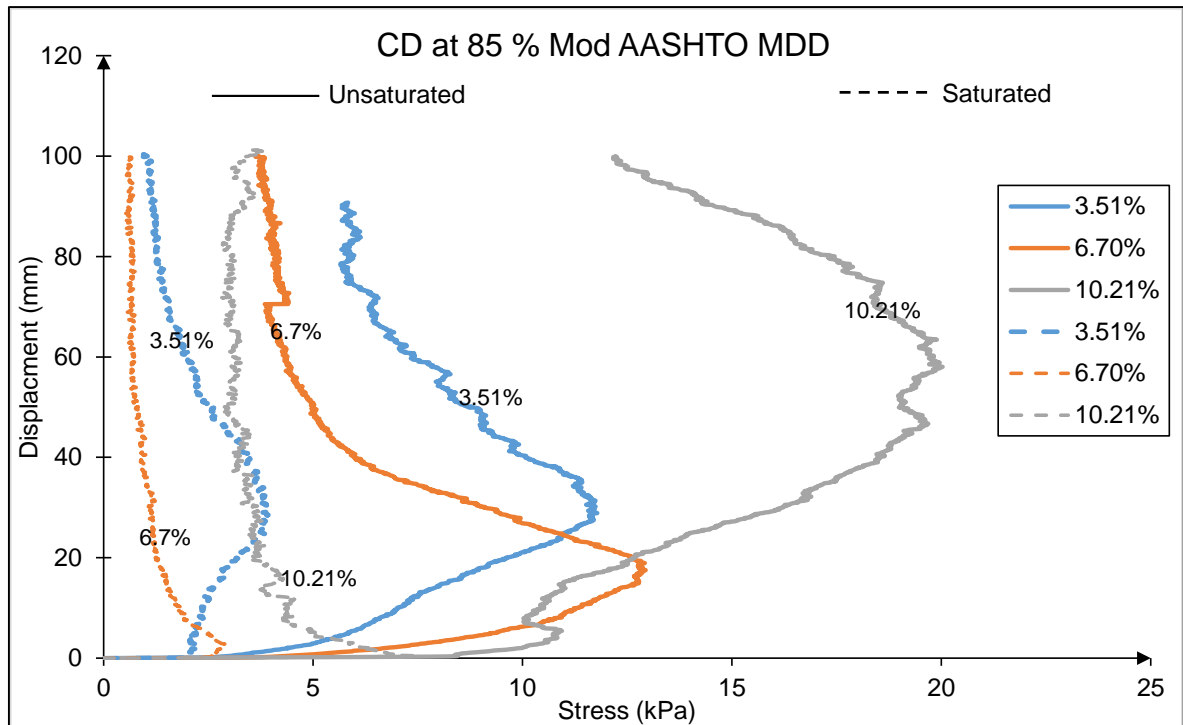


Figure 5-5 Axial pull-out resistance versus displacement of CD at different area ratio in unsaturated and unsaturated condition

c) Comparison of Pull-out Capacity Compacted at OMC and Dry

Figure 5-6 represents the comparison of axial pull-out resistance performed when the material was compacted dry and at OMC and tested at dry and unsaturated conditions. The results show that drive-in post of the specimen compacted at dry conditions exhibited a lower axial pull-out force than the one compacted in unsaturated conditions.

An axial maximum pull-out resistance of 0.35kPa and 4.78kPa were recorded for tests on materials compacted dry using the compaction effort required for 80% and 90% Mod AASHTO MDD whereas 7.28kPa and 66.52kPa were recorded when the material was compacted at OMC using the same compaction effort. As noted above, the compaction densities achieved with compaction of the dry material were only 74.6% and 81.92% MDD whereas the compaction density achieved with compaction at OMC was 79.89% and 90.18%. This is probably the main contributor to the lower axial pull-out resistance recorded for the dry compacted material.

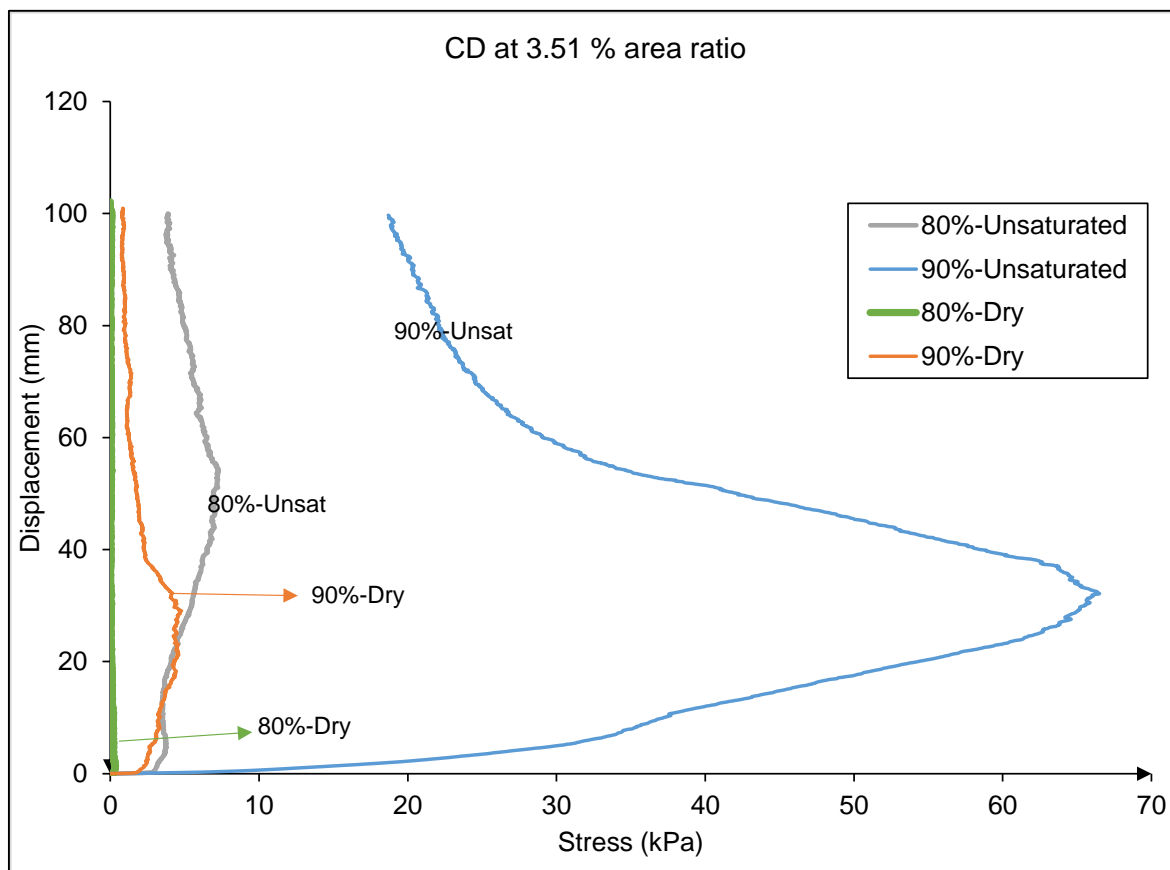


Figure 5-6 Axial pull-out resistance tested for dry and unsaturated conditions at 80% and 90% Mod AASHTO compaction density

d) Effect of Aging on Axial Pull-out Capacity

The above tests were all conducted the day after driving the post (1 day). To investigate the effects of aging of the backfill, one test specimen was tested 21 days after driving the post. The material was compacted at OMC and the pull-out tests at unsaturated conditions.

Figure 5-7 illustrates the relationship between the axial pull-out force and displacement obtained from tests performed at 1 day and 21 days after driving the post. Both the specimens were compacted at 90% Mod AASHTO MDD. The axial pull-out capacity increased significantly with aging of the fill. The axial pull-out resistance at 21 days was 3.5 times higher than the axial pull-out at 1 day. An axial maximum pull-out resistance value of 66.52kPa and 247.86kPa were recorded for 1 day and 21 days. This increase could be related to the increase of shear stiffness and dilation of the soil around the post, increase of interface roughness due to sand bonding and the relaxation of stress generated during the installation as it has been stated by (Chow & Jardine 1998; Gavin *et al.* 2013; Lim & Lehane 2015). This thus implies an increase of radial effective stress on the post.

A possible additional contributor was the drying out of the backfill during the aging period. An 18.6% reduction in water content was recorded.

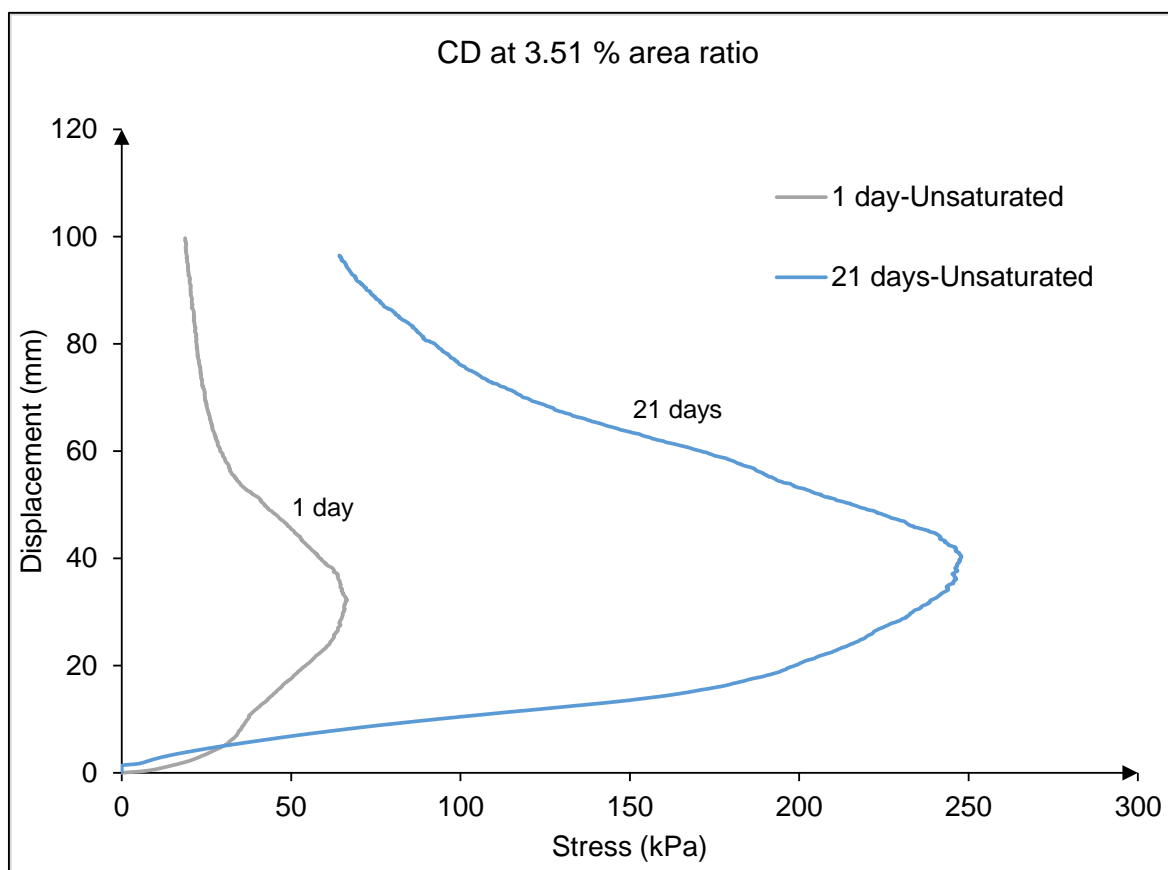


Figure 5-7 Effect of aging on axial pull-out capacity of CD compacted at 90% Mod ASSHTO

e) Effect of Compaction Density and Area Ratio on Axial Pull-out Resistance

Figure 5-8 illustrates the effect of compaction density and area ratio on axial pull-out capacity of the post tested under unsaturated and saturated conditions. The effect of compaction density is more pronounced on axial pull-out capacity than the area ratio effect at unsaturated condition whereas the trends at saturated condition are more-or-less the same for both compaction density and area ratio.

As a general statement, the axial pull-out capacity increases with increases in both compaction density and area ratio. In both cases, this increment is due to the densification of material surrounding the post. The compaction density exerted a greater influence on the axial pull-out capacity than area ratio.

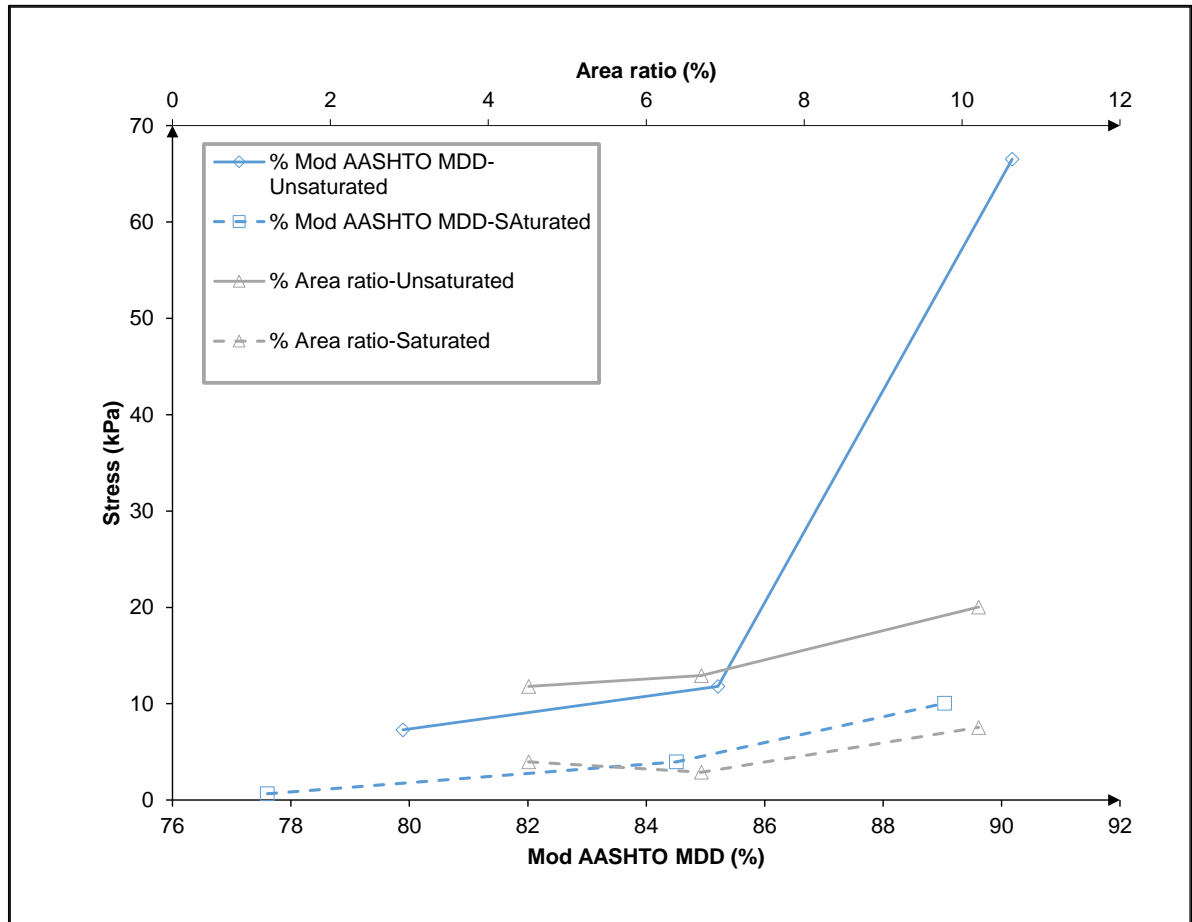


Figure 5-8 Comparison between the effect of compaction density and area on axial pull-out capacity of crusher dust (CD)

5.2.2 MALMESBURY SAND

5.2.2.1 Drive-in Force

Figure 5-9 illustrates the relationship between the drive-in force of the post and penetration in Malmesbury sand (MS) at unsaturated condition. A general increase in drive-in force was observed with penetration. The maximum drive-in force was approximately 3.5kN at 535mm of penetration. The local peaks in resistance can be attributed to the effect of compaction layering of the sand on the end bearing resistance of the post.

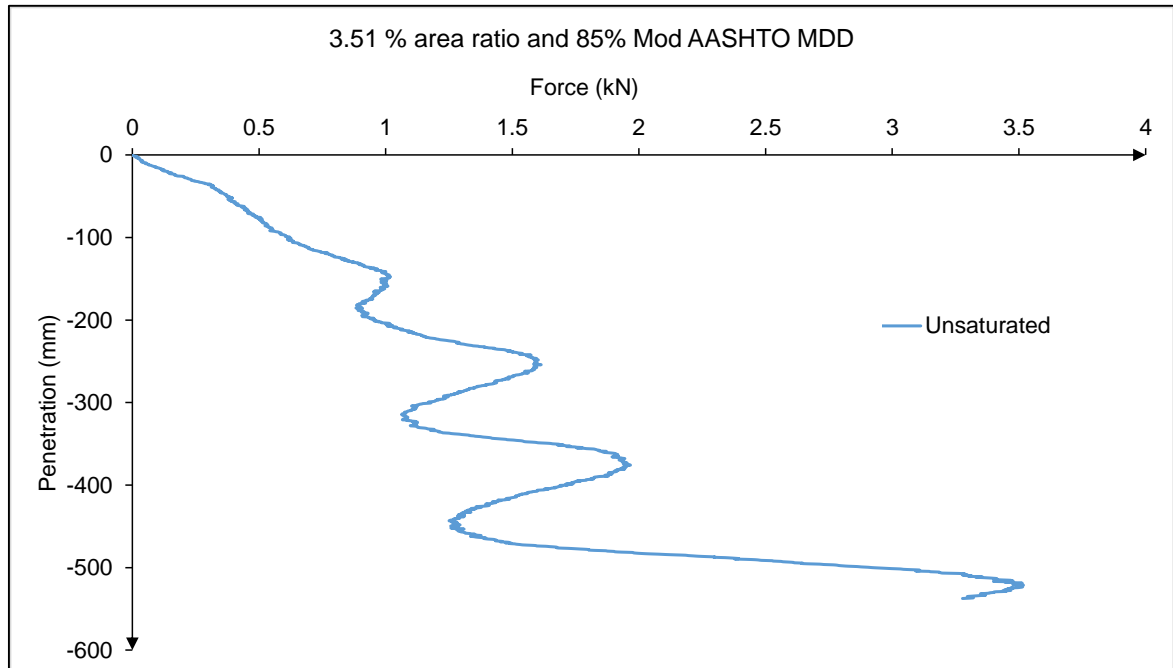


Figure 5-9 Drive-in force versus penetration of MS at unsaturated conditions

5.2.2.2 Axial Pull-out Capacity

Figure 5-10 shows the relationship between the pull-out force and displacement for 85% Mod AASHTO MDD compaction density and a 3.51% of area ratio. When the test was done without saturation of the sample, the pull-out force increased with displacement until the failure of soil occurs thereafter the pull-out force decreased with displacement. Saturation of the MS sample prior to testing resulted in a dramatic decrease in pull-out resistance. At unsaturated condition, the MS exhibited a maximum pull-out resistance of 10.09kPa at 23 mm of displacement, while a mere 0.27kPa was registered at 3.25mm for the saturated test.

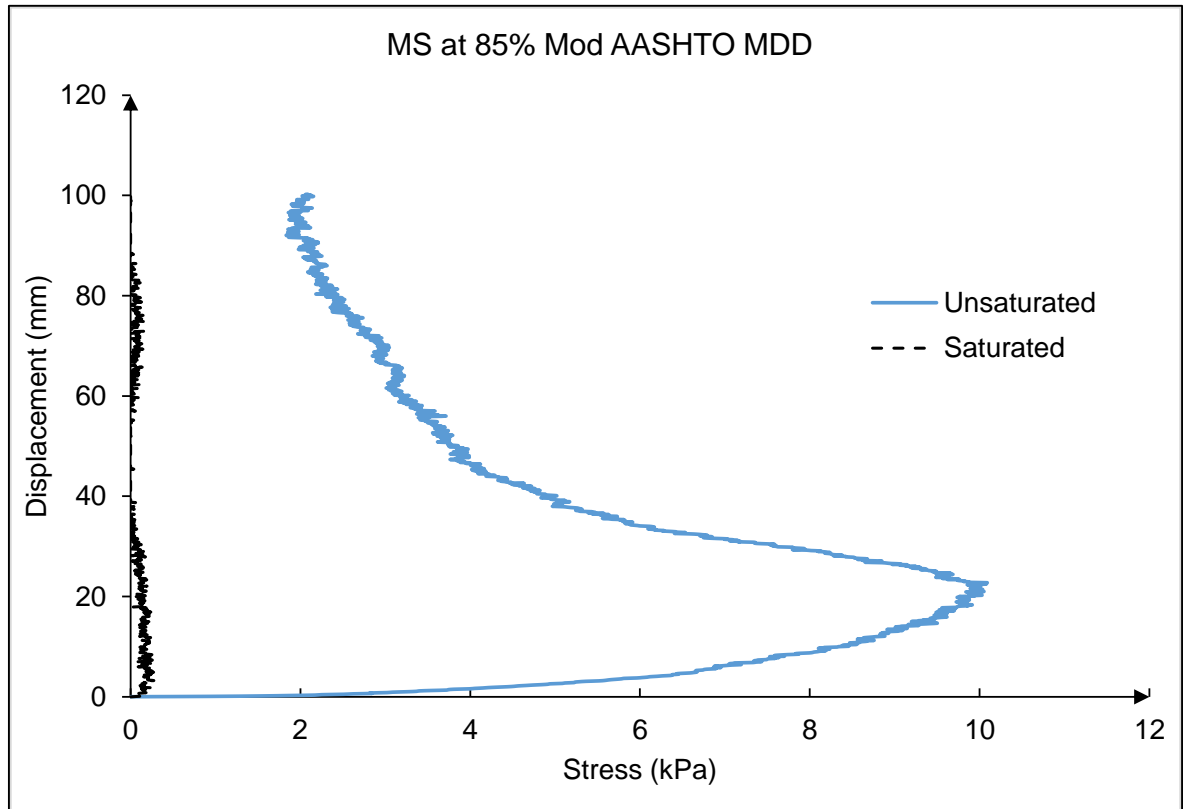


Figure 5-10 Axial pull-out resistance versus displacement at unsaturated and saturated conditions of MS

5.2.3 PHILIPPI SAND

5.2.3.1 Drive-in Force

Figure 5-11 shows the relationship between the drive-in force and penetration of Philippi sand material for an area ratio of 3.51 % and compaction of the backfill to 85% Mod AASHTO MDD. The test was performed in the unsaturated condition. The maximum drive-in force of 4kN was recorded at a penetration of about 550 mm. No compaction layering effects are evident.

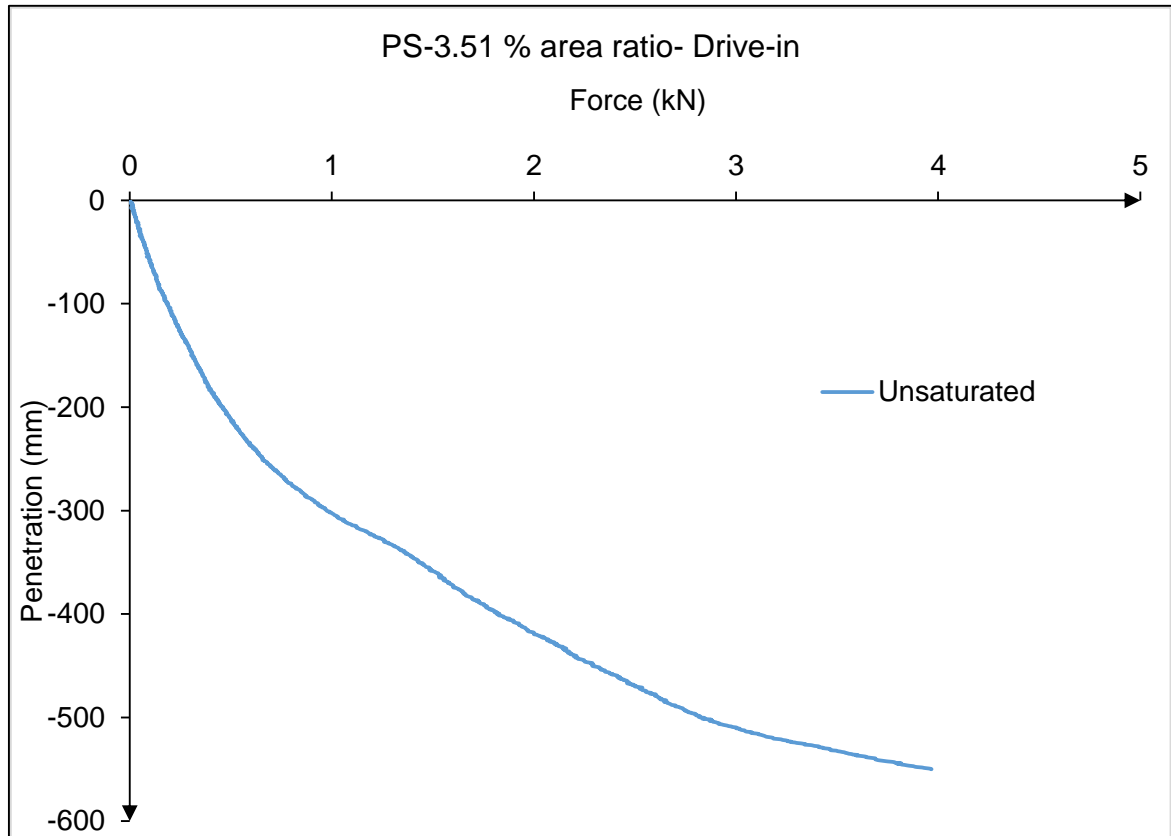


Figure 5-11 Drive-in force versus penetration of PS tested at 3.51% area ratio at 85% Mod AASHTO

5.2.3.2 Pull-out Capacity

Figure 5-12 shows the relationship of the axial pull-out force to displacement of PS for a 3.51% area ratio and compaction to 85% Mod AASHTO MDD for a test conducted under unsaturated and saturated conditions. The axial pull-out resistance increased with displacement until the failure in material occurred then decreased. In the unsaturated test, a maximum axial pull-out capacity of 7.87kPa was recorded after a displacement of about 20mm. The reduction in pull-out capacity in saturated conditions was even more dramatic than with the MS with the pull-out resistance being too small to measure. Moisture content influences significantly the pull-out capacity of PS material.

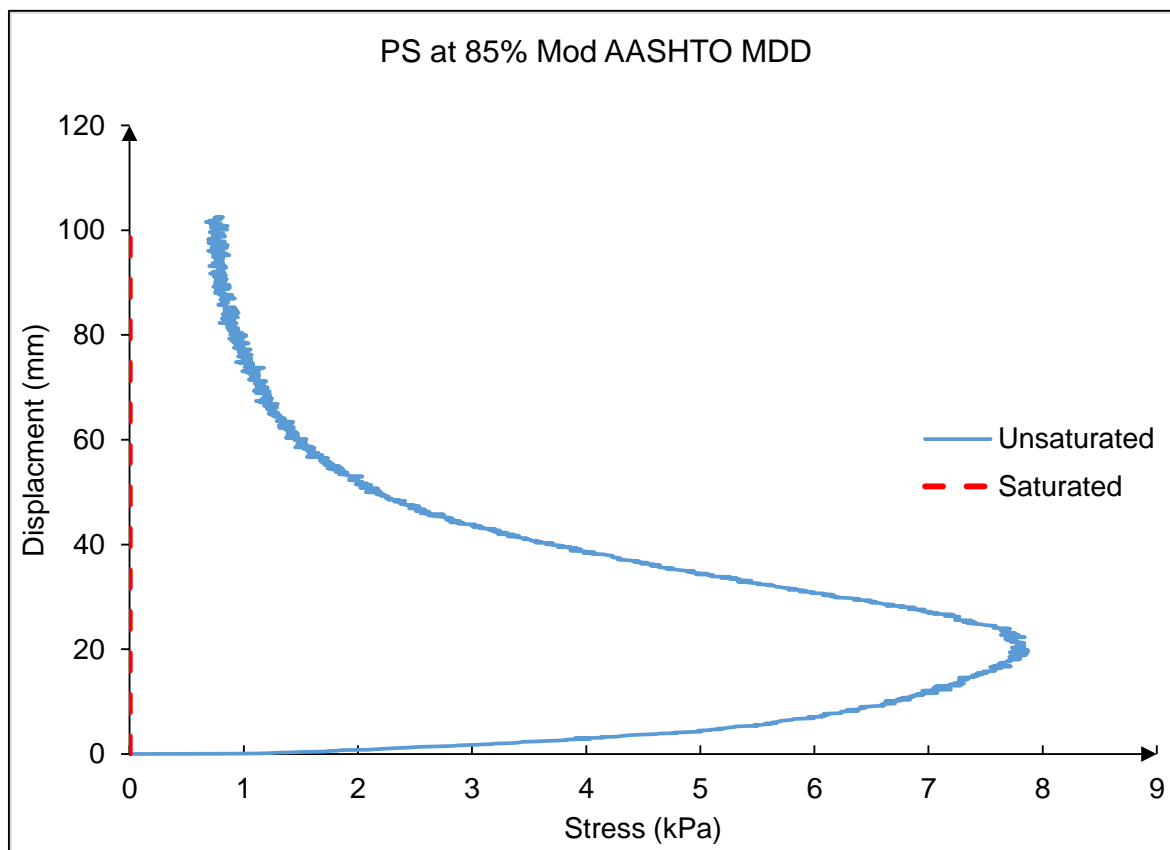


Figure 5-12 Axial pull-out resistance versus displacement of PS

5.2.4 COMPARISON OF DIFFERENT MATERIAL TYPES

5.2.4.1 Drive-in Force

Figure 5-13 illustrates the relationship of the drive-in force to penetration for all the research materials for an area ratio of 3.51% and a compaction density of 85% Mod AASHTO MDD. The drive-in force increases generally with depth. CD material exhibited higher drive-in force than MS and PS materials. This is attributed to the particle size distribution, maximum aggregate size, and particle shape of the materials. CD is an angular, well graded material with a maximum particle size of 6.7 mm while MS and PS have more rounded particles, are poorly graded with 6.7 and 2.3mm maximum particle sizes respectively.

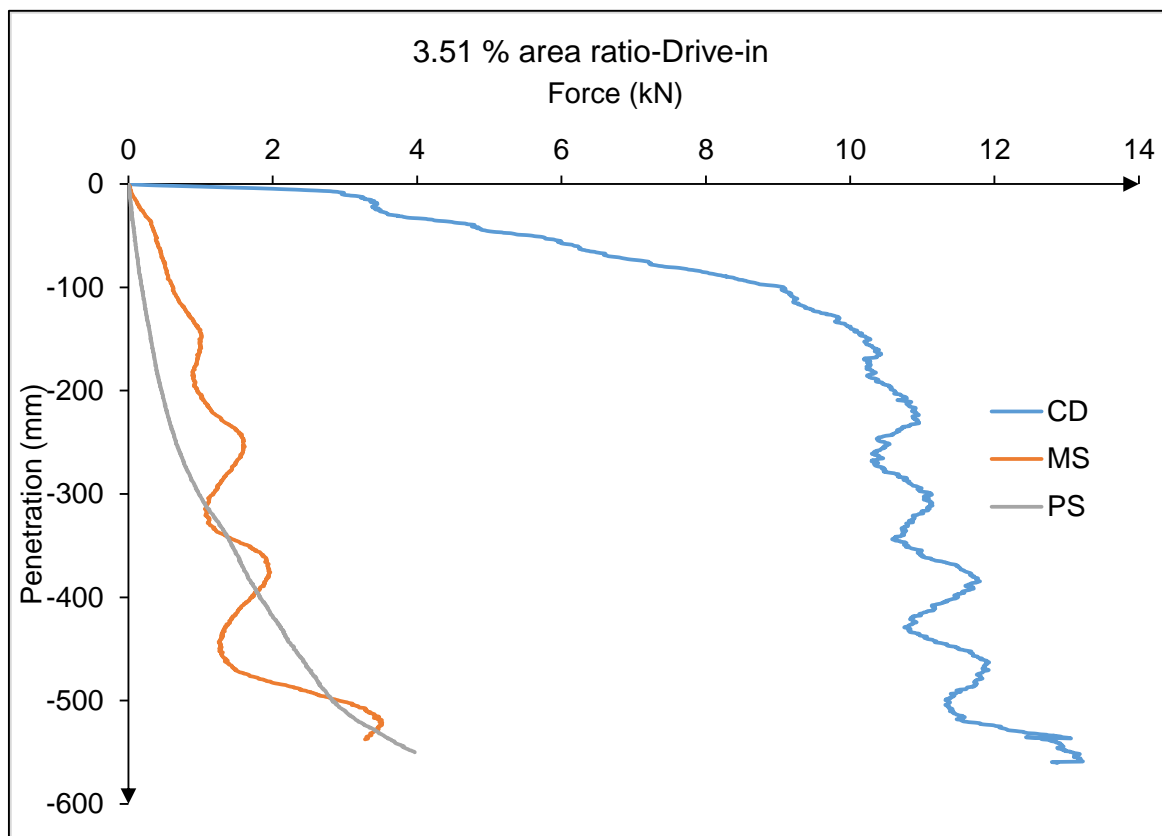


Figure 5-13 Driven in force versus displacement of research materials at 85% Mod AASHTO MDD

5.2.4.2 Pull-out Capacity

Figure 5-14 shows the axial pull-out resistance of the research materials tested at the same compaction effort (85% MDD) and area ratio (3.51%). Generally, the pull-out resistance increased until it reached its maximum capacity then started decreasing after the material failure occurred. The CD material exhibited a higher pull-out capacity than MS and PS materials.

For the tests conducted under unsaturated conditions, pull-out capacities of 11.79kPa, 10.09kPa and 7.87kPa were recorded for CD, MS and PS respectively. The differences in the performance of the CD, MS and PS materials are attributed to differences in their maximum dry density (MDD), dilation and shear strength. Higher maximum density was developed in CD compared to MS material and lower maximum density was recorded in PS. Moreover, CD exhibited dilation and higher shear strength while MS and PS either did not dilate on shear or dilated only at low stresses.

For all materials, the axial pull-out capacity decreased when the tests were conducted under saturated conditions. Pull-out values of 3.98kPa, 0.27kPa and 0.00kPa were registered for DC, MS and PS respectively at saturation condition.

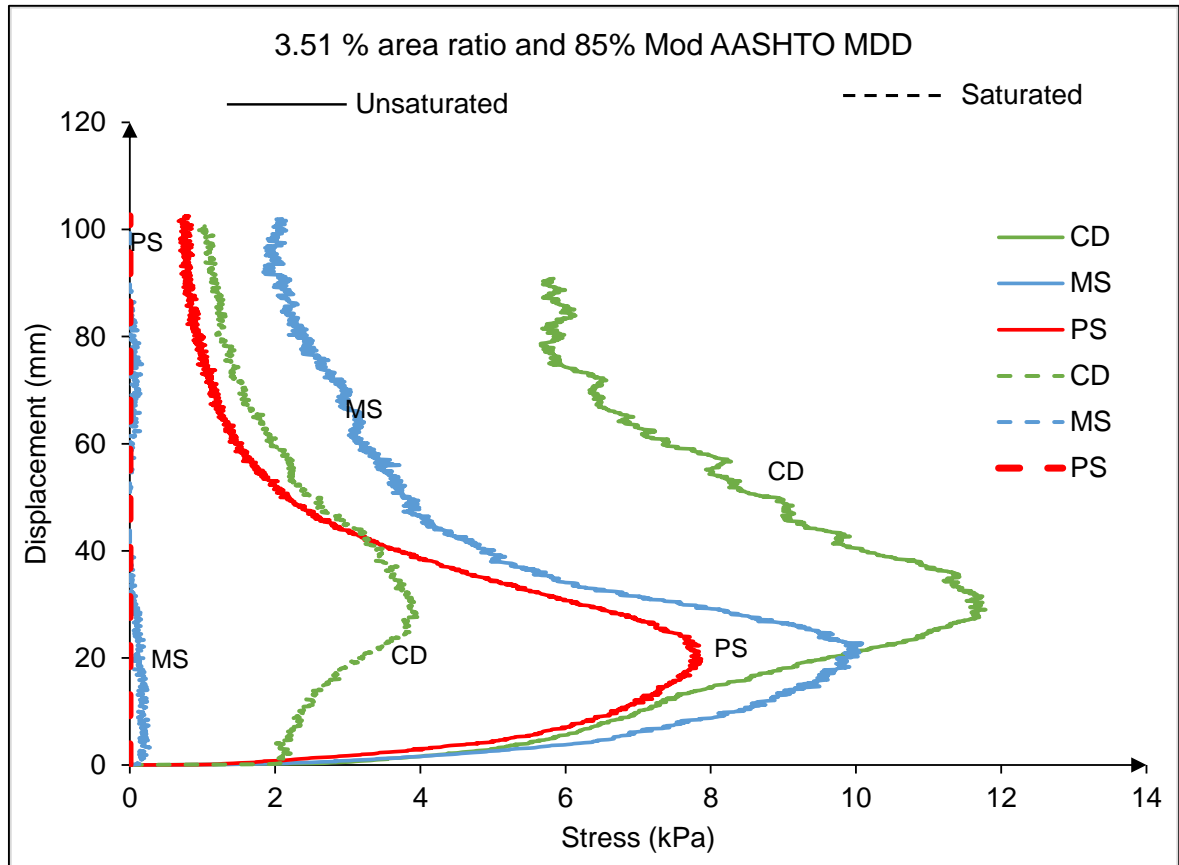


Figure 5-14 Axial pull-out resistance versus displacement of research materials compacted at 85% Mod AASHTO MDD

Table 5-2 Summary of maximum of axial pull-out resistance force of the research materials

| Material type | Maximum size of aggregate (mm) | Number of days prior to test | Compaction moisture content | Testing moisture condition | Mod AASHTO MDD (%) | Area ratio A/A _p (%) | Maximum axial pull-out resistance in stress (kPa) | Maximum axial pull-out force (kN) | Distance at the failure (mm) |
|---------------|--------------------------------|------------------------------|-----------------------------|----------------------------|--------------------|---------------------------------|---|-----------------------------------|------------------------------|
| CD | 6.7 | 1 | OMC | Unsaturated | 79.89 | 3.51 | 7.28 | 0.74 | 54.40 |
| | | 1 | | | 85.21 | 3.51 | 11.79 | 1.25 | 28.90 |
| | | 1 | | | 90.18 | 3.51 | 66.52 | 6.59 | 32.14 |
| | | 1 | | | 84 | 6.7 | 12.94 | 1.40 | 17.54 |
| | | 1 | | | 85.62 | 10.21 | 20.03 | 1.97 | 58.02 |
| | | 1 | OMC | Saturated | 77.79 | 3.51 | 0.66 | 0.07 | 1.00 |
| | | 1 | | | 84.51 | 3.51 | 3.98 | 0.41 | 28.12 |
| | | 1 | | | 89.04 | 3.51 | 10.06 | 1.01 | 29.00 |
| | | 1 | | | 84.37 | 6.7 | 2.90 | 0.31 | 2.85 |
| | | 1 | | | 85.19 | 10.21 | 7.54 | 0.82 | 0.49 |
| | | 1 | Dry | Dry | 74.61 | 3.51 | 0.35 | 0.04 | 1.41 |
| | | | | | 81.92 | 3.51 | 4.78 | 0.48 | 29.05 |
| | | 21 | OMC | Unsaturated | 90.05 | 3.51 | 247.86 | 23.51 | 40.15 |
| MS | 6.7 | 1 | OMC | Unsaturated | 85.86 | 3.51 | 10.09 | 0.79 | 22.74 |
| | | 1 | OMC | Saturated | 84.97 | 3.51 | 0.27 | 0.03 | 3.25 |
| PS | 2.3 | 1 | OMC | Unsaturated | 87.1 | 3.51 | 7.87 | 0.84 | 19.81 |
| | | 1 | OMC | Saturated | 87.13 | 3.51 | 0.00 | 0.00 | 0 |

5.3 OBLIQUE PULL-OUT TEST

In this section, oblique pull-out resistance plotted against displacement are presented for CD, MS and PS materials at 80%, 85% and 90% compaction density and 3.51%, 6.7% and 10.21% area ratios. Each of the tests was performed under unsaturated and saturated conditions.

In the oblique tests, the force was applied at an angle of 20° to the post axis.

5.3.1 CRUSHER DUST

5.3.1.1 Unsaturated and Saturated Conditions at Different Compaction Densities

Figure 5-15 shows the relationship between oblique pull-out forces and displacement of CD material compacted at 80%, 85% and 90% Mod AASHTO MDD under unsaturated and saturated conditions for a 3.51% area ratio. Generally, the oblique pull-out forces increased continuously with displacement except at 90% Mod AASHTO MDD and unsaturated. Due to the continuous increase of the oblique pull-out forces, each of the tests failure of CD was taken as occurring at the same displacement as the peak resistance at 90% Mod AASHTO MDD i.e. at 40mm.

The oblique pull-out capacity, taken as occurring at 40mm, increased with the increase of compaction density and reduced with saturation. When tested in the unsaturated condition, oblique pull-out capacities of 20.13, 32.42, and 129kPa were developed for compaction densities of 80%, 85% and 90% MDD respectively. As with the axial pull-out tests, the pull-out resistance under oblique loading decreased when the tests were carried out under saturated conditions. However, the decrease was not as dramatic as in the axial tests. The reduced oblique pull-out resistances for saturated tests were 7.11kPa, 13.03kPa and 43.18kPa at the above three densities respectively.

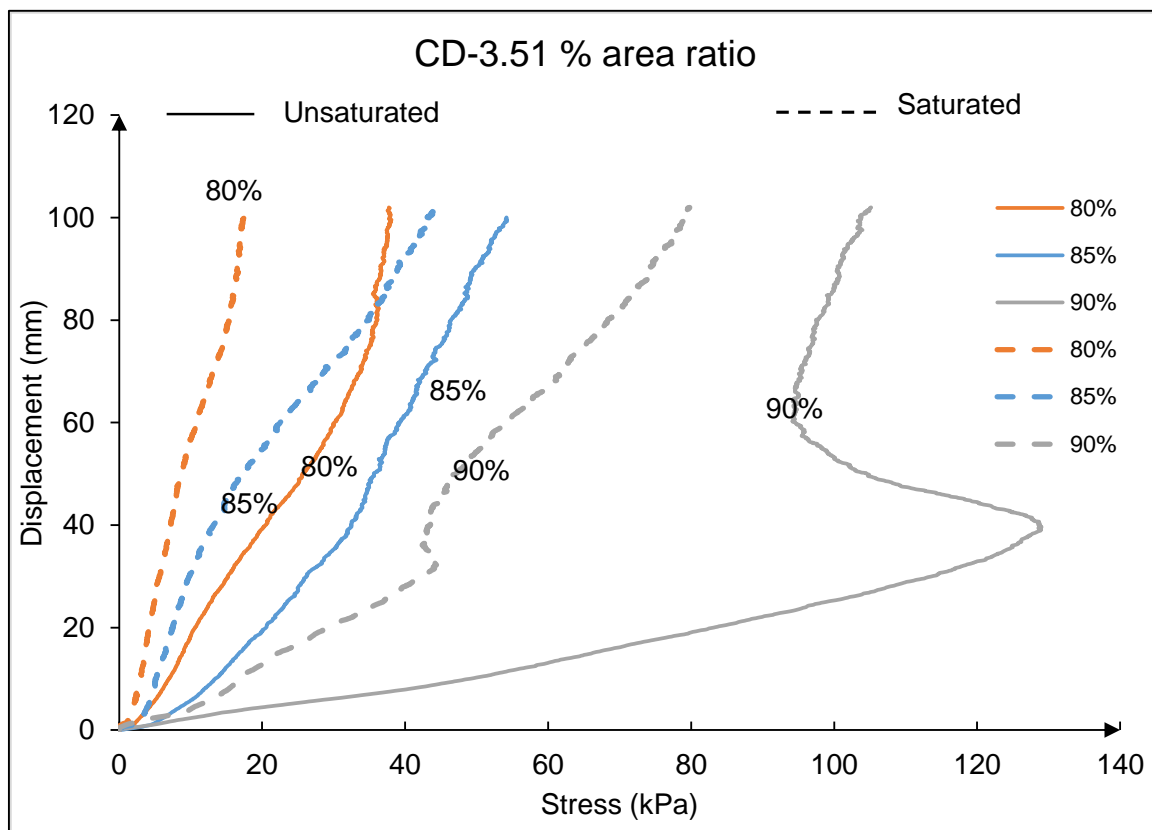


Figure 5-15 Oblique pull-out resistance versus displacement of CD at different compaction densities

5.3.1.2 Unsaturated and Saturated Conditions at Different Post Area Ratios

Figure 5-16 illustrates the relationship between oblique resistance and displacement at different area ratios under unsaturated and saturated conditions. The oblique pull-out forces increased continuously with displacement due to the lateral force component and also increased with an increase in area ratio. The resistance was lower in the saturated tests compared to the tests on unsaturated soils.

In the unsaturated condition, an oblique pull-out resistance of 32.42kPa, 23.94kPa and 70.37kPa at 40mm displacement were recorded for area ratios of 3.51%, 6.7% and 10.21% respectively. The oblique pull-out reduced at 6.7% area ratio. This unexpected result was due to limited increase in resistance from 15 mm to 40mm. The resistance recovered with further displacement and its resistance exceeded the resistance of the 3.51 area ratio post at higher deflections. The higher oblique pull-out resistance for the 10.21% area ratio post was due to the higher displacement during drive-in causing densification of material.

In the saturated tests, the oblique pull-out resistance was lower than in the unsaturated tests. Resistances of 13.03kPa, 14.17kPa, and 26.57kPa shown in Table 5-3 were recorded for the 3.51%, 6.7%, and 10.21% area ratio posts respectively. This is reduction a 60%, 41%, and 62.24 % respectively.

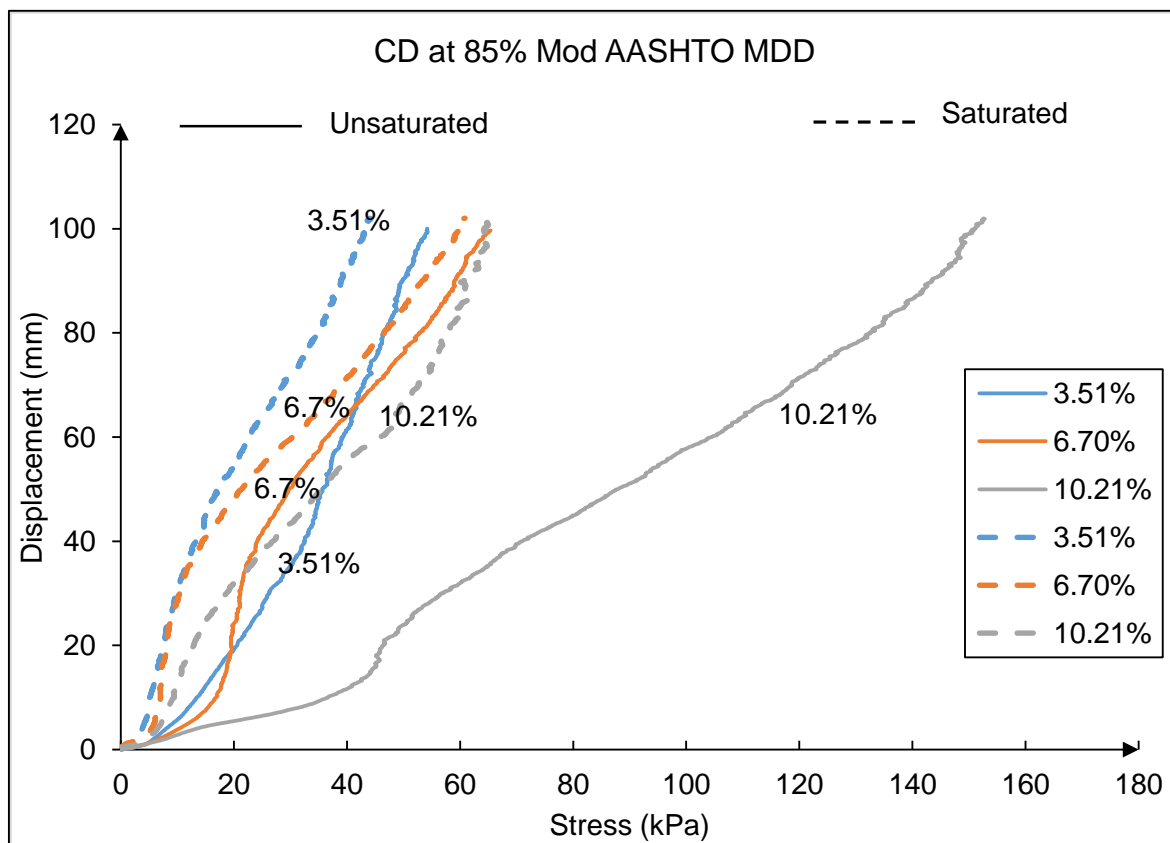


Figure 5-16 Oblique pull-out resistance versus displacement of CD at different area ratios in unsaturated and unsaturated conditions

5.3.2 MALMESBURY SAND

The results of the saturated and unsaturated oblique pull-out test of MS material for a 3.51 area ratio are plotted in Figure 5-17. In the unsaturated test, the oblique pull-out stress increases with displacement before becoming more-or-less constant from 25mm onward. The peak oblique pull-out resistance of 19.99kPa occurred at about 35mm displacement. The pull-out resistance for the saturated test was considerably lower throughout the full displacement range. In the saturated test, the pull-out stress increased continuously with displacement. Therefore, “failure” was taken as occurring at the same displacement as the peak in the unsaturated test. This gives a pull-out resistance of 2.41kPa at 35mm.

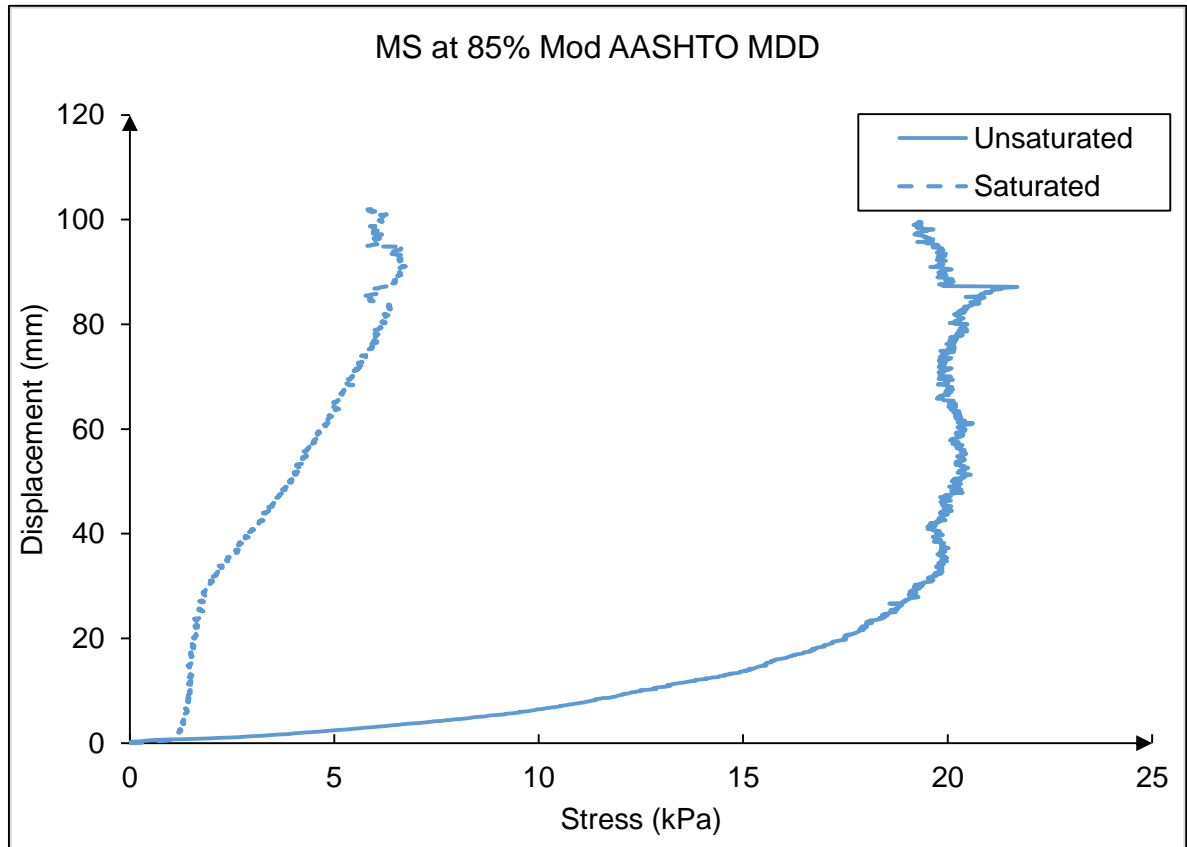


Figure 5-17 Oblique pull-out force versus displacement of MS at unsaturated and saturated conditions

5.3.3 PHILIPPI SAND

Figure 5-18 presents the relationship between the oblique pull-out resistance and displacement in PS material under both unsaturated and saturated conditions. The tests were both performed at 85% Mod AASHTO MDD with a 3.51% area ratio post. In the unsaturated test, the oblique pull-out resistance increased with displacement until it reached its maximum of 15.67kPa at 23mm. In the saturated test, a pull-out resistance of 4.26kPa was developed, which is a reduction of approximately 73%.

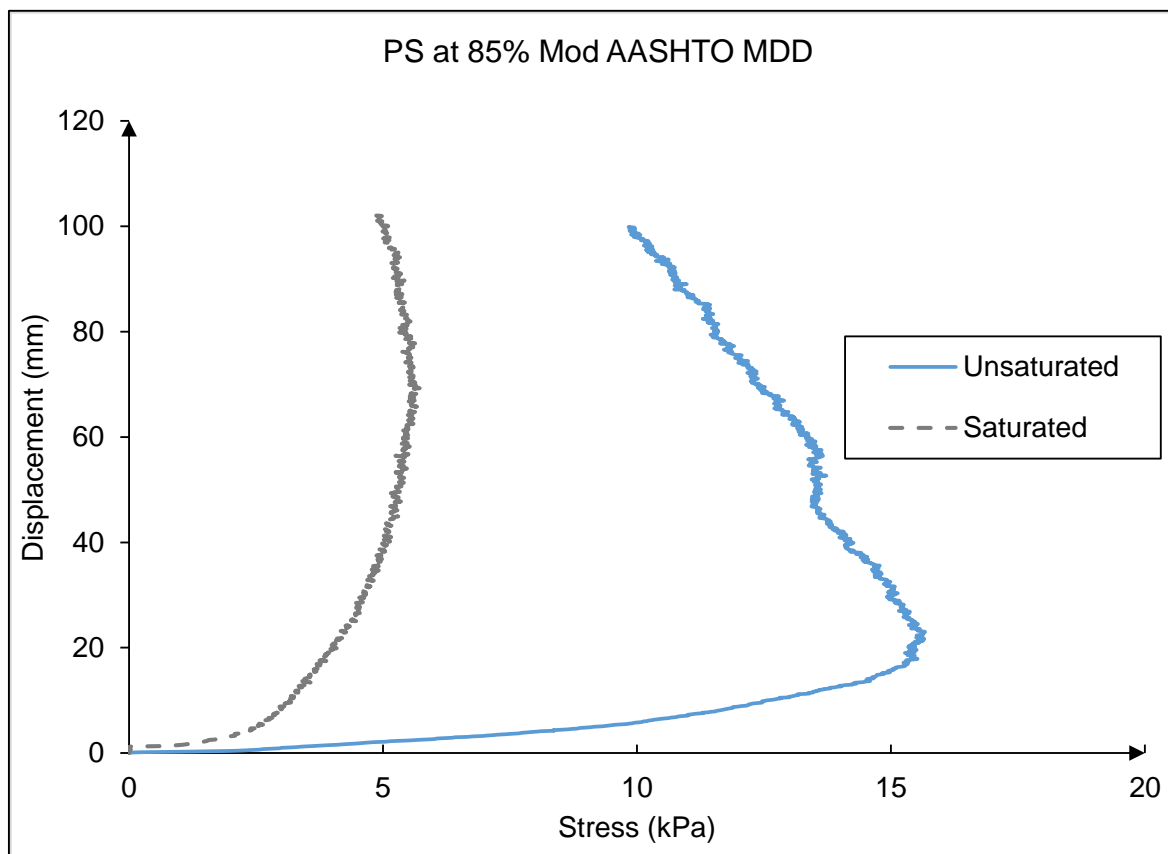


Figure 5-18 Axial pull-out force versus displacement of PS at unsaturated and saturated conditions

5.3.4 COMPARISON OF DIFFERENT MATERIAL TYPES

The influence of material types on oblique pull-out resistance is presented in Figure 5-19 for all the research materials at 85% Mod AASHTO using the 3.51% area ratio post. Both saturated and unsaturated test results are presented. Oblique pull-out resistance for CD material is higher than for MS and PS sand. The higher resistance recorded for the posts in CD is attributed to its higher shear strength and dilation as discussed in section 4.2 of chapter 4, particularly the Figure 4-6 and Figure 4-13.

Saturation of the material prior to testing reduced the oblique pull-out resistance from 32.42 to 13.03kPa, 19.99 to 2.41kPa and 15.67 to 4.26kPa for CD, MS and PS respectively. This is the effect of water acting as lubricant on the interface of material and the post.

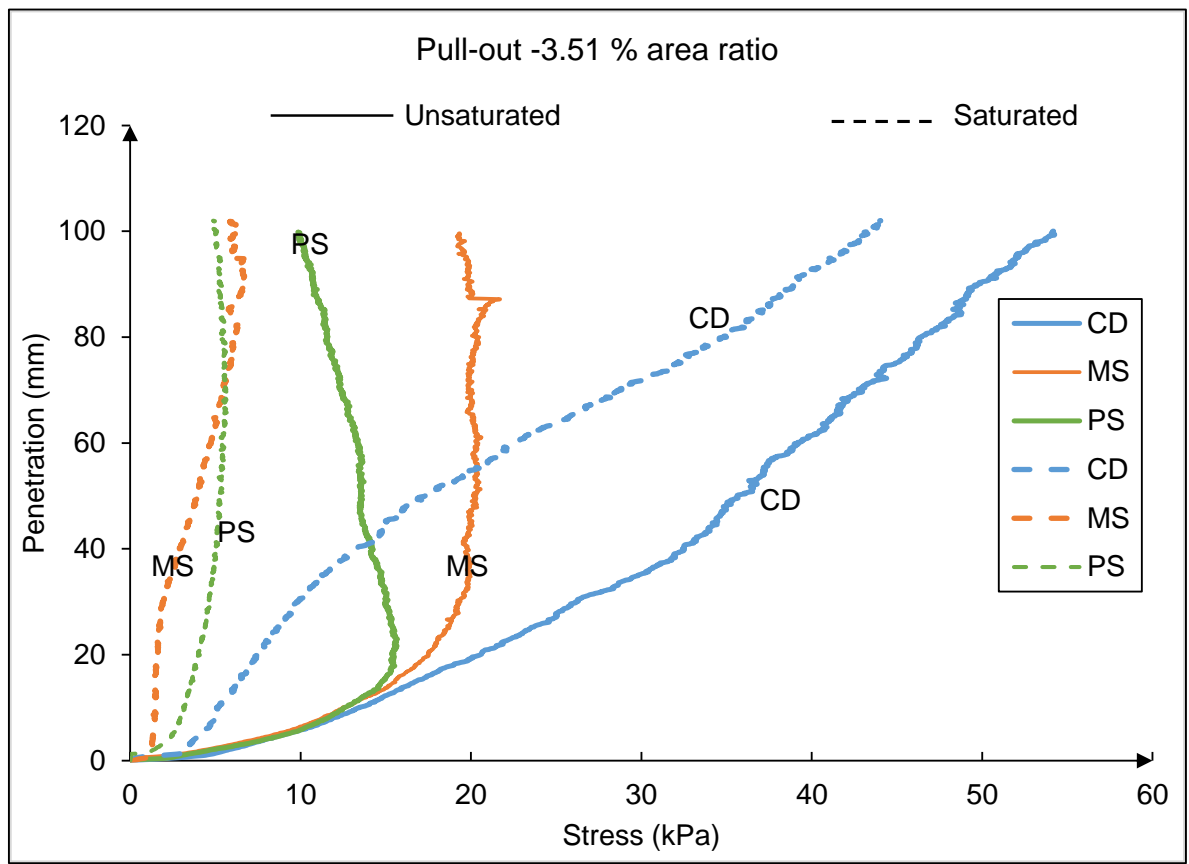


Figure 5-19 Oblique pull-out force versus displacement of research materials compacted at 85% Mod AASHTO MDD

Table 5-3 Summary of maximum of oblique pull-out resistance and force of the research materials

| Material type | Maximum size of aggregate (mm) | Number of days prior to test | Compaction moisture content | Testing moisture condition | Mod AASHTO MDD (%) | Area ratio (%) | Maximum oblique pull-out resistance (kPa) | Maximum oblique pull-out force (kN) | Distance at the failure (mm) |
|---------------|--------------------------------|------------------------------|-----------------------------|----------------------------|--------------------|----------------|---|-------------------------------------|------------------------------|
| CD | 6.7 | 1 | OMC | Unsaturated | 78.61 | 3.51 | 20.13 | 1.96 | 39.58 |
| | | 1 | | | 85.76 | 3.51 | 32.42 | 3.26 | 39.58 |
| | | 1 | | | 90.79 | 3.51 | 129.00 | 12.13 | 39.58 |
| | | 1 | | | 83.06 | 6.70 | 23.94 | 2.35 | 39.58 |
| | | 1 | | | 83.16 | 10.21 | 70.37 | 6.98 | 39.58 |
| | | 1 | OMC | Saturated | 78.69 | 3.51 | 7.11 | 0.67 | 39.58 |
| | | 1 | | | 84.58 | 3.51 | 13.03 | 1.22 | 39.58 |
| | | 1 | | | 89.59 | 3.51 | 43.18 | 6.56 | 39.58 |
| | | 1 | | | 83.50 | 6.70 | 14.17 | 1.34 | 39.58 |
| | | 1 | | | 83.59 | 10.21 | 26.57 | 2.47 | 39.58 |
| MS | 6.7 | 1 | OMC | Unsaturated | 85.84 | 3.51 | 19.99 | 2.02 | 34.75 |
| | | 1 | OMC | Saturated | 84.97 | 3.51 | 2.41 | 0.24 | 34.75 |
| PS | 2.3 | 1 | OMC | Unsaturated | 85.83 | 3.51 | 15.67 | 1.63 | 23.00 |
| | | 1 | OMC | Saturated | 87.13 | 3.51 | 4.26 | 0.41 | 23.00 |

5.4 DISCUSSION OF RESULTS

This chapter has dealt with the pull-out capacity of posts installed into three types of sand materials. The materials were crusher dust (CD), Malmesbury and Philippi sands (MS & PS). CD material was tested at three compaction densities, three area ratios, two compaction moisture contents, saturated and unsaturated test conditions and aging. MS and PS materials were tested at one compaction density, one area ratio and two testing moisture contents.

The pull-out capacity was determined using static load test. The most important results regarding the investigated influence factors (i.e. compaction density, area ratio, moisture content and time effect) are presented in following:

- The drive-in force increases with both compaction density and area ratio in CD material. The drive-in is also higher in CD material than in MS and PS sands. This is indicative of difference in particle size distribution and maximum particle aggregate size.
- The compaction density influences the pull-out capacity of the post. With an increase of compaction density, the pull-out capacity increases. This increase varied with the compaction density. A higher increase of pull-out resistance was developed from 85% to 90% Mod AASHTO MDD than from 80% to 85%.
- The pull-out capacity values have shown the effect of varying the area ratio. The pull-out capacity generally increases with an increase in area ratio, i.e. posts with an area ratio of 10.21% exhibited higher pull-out capacity than the 6.7% and 3.51% posts. However, it is important to mention that the influence was not significant compared to the effect of compaction density. In the absence of any heave in the surface of the backfill, the insertion of the post must increase the density of the fill by a percentage roughly equal to the area ratio due to the reduction in volume occupied by the soil. However, the increase in pull-out resistance is less than what one would expect based on this density increase. This could be due to the fact the effect of the increase in density is offset by crushing of the particles and remoulding of the soils immediately adjacent to the post/soil interface.
- Based on the single test carried out, it appears that aging has a significant effect on the pull-out resistance. A large increase in pull-out capacity developed when the test was performed after 21 days after driving the post.
- The significant influence of moisture content was observed in pull-out capacity. For all the materials, saturation of the material prior to testing results in a pull-out capacity reduction. This is due to water acting as lubricant.
- Material types influence the pull-out capacity of the post. CD material exhibited higher pull-out capacity than MS and PS materials at the same Mod AASHTO MDD degree. This is due to several factors including the particle size distribution, particle shape, shear strength and angle of dilation. CD material is a well graded material whereas MS and PS materials are poorly graded materials.

- The oblique pull-out capacity was higher than the axial pull-out capacity due to the lateral component in oblique pull-out.

CHAPTER 6 CONCLUSIONS AND RECOMMENDATIONS

The purpose of this study was to investigate factors that affect the shaft pull-out capacity of driven posts used to support solar panels. Three steps were followed to achieve the study objectives. The first step was a critical review of literature as described in Chapter 2 in order to understand the post shaft capacity mechanism and document the factors that affect its pull-out capacity. The second step, presented in Chapter 3, covers the testing methods and procedures as well as the design of the experimental work. The last step presented in Chapters 4 and 5 covers the analysis and interpretation of tests undertaken to evaluate characteristics of the backfill materials used, then the shaft pull-out resistance.

This chapter presents a summary of the main findings provided in the chapters mentioned above together with recommendations for further study.

6.1 CONCLUSIONS

Based on the results of the study, the main conclusions are presented below:

- Particle size distribution has a significant influence on material strength. The well-graded crusher dust has a higher shear strength and dilation than the poorly graded-Malmesbury and Philippi sands. In addition to the particle size distribution, the subangular particle shape of the crusher dust contributed to the higher shear strength and dilation of this material.
- Shear strength and dilation of CD material also increases with the degree of compaction.
- The shear strength of the research materials increases with an increase in normal stress. However, the dilation reduces with an increase in normal stress.
- Saturation of specimen reduces both the shear strength and dilation of the research materials.
- Drive-in force depends on the material type. It also increases with the compaction density and area ratio. Drive-in force for crusher dust is higher than for Malmesbury and Philippi sands.
- Due to the physical properties of the materials mentioned above, the shaft pull-out capacity of the post is higher for the crusher dust material than for Malmesbury and Philippi sands.
- In addition, the shaft pull-out capacity increases with an increase in the degree of compaction for crusher dust material.
- Saturation of the backfill was found to have a very significant effect on the shaft pull-out capacity, particularly in the Malmesbury and Philippi sands.
- The effect of area ratio was found to be less significant in most instances.
- Aging of the backfill after driving of the post increases the shaft capacity of the post. A more than threefold increase in shaft pull-out capacity was recorded when the test was performed 21 days after driving of the post. Drying out of the backfill during the aging period may have contributed to this increase.

- For a given compactive effort, compacting material in a dry state gives a lower degree of compaction compared to compaction at or near optimum moisture content. Therefore, the shaft pull-out capacity of the post is lower with dry compaction than with compaction near the optimum moisture content despite the application of the same compaction energy.
- The oblique pull-out capacity of the post is higher than the axial pull-out capacity due to the increased normal stress on one side of the post both at the top and bottom of the embedded length.
- In relation to the solar panel supports, it is concluded that compaction density of the backfill material, the backfill type, saturation of the backfill prior to loading and the direction of loading all have an effect on the pull-out resistance of the post. The increase in capacity under oblique loading lateral load explains why incorrectly installed posts in solar panel project may settle under modest dead loading but is able to resist significant wind loading.

In summary, it can be concluded that based on the study, the key factors affecting the shaft pull-out capacity of the post are the degree of compaction, types of material, effect of aging and saturation of the backfill. The results of the study showed that crusher dust material could be a good backfill material for the driven post.

6.2 RECOMMENDATIONS

The research identifies keys factors affecting the shaft pull-out capacity. However, to improve the evaluation and performance of the shaft pull-out capacity of the driven post for further studies and field construction practices, the following recommendations are made:

6.2.1 RECOMMENDATIONS FOR SOLAR PANELS POSTS FIELD CONSTRUCTION

- A well graded backfill, preferably with angular particle shape, should be used. Materials, which have a high angle of internal friction and high angle of dilation, will perform better than weaker, non-dilatant materials.
- Compaction of the backfill should take place in layers as the hole is filled, with the backfill at optimum moisture content. Placement of the backfill in a dry condition will lower the density of the fill and reduce the pull-out capacity of the post.

6.2.2 RECOMMENDATIONS FOR FURTHER STUDIES

- As it has been noted in literature review, average particle size (d_{50}) reduction increases the interface angle of friction. Therefore, it is recommended that the effect of reducing the average particle size on the shaft pull-out capacity should be evaluated. For example, will 6mm crusher dust perform better than a 26.5mm crusher run.
- The experimental model was conducted at half scale and the shaft capacity increases with an increase in confinement. For this reason, an effect of pipe diameter should be investigated to evaluate the shaft pull-out capacity of the post.

- An angle section post was used in the investigation study to due to the availability and the simplification. Further tests should be undertaken using a “top hat” section, which is the section commonly used on solar projects.
- Further study on the effect of driven post length on the shaft pull-out capacity.
- A steel pipe was used to simulate a hole was drilled into rock. To gain a better understanding of the shaft pull-out capacity, field trials in various ground conditions are recommended.
- In the field, solar panel driven posts are subjected to dynamic load caused by winds. Therefore, a detailed analysis of shaft pull-out is recommended by using a dynamic load.
- The study showed a significant improvement in shaft pull-out capacity when testing was carried out 21 days after driving of the post. The result of this single test should be verified and more tests undertaken at different times to evaluate the effect of aging on shaft pull-out capacity of the post. To reduce the influence of drying of the backfill during the aging period, loss of moisture during aging should be prevented. Tests should be conducted in both the saturated and “dry” condition.
- Due to the various tilt angles used for solar panels at different latitudes, it is recommended to evaluate the shaft pull-out capacity at different angles of oblique loading.

REFERENCES

- Alawneh, A.S., Malkawi, A.I.H. & Al-deeky, H., 1999. Tension tests on smooth and rough model piles in dry sand. *Canadian Geotechnical Journal*, 753, pp.746–753.
- API, 2000. Recommended Practice for Planning , Designing and Constructing Fixed Offshore Platforms - Working Stress Design 21st Edition. API Publishing.Washington, D.C., USA.
- ASTM, 2003. D3080: Standard Test Method for Direct Shear Test of Soils Under Consolidated Drained. ASTM international, West Conshohocken, PA, USA.
- Axelsson, G., 2000. Long Term Set Upt of Driven Piles In Sand. Doctoral Dissertation.Stockholm: Royal Institute of Technology.
- Axelsson, G., 1998. Long-term increase in shaft capacity of driven piles in sand. In *Proceeding of Fourth International Conference on Case History in Geotechnical Engineering*. St. Louis, Missouri: Missouri University of Science and Technology Scholars' Mine.
- Bareither, C.A. *et al.*, 2008. Geological and Physical Factors Affecting the Friction Angle of Compacted Sands. *Journal of Geotechnical and Geoenvironmental Engineering*, 134(10), pp.1476–1489.
- Bareither, C.A., Benson, C.H. & Edil, T.B., 2008. Comparison of Shear Strength of Sand Backfills Measured In Small-Scale and Large-Scale Direct Shear Tests. *Canadian Geotechnical Journal*, 45(9), pp.1224–1236.
- Bell, A. & Robinson, C., 2012. Single Piles. In *ICE Manual of Geotechnical Engineering: Geotechnical Design, Construction and Verification*, Burland J. *et al.*, (eds). Thomas Telford, London, UK,vol.2, pp. 803-821.
- Bhardwaj, S. & Singh, S.K., 2013. Pullout capacity of model micropiles under oblique loads. In *Proceedings of Indian Geotechnical Conference-GANGA*. Roorkee, India.
- Bolton, M.D., 1986. The strength and dilatancy of sands. *Géotechnique*, 36, No.1, 65-78.
- Boulon, M. & Foray, P., 1986. Physical and numerical simulation of lateral shaft friction along offshore piles in sand. 3rd *International Conference on Numerical Methods in Offshore piling*, Nantes, France. pp.127–147.
- Briaud, J.-L., 2013. *Geotechnical Engineering: Unsaturated and Saturated Soils*. New Jersey, USA: John Wiley & Sons.
- BSI, 1990. BS 1377-7. British Standard Methods of Test for soils for civil engineering purposes. Shear strength tests. BSI, London, UK.

- Burland, J., 2012. Soils as Particulate Materials. In *ICE Manual of Geotechnical Engineering: Geotechnical Engineering Principles, Problematic Soils and Site Investigation*, Burland, J. et al., (eds). Thomas Telford, London, UK, vol.1, pp.153-161.
- Byrne, G. & Berry, A.D., 2008. *A Guide to Practical Geotechnical Engineering in Southern Africa* 4th edition, South Africa: Franki Afrika.
- Cerato, A.B. & Lutenecker, A.J., 2006. Specimen size and scale effects of direct shear box tests of sands. *Geotechnical Testing Journal*, 29(6), pp.507–516.
- Cho, G.-C., Dodds, J. & Santamarina, J.C., 2006. Particle Shape Effects on Packing Density, Stiffness, and Strength: Natural and Crushed Sands. *Journal of Geotechnical and Geoenvironmental Engineering*, 132(5), pp.591–602.
- Chow, F. & Jardine, R., 1998. Effects of time on capacity of pipe piles in dense marine sand. *Journal of Geotechnical and Geoenvironmental Engineering*, 124(3), pp.254–264.
- Craig, R.F., 2004. *Craig's Soil Mechanics* 7th Edition, London: Taylor & Francis.
- Das, B. & Sivakugan, S., 2014. *Introduction to Geotechnical Engineering* 2nd Edition, Boston, USA:Cengage Learning.
- Das, B. & Sobhan, K., 2013. *Principles of Geotechnical Engineering*, 8th Edition, Stamford, USA:Cengage Learning.
- Das, B.M., 2009. *Principles of Geotechnical Engineering*, 7th Edition, Stamford, USA: Cengage Learning.
- Day, P.W., 2014a. *Advanced Foundation Design*, Stellenbosch, South Africa: Unpublished Lecture.
- Day, P.W., 2014b. *driven piles installation method*, e-mail to A. Uwimana [Online], 17 June. Available e-mail: aim05fr@gmail.com.
- De-Aar Solar Power, 2014. Aerial photographs of De Aar Solar Power [Online]. Available: <http://deaarsolar.co.za/aerial-photographs-of-de-aar-solar-power/> [2014, August 28]
- Department of Energy of South Africa, 2014. Solar Power [Online]. Available: http://www.energy.gov.za/files/esources/renewables/r_solar.html [2014, August 2]
- Duncan, J.M. & Wright, S.G., 2005. *Soil strength and slope stability*, New Jersey, USA: John Wiley & Sons.
- Fleming, W.G.K. et al., 1992. *Piling Engineering* 2nd Edition, USA: John Wiley & Sons.

- Gavin, K. & Lehane, B., 2003. The shaft capacity of pipe piles in sand. *Canadian Geotechnical Journal*, 40(1), pp.36-45.
- Gavin, K.G., Igoe, D.J.P. & Kirwan, L., 2013. The effect of ageing on the axial capacity of piles in sand. *Proceedings of the Institution of Civil Engineers-Geotechnical Engineering*, 166(2), pp.122–130.
- Germaine, J.T. & Germaine, A. V., 2009. *Geotechnical Laboratory Measurements for Engineers*, New jersey: USA. John Wiley & Sons. [Online]. Available: <https://books.google.com/books?id=Ln5EpwZooPQC&pgis=1>. [2015, July 29]
- Head, K., 2011. *Manual of soil Laboratory Testing: Permeability, Shear Strength and Compressibility tests*, vol 2. Scotland, UK: Whittles Publishing.
- Holtz, R.D. & Kovacs, W.D., 1981. *An Introduction to Geotechnical Engineering*, New Jersey, USA: Prentice-Hall.
- Houlsby, G.T., 1991. How the Dilatancy of Soils Affects their Behaviour. In *Tenth European Conference of Soil Mechanics and Foundation Engineering*, Florence, Italy.
- Igoe, D.J.P., Gavin, K.G. & Kelly, B.C.O., 2011. Shaft Capacity of Open-Ended Piles in Sand. *Journal of Geotechnical and Geoenvironmental Engineering*, 137(10). pp.903–913.
- Jardine, R., 2009. *Review of technical issues relating to foundations and geotechnics for offshore installations in the UKCS*, London: Imperial College London.
- Jardine, R., Overy, R.F. & Chow, F.C., 1998. Axial Capacity of Offshore Piles in Dense North Sea Sands. *Journal of Geotechnical and Geoenvironmental Engineering*, (February), pp.171–178.
- Jardine, R. J. & Chow, F.C., 2007. Some Recent Developments in Offshore Piles Design. In *Proceedings of the 6th International Offshore Site Investigation and Geotechnics Conference: Confronting New Challenges and Sharing Knowledge*. London, UK.
- Jewell, R.A. & Wroth, C.P., 1987. Direct Shear Tests on Reinforced Sand. *Géotechnique*, 37(1), pp.53–68.
- Kansas Department of Transportation, Undated. *Driven pile*, Kansas, USA [Online]. Available at: <http://www.ftandc.com/specs/1292195812-pile.pdf> [2014, October 24]
- Kraft, L.J., 1991. Performance of Axially Loaded Pipe Piles in Sand. *Journal of Geotechnical Engineering*, 117(2), pp.272–296.
- Kruger, A.G. et al., 2010. Strong Wind Climatic Zones in South Africa. *Wind and Structures, An International Journal*, 13(1), pp.37–55.

- Kruger, A.G., Retief, J.V. & Goliger, A.M., 2013. Strong Winds in South Africa : Part 1. *Journal of the South African Institution of Civil Engineering*, 55(2), pp.29-45.
- Krumbein, W.C., 1941. Measurement and geological significance of shape and roundness of sedimentary particles. *Journal of Sedimentary Petrology*, 11(2), pp.64–72.
- Lambe, T. & Whitman, R., 1969. *Soil Mechanics*, New York, USA: John Wiley & Sons.
- Lehane, B.M., Schneider, J.A. & Xu, X., 2007. Development of the UWA-05 Design Method for Open and Closed Ended Driven Piles in Siliceous Sand. Geo-Denver 2007: New Peaks in Geotechnics, Virginia, USA.
- Lehane, B.M. *et al.*, 1993. Mechanisms of Shaft Friction in Sand from Instrumented Pile Tests. *Journal of Geotechnical Engineering*, 119(1), pp.19–35.
- Lehane, B.M., Schneider, J.A. & Xu, X., 2005. *A review of Design Methods for Offshore Driven Piles in Siliceous Sand*, Australia: University of Western Australia.
- Lim, J.K. & Lehane, B., 2015. Time effects on the shaft capacity of jacked piles in sand. *Canadian Geotechnical Journal*. pp.1–38.
- Maffei, J. *et al.*, 2013. Wind Design Practice and Recommendations for Solar Arrays on Low-Slope Roofs. *American society of Civil Engineers*, pp.1–10.
- Meyerhof, G.G. & Adams, J.I., 1968. The Ultimate Uplift Capacity of Foundations. *Canadian Geotechnical Journal*, 5(4), pp.225–244.
- Mitchell, J.K. & Soga, K., 2005. *Fundamentals of Soil Behaviour* 3rd Edition, New Jersey, USA: John Wiley & Sons.
- Mulaudzi, S.K., Mammo, M. & Rudzani, M., 2012. Investigation of Solar Energy Production and Contribution in South Africa. *Africa Journal of Science, Technology, Innovation and Development*, pp.233-254.
- Nicola, B.A. De & Randolph, M.F., 1993. Tensile and Compressive Shaft Capacity of Piles in Sand. *Journal of Geotechnical Engineering*, 119(12), pp.1952–1973.
- Nowak, P. & Gilbert, P., 2015. *Earthworks: A Guide* 2nd Edition, London, England: Thomas Telford.
- Ntirenganya, N., 2015. *An Investigation of the Interlayer Adhesion Strength between the Granular Base and Lightly Cemented Subbase and Its Influence on the Pavement Performance*. Masters Dissertation. Stellenbosch: University of Stellenbosch.

Oldcastle Precast Inc., 2009. *Keeping Solar Panels Secure on Unstable Ground*. [Online] Available: [http://www.oldcastleprecast.com/news/Documents/Keeping Solar Panels Secure on Unstable Ground.pdf](http://www.oldcastleprecast.com/news/Documents/Keeping_Solar_Panels_Secure_on_Unstable_Ground.pdf) [2014, October 24]

Poulos & Davis, 1980. *Pile Foundation Analysis and Design*, Canada: John Wiley & Sons.

Prakash, S., 1990. *Piles Foundations in Engineering Practice*, Toronto: John Wiley & Sons.

Rajapakse, R., 2007. *Pile Design for Structural and Geotechnical Engineers* 1st Edition. UK: Butterworth-Heinemann.

Raymond, 2010. *Photovoltaics Solar Energy in South Africa*. Johannesburg: Scatec Solar [Online] Available: <http://www.doe-irp.co.za/irpcpt/scatec.pdf> [2014, August 2]

Reddy, K.M. & Ayothiraman, R., 2015. Experimental Studies on Behavior of Single Pile under Combined Uplift and Lateral Loading. *Journal of Geotechnical and Geoenvironmental Engineering*, pp.1–10.

REN21, 2014. *Renewable global Status report 2014*, Paris [Online]. Available: http://www.ren21.net/Portals/0/documents/Resources/GSR/2014/GSR2014_full%20report_low%20res.pdf [2014, October 24]

Rowe, P.W., 1962. The Stress-Dilatancy Relation for Static Equilibrium of an Assembly of Particles in Contact. *Proceedings of the Royal Society A: Mathematical, Physical and Engineering Sciences*, 269(1339), pp.500–527.

Sakr, M., Undated. Helical piles - An effective foundation system for solar plants. *Foundations*, pp.1–8.

SANS10160-3, 2011. South Africa Nation Standard: Basic of structure design and actions for building and industrial structures: wind actions 1.1 Edition. South Africa Bureau of Standards. Pretoria, Republic of South Africa.

SAPEM, 2014. South African Pavement Engineering Manual 2nd Edition. South African National Roads Agency. Pretoria, Republic of South Africa.

Schletter, 2010. Professional Solar Mounting Systems [Online]. Available at: http://www.schletter.ca/support/l400111_Ground_Mt_System_OV.pdf [2015, May 25]

Schwartz, K., 1985. Problem Soils in South Africa - State-of-the-Art: Collapsible Soils. *The Civil Engineer in South Africa*, Vol. 27 No.7. pp. 379-393

Semmelink, C. J. and Visser, A.T., 1994. Effect of Material Properties on Compactability and Bearing Capacity. *Journal of Transportation Engineering*, 120(4), pp.570–589.

Simoni, A. & Houlsby, G.T., 2006. The direct shear strength and dilatancy of sand-gravel mixtures. *Geotechnical and Geological Engineering*, 24(3), pp.523–549.

Smith, G. & Smith, I.G.N., 1998. *Elements of Soil Mechanics* 7th Edition., UK: Blackwell Science Ltd.

Solargis, 2015. Solar resource map for South Africa [Online]. Available: http://solargis.info/doc/_pics/freemaps/1000px/ghi/SolarGIS-Solar-map-South-Africa-en.png [2015, July 9]

South African Government, 2015. About Geography and climate.[online]. Available at: <http://www.gov.za/node/65> [2015, July 10]

Taylor, D.W., 1948. *Fundamentals of Soil Mechanics*. New York: Wiley.

Terzaghi, K., Peck, R.B. & Mesri, G., 1996. *Soil Mechanics in Engineering Practice*, New York: John Wiley & Sons.

TMH1, 1986. Standard Methods of Testing Road Construction Materials. 2nd Edition. Department of Transport, Pretoria, South Africa, pp.1-132.

Tomlinson, M.J., 1994. *Pile Design and Construction Practice* 4th Edition, London: E & FN Spon.

Uesugi, M. & Kishida, H., 1986. "Influential factors of friction between steel and dry sands. *Japanese Society of Soil and Foundations and Foundations*, 37(12), pp.3229–3235.

Whitlow, R., 1995. *Basic Soil Mechanics* 3rd Edition, England: Longman Group Limited.

Wikipedia, 2015. Solar power in South Africa [Online]. Available at: https://en.wikipedia.org/wiki/Solar_power_in_South_Africa#cite_note-iea-pvps-snapshot-1992-2014-7 [2015, August 18]

Yu, F. & Yang, J., 2012. Improved Evaluation of Interface Friction on Steel Pipe Pile in Sand. *Journal of Performance of Constructed Facilities*, 26(2), pp.170–179.

APPENDIX

A. DILATION RATE CURVES

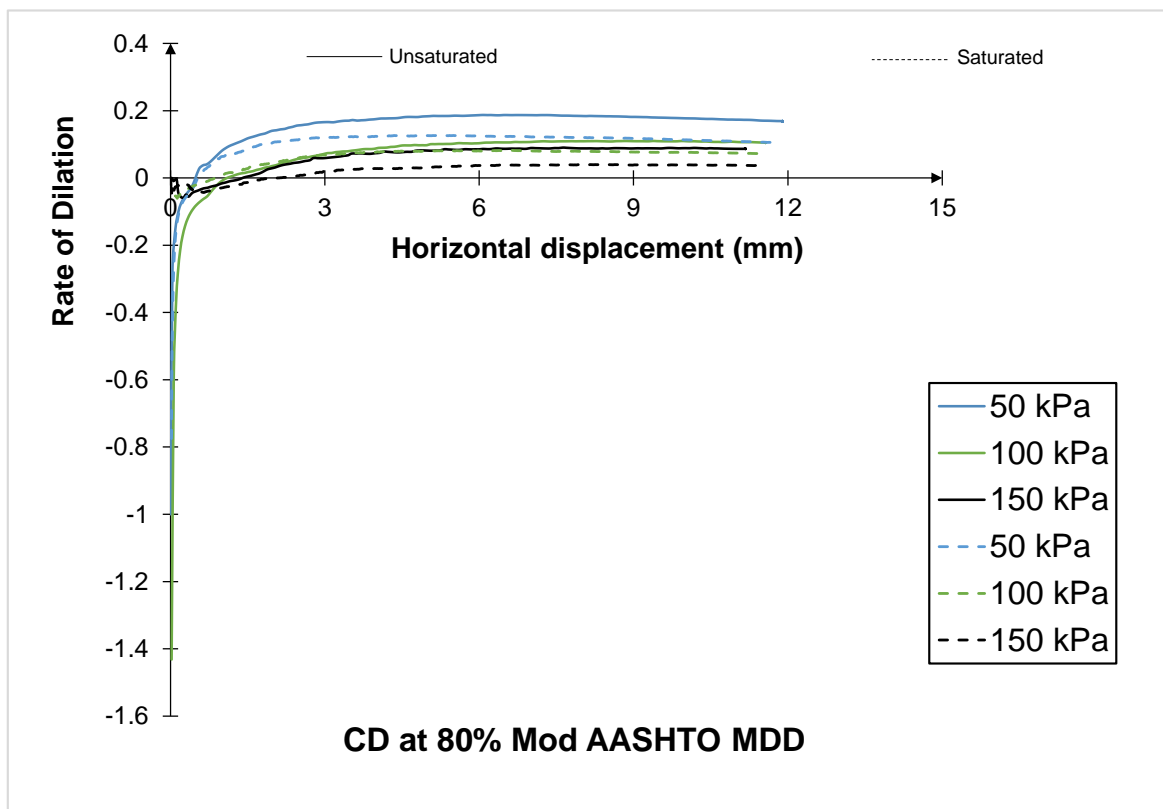


Figure A-1 Crusher dust (CD) at 80% Mod AASHTO MDD

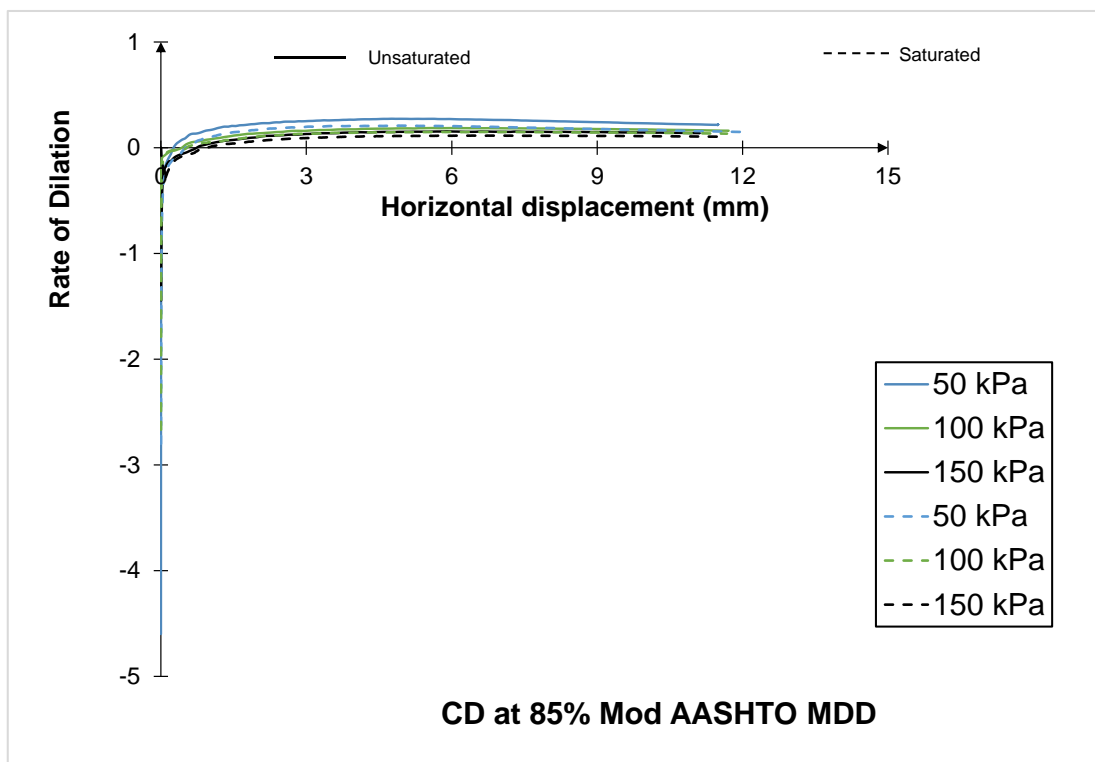


Figure A-2 Crusher dust (CD) at 85% Mod AASHTO MDD

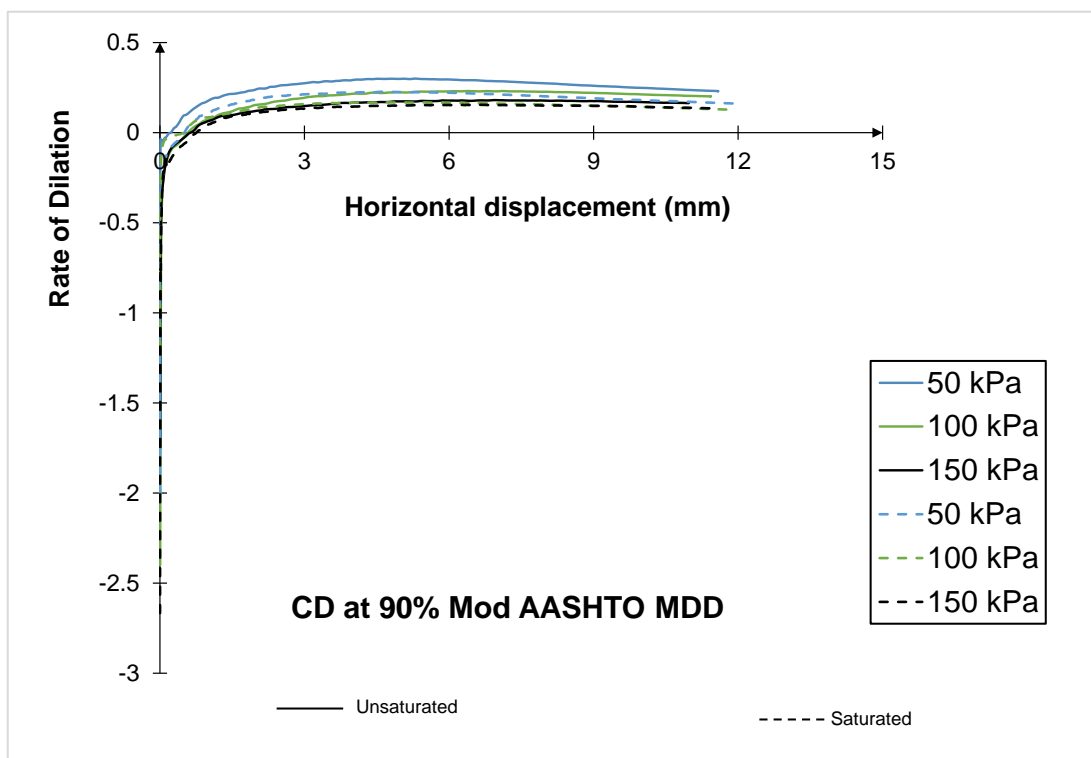


Figure A-3 Crusher dust (CD) at 90% Mod AASHTO MDD

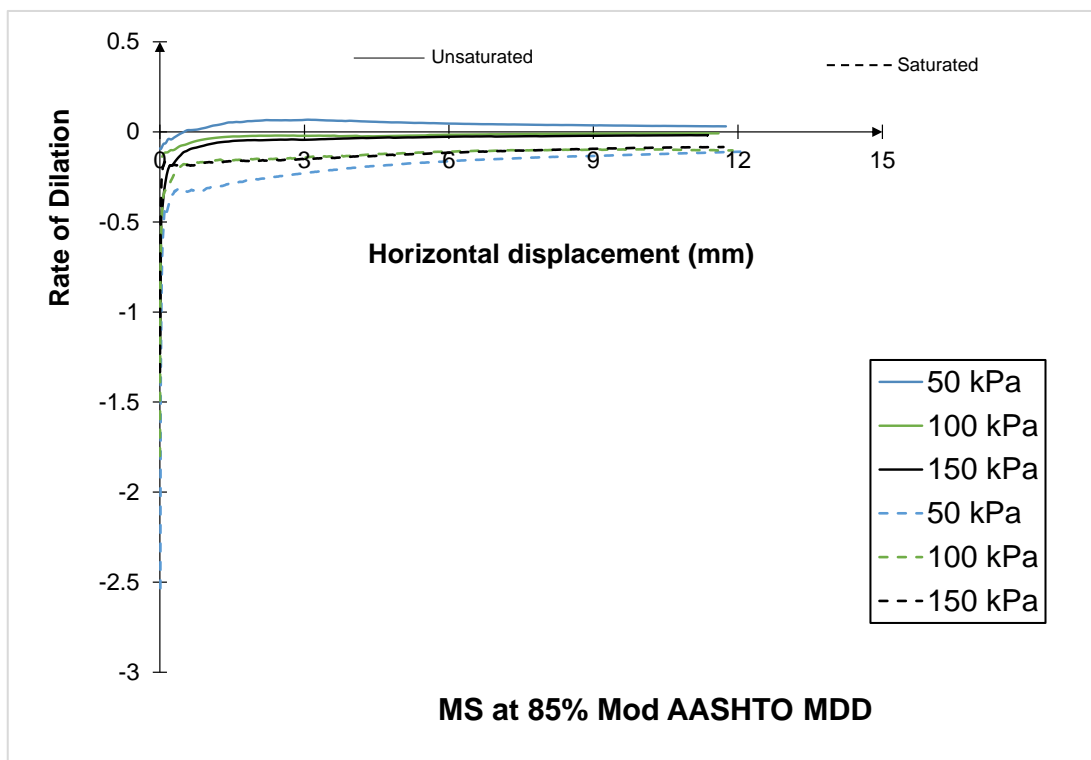


Figure A-4 Malmesbury sand (MS) at 85% Mod AASHTO MDD

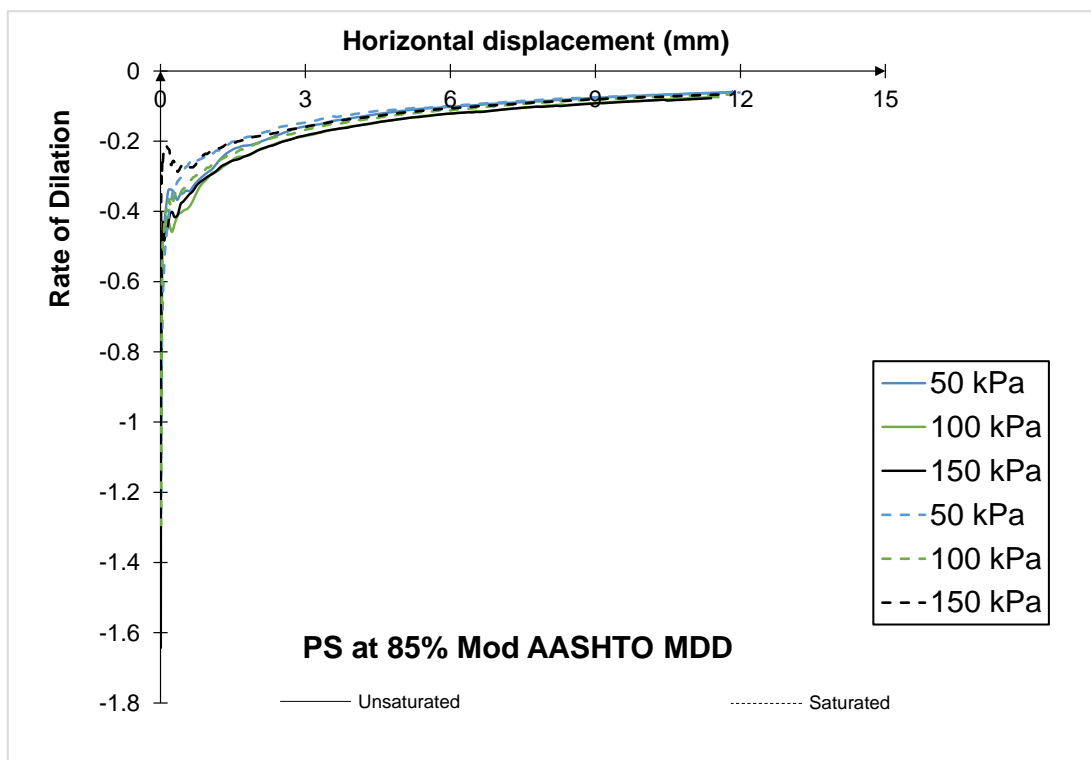


Figure A-5 Philippi sand (PS) at 80% Mod AASHTO MDD

B. WORK SHEETS FOR DIRECT SHEAR AND PULL-OUT COMPACTION TESTING**Figure B-1 Worksheet for Direct shear**

| Type of material | | | |
|--|--------|---------|---------|
| Normal pressure | 50 kPa | 100 kPa | 150 kPa |
| Mass of dry sample (g) | 500 | 500 | 500 |
| Initial water content (g) | | | |
| Water to add | | | |
| 1. APPROXIMATE VALUES | | | |
| Mass of the shear box (SB)in (g) | | | |
| Mass of the SB + soil (g) | | | |
| Mass of soil (g) | | | |
| Percentage of water (%) | | | |
| Thickness of porous plates (t) in cm | 1.125 | 1.125 | 1.125 |
| Mean depth from top surface of upper half of the box to the top of upper porous (h2) in cm | | | |
| Mean depth from top surface of upper half of the box to the top of baseplate (h1) in cm | 3.8 | 3.8 | 3.8 |
| Volume (m3) | | | |
| Relative Density (Kg/m3) | | | |
| Dry Density (Kg/m3) | | | |
| MDD from Mod compaction | 2053 | 2053 | 2053 |
| Degree of compaction (Kg/m3) | | | |
| 2.ACTUAL VALUES | | | |
| Container No | | | |
| Container weight (g) | | | |
| Container + Mass wet soil | | | |
| Container +Mass dry soil (g) | | | |
| Mass dry soil (g) | | | |
| Mass of water (g) | | | |
| Water content | | | |
| Actual Dry Density | | | |
| Actual Degree of Compaction | | | |

Figure B-2 Work sheet for pull-out compaction testing

| Type of material | | |
|---|--------|--------|
| Normal pressure | Test 1 | Test 2 |
| Mass of dry prepared sample (g) | 10500 | 10500 |
| Initial water content (g) | | |
| Water to add | | |
| 1. APPROXIMATE VALUES | | |
| Mass of pipe (P) in (g) | | |
| Mass of P + soil (g) | | |
| Mass of soil (g) | | |
| Percentage of water (%) | | |
| Height of pipe H (mm) | 650 | 650 |
| Height from top of pipe to the level of soil D (mm) | | |
| Diameter of pipe (mm) | 104 | 104 |
| Height of specimen H-D (mm) | | |
| Volume (m ³) | | |
| Relative Density (Kg/m ³) | | |
| Dry Density (Kg/m ³) | | |
| MDD from Mod compaction | | |
| Degree of compaction (Kg/m ³) | | |
| 2. ACTUAL VALUES | | |
| Container No | | |
| Container weight (g) | | |
| Container + Mass wet soil | | |
| Container + Mass dry soil (g) | | |
| Mass dry soil (g) | | |
| Mass of water (g) | | |
| Water content | | |
| Actual Dry Density | | |
| Actual Degree of Compaction | | |